ALMA MATER STUDIORUM – UNIVERSITÁ DI BOLOGNA

DOTTORATO DI RICERCA IN

Bioingegneria

XXVI ciclo

Settore Concorsuale di afferenza: 09/G2
Settore Scientifico disciplinare: ING-IND/34

THREE-DIMENSIONAL JOINT KINEMATICS OF SWIMMING USING BODY-WORN INERTIAL AND MAGNETIC SENSORS PhD

Presentata da: Fabrício Anício de Magalhães

Coordinatore
Prof. Elisa Magosso

Relatore
Prof. Silvia Fantozzi

Correlatore
Prof. Giorgio Gatta

Revisori:
Prof. Ugo Della Croce
Prof. Kamiar Aminian

---

esame finale 2014

“There is one God and one Mediator who can reconcile God and humanity, the man Christ Jesus”. 1 Timothy 2:5.

THIS THESIS IS BASED ON:

Magalhães, F.A., Giovanardi, A., Di Michele, R., Cortesi, M., Gatta, G., Fantozzi, S., 2014. Swimming motion analysis: 3D joints kinematics of the upper limb using wearable inertial and magnetic sensors. In 3D Analysis of Human Movement. Lausanne, Switzerland.

Magalhães, F.A., Giovanardi, A., Cortesi, M., Gatta, G., Fantozzi, S., 2013a. Three-dimensional kinematic analysis of shoulder through wearable inertial and magnetic sensors during swimming strokes simulation. In XXIV Congress of the International Society of Biomechanics. Natal, Brazil.

Giovanardi, A., Magalhães, F.A., Cortesi, M., Fantozzi, S., Gatta, G., 2013. L'utilizzo dei sensori inerziali nell'analisi biomeccanica del nuoto, La Tecnica del Nuoto, Verona, Italy, pp. 10-13.

Magalhães, F.A., Sawacha, Z., Di Michele, R., Cortesi, M., Gatta, G., Fantozzi, S., 2012. Performance analysis of an automatic tracking software in underwater exercises. In 3D Analysis of Human Movement. Bologna, Italy.

Magalhães, F.A., Sawacha, Z., Di Michele, R., Cortesi, M., Gatta, G., Fantozzi, S., 2013b. Effectiveness of an Automatic Tracking Software in Underwater Motion Analysis. Journal of Sports Science and Medicine 12, 660-667.

Magalhães, F.A., Vannozzi, G., Gatta, G., Fantozzi, S., In review. Wearable inertial and magnetic sensors in swimming motion analysis: a systematic review. Submitted to the Journal of Sports Sciences.

ABSTRACT

The knowledge of the joint kinematics during swimming plays a fundamental role in sports conditioning and clinically. The analysis of video recordings obtained using underwater cameras is the most typical method used to evaluate swimming kinematics However, video-based analysis is often limited to a single stroke; the examined movement is limited to underwater arm stroke phases; and is time-consuming and requiring off-line post-processing procedures. On the other hand, wearable inertial and magnetic measurements units (IMMU) are an alternative tool for underwater motion analysis because they are swimmer-centric, they require only simple measurement set-up and they provide the performance results very quickly. In order to estimate 3D joint kinematics during motion, protocols were developed to transpose the IMMU orientation estimation to a biomechanical model. The aim of the thesis was to validate a protocol originally propositioned to estimate the joint angles of the upper limbs during one-degree-of-freedom movements in dry settings and herein modified to perform 3D kinematics analysis of shoulders, elbows and wrists during swimming. Eight high-level swimmers were assessed in the laboratory by means of an IMMU while simulating the front crawl and breaststroke movements. A stereo-photogrammetric system (SPS) was used as reference. The joint angles (in degrees) of the shoulders (flexion-extension, abduction-adduction and internal-external rotation), the elbows (flexion-extension and pronation-supination), and the wrists (flexion-extension and radial-ulnar deviation) were estimated with the two systems and compared by means of root mean square errors (RMSE), relative RMSE, Pearson's product-moment coefficient correlation (R) and coefficient of multiple correlation (CMC). Subsequently, the athletes were assessed during pool swimming trials through the IMMU. Considering both swim styles and all joint degrees of freedom modeled, the comparison between the IMMU and the SPS showed median values of RMSE lower than 8°, representing 10% of overall joint range of motion, high median values of CMC (0.97) and R (0.96). These findings suggest that the protocol accurately estimated the 3D orientation of the shoulders, elbows and wrists joint during swimming with accuracy adequate for the purposes of research. Furthermore, an overall correspondence was verified among the swim phases in both simulated and real swimming, and no difference in the overall joint ranges of motion between the real and the simulated swims were observed. In conclusion, the proposed method to evaluate the 3D joint kinematics through IMMU was revealed to be a useful tool for both sport and clinical contexts.

LIST OF ACRONYMS

2D	Bi-Dimensional
3D	Three-Dimensional
APDM	Ambulatory Parkinson's Disease Monitoring
ASOR	Anatomical System of Reference
CAST	Calibration of Anatomical System Technique
CMC	Coefficient of Multiple Correlation
DLT	Direct Linear Transformation
DOF	Degree of Freedom
GPS	Global Positioning System
H1	Proximal Humerus
HF1	Distal Humerus
HND	Hand
IMMU	Inertial And Magnetic Measurements Units
IQR	Interquartile Range
MAD-system	Measuring Active Drag System
MHA	Mean Helical Axis
PF	Proximal Forearm
R	Pearson Product-Moment Correlation Coefficients
RMSE	Root Mean Square Error
SOR	System of Reference
SPS	Stereo-Photogrammetry System
THX	Thorax
UNIBO	University of Bologna

LIST OF FIGURES

LIST OF TABLES

CONTENTS

CHAPTER 1

INTRODUCTION

1 Introduction

Swimming is a physical activity practiced by millions of people in the whole world for recreation, sport and fitness. Regarding competitive swimming, sport scientists have proposed different methodologies to improve performance with minimal musculoskeletal damage. Consequently, swimming world records have been broken year after year much more frequently than in other sports like track and field. The identification of the key factors that allows the best propulsive efficiency is important not only to achieve high sports performance but also to acquire valuable information for teaching the right swimming technique. A further significant issue is that of injury prevention in competitive swimmers. For example, shoulder pain is frequent in swimmers, being caused by a set of factors like gleno-humeral laxity, biceps or rotator cuff lesions, and impingement syndrome (Allegrucci et al., 1994; McMaster and Troup, 1993; Pink and Tibone, 2000; Pollard and Croker, 1999; Sein et al., 2010). Joint range of motion, joint laxity, and anthropometric and epidemiologic data were evaluated to investigate the mechanisms leading to injuries.

Therefore, from both a sports conditioning and clinical perspective, the knowledge of the joint kinematics during swimming plays a fundamental role. In the first case, it can give essential information for planning a training program specific for each athlete. Moreover, measuring biomechanics variables throughout a whole race or training session can be very useful to prevent both overtraining and decreased performance phenomena. Concerning the clinical aspects, the biomechanical analysis can support the design of appropriate prevention programs for the most common upper limb injuries that typically affect the swimmers.

The analysis of video recordings obtained using underwater cameras is the most typical method used to evaluate swimming kinematics. Traditionally, tracking markers placed or drawn on the swimmers' skin is the most common way to perform underwater motion analysis (Magalhães et al., 2013; McCabe and Sanders, 2012; Psycharakis and McCabe, 2011; Sanders, 2007; Seifert et al., 2008). Recently, an alternative method has been proposed by Ceseracciu et al. (2011) through the markerless approach. However, in both the marker-based and markerless approaches, only the 3D position of the anatomical landmarks and 2D joint angles were analyzed. Only the study conducted by Ceccon and co-workers was found that have used the video recording analysis to perform the 3D kinematics of the shoulder and elbow joints during front crawl swimming (Ceccon et al., 2012). Nevertheless, all studies based on video analysis have a number of drawbacks. This analysis is often limited to a single stroke due to the restricted field of view associated with the number of cameras. Furthermore, the examined movement is limited to underwater phases, a long elaboration time is required even when an automatic tracking procedure is used, and time-consuming set-up and

calibration procedures are required (Magalhães et al., 2013). Finally, quantitative video analysis can only be performed off-line and thus cannot be used by coaches during training sessions for detecting and immediately correcting technical mistakes.

To overcome the limitations of methods based on the video analysis, in the last 15 years the wearable inertial and magnetic measurements units (IMMU) have been applied in swimming performance analysis. These systems are based on swimmer-centric waterproofed devices that allow a continuous data acquisition throughout a swim, requiring a simple measurement set-up. Furthermore, IMMU have the value to provide in real time useful performance variables to the coaches during training sessions. Duration of the swimming stroke phases, stroke frequency, time parameters and velocities have been measured using IMMU and validated with appropriate measurement systems (Dadashi et al., 2011; Daukantas et al., 2008; Le Sage et al., 2011; Ohgi, 2002). More recently, two or more monitors have been attached to the swimmers' wrists, lower back, arms or legs, in order to better estimate the biomechanical variables (Bächlin and Tröster, 2012; Dadashi et al., 2013; Fulton et al., 2009a; Hou, 2012; James et al., 2011).

However in a systematic review about the use of IMMU for underwater motion analysis (Magalhães et al.), no study on 3D joints kinematics of the upper limbs was found in the literature. Additionally, it was found a protocol for the estimation of the 3D joint angles of shoulder and elbow in the clinical context throughout an IMMU system developed by Cutti et al. (2008), which is adaptable for the use of different IMMU systems, for the use of other joints and for the use of different situations like the sports context.

1.1 Aim of the Study

The aim of this study is to analyze the 3D joint kinematics of the upper limbs during swimming using IMMU by extending a protocol previously developed for simple and slow movements of shoulder and elbow, validated in ambulatory context. The present protocol was validated in simulated swimming performed in dry condition using the stereo-photogrammetry as reference, and tested in actual in-water swimming.

CHAPTER 2

LITERATURE REVIEW

2 Literature Review

2.1 Introduction

Swimming is one of the most challenging sports to analyze scientifically. Not only the human movement analysis is quite complex, but also the aquatic environment involves specific physical effects, like the thrust and drag, that must be considered. Several biomechanical methods have been proposed in the literature with the aim of acquiring valid data to analyze swimming performance. The most frequently investigated areas include kinematics, kinetics, energetics, neuromuscular biomechanics and anthropometrics.

In competitive swimming, the performance can be subdivided into four phases: starting, swimming, turning, and finishing. During any swimming event, athletes spend most of the time in the swimming phase. Therefore, the swimming phase is the most determinant of swimming performance, and the majority of research efforts in swimming biomechanics have been dedicated to analyzing the four competitive strokes: Front Crawl, Backstroke, Breaststroke and Butterfly.

This chapter summarizes the-state-of-the-art on the biomechanics of swimming. The literature review provided groundwork for the development of the methods described in Chapter 3, and for the discussion of the results in Chapter 4. In accordance with the main purpose of the thesis, only the kinematics of the upper limbs during front crawl and breaststroke were considered. The front crawl is the most frequently performed swim style among practitioners; and both front crawl and breaststroke are easily adapted to be simulated in laboratory.

2.2 Swimming biomechanics

A large part of the swimming research is dedicated to the swimming strokes kinematics. Hence, the main aspects related to the stroke cycle kinematics, limbs kinematics, body kinematics and kinetics will be summarized in this section.

2.2.1 Stroke cycle kinematics

Velocity is the critical variable to assess swimming performance. Stroke length (horizontal distance traveled by the body during a full stroke cycle) and stroke frequency (number of full stroke cycles completed within a unit of time) are the independent variables usually used to define swimming velocity. Variations in velocity are determined by increases or decreases in stroke frequency and stroke length (Craig et al., 1985; Kjendlie et al., 2006; Toussaint and Truijens, 2005). A swimmer usually has a stroke length that is as long in distance as possible, therefore, velocity is manipulated chiefly by changing the stroke frequency (Craig and Pendergast, 1979).

Another variable often used to assess the stroke cycle kinematics is the stroke index, an estimator of overall swimming efficiency. The stroke index was defined by Costill et al. (1985) as the product of average velocity and stroke length. At a given velocity, swimmers with the most efficient swimming technique are those presenting the higher stroke length (Barbosa et al., 2011).

2.2.2 Upper- and Lower-Limb kinematics

Stroke mechanics variables including stroke frequency and length are related to the overall limb kinematics. Many researchers have attempted to determine the exact contribution of the limbs to swimming performance. Deschodt et al. (1996) observed a significant high relationship between hip velocity and upper limb horizontal and vertical motion, i.e. an increase of upper limb velocity was associated with an increase in swimmers' horizontal velocity. Thus, the upper-limb action has a major influence on swimming performance (Deschodt et al., 1996; Zamparo, 2006). Furthermore, the contribution of the legs to overall propulsion was found to be small during front crawl, varying from about 10 to 15% (Deschodt et al., 1996; Hollander et al., 1988).

Another issue is the contribution of the body roll to the upper-limb kinematics and consequently to the swimming performance. For the front crawl, Psycharakis et al. (2010) reported a strong influence of the body roll on the upper limb's kinematics: a more efficient body rolls enabled a more efficient hand trajectory, leading to an effective push. For the breaststroke, the timing between the upper- and lower- limbs is a major concern. Chollet et al. (1999) verified a significant high relationship between both upper- and lower-limb coordination and swimming velocity. Tourny et al. (1992) suggested that higher velocities can be achieved by reducing the gliding phase.

2.2.3 Body kinematics

Normally the body kinematics are calculated using markers placed either on the body's center of mass or on the hip joint. However, the hip seems not to be a valid estimator of the center of mass for kinematics because: 1) it displays more variability in velocity than the center of mass; 2) its temporal estimation does not always represent the stroke cycle; 3) during the stroke cycle, the limb movements affect the estimation of the center of mass position; and 4) it is a fixed anatomical landmark, so it is not dynamically adaptable during the swimming phases (Barbosa et al., 2011; Psycharakis and Sanders, 2009; Vilas-Boas et al., 2010). Although estimation of the center of mass using the hip joint presents these drawbacks, some researchers use this kind of estimation anyway.

Intra-cyclic variation of the horizontal velocity is the most frequently measured variable related to the center of mass. The body's velocity is not constant during a stroke cycle since the

body's velocity increases and decreases due to the limb action. The horizontal velocity can be described with non-linear functions, since swimmers present different individual horizontal velocity curves (Barbosa et al., 2010b). So, individual curves may not coincide with the mean curves of a sample of subjects, thus expressing the individual interpretation of the swimming technique (Barbosa et al., 2011).

Barbosa et al. (2010a) analyzed the horizontal velocity of swimmers during the front crawl stroke and found a multi-model profile where higher peaks were related to arm actions and lower peaks to leg actions. For some athletes two distinct peaks with different velocities were found that were related to the most propulsive phases of each arm. Moreover, it seems that for some subjects there is an asymmetrical application of the propulsive force from the arms. For the breaststroke, (Barbosa et al., 2010a) characterized the horizontal velocity as a bi-modal profile. One peak was related to the arm actions and the other to the leg action, and both the peaks were almost comparable. After that peak, the gliding phase occurs with a decrease in the velocity. Good swimmers know the exact moment in which to start a new stroke cycle, avoiding a major decrease in the instantaneous velocity (Capitão et al., 2006).

2.2.4 Strokes kinetics

Kinetic analysis in swimming can be associated to two main topics of interest: the propulsive force generated by the propelling segments, and the drag forces resisting to the forward motion. The balance between these two forces influences a given swimmer's speed.

2.2.5 Propulsive force

Propulsive force is the total force produced by the swimmer to push his/her body forward. In this sense, performance is strictly connected to the swimmer's ability to produce effective propulsive force. The direct measure of the propulsive forces acting on a swimmer is practically impossible but several methods have been proposed in order to give an indirect estimation of them. Hollander et al. (1986) developed a system for measuring active drag (MAD system) that determines the propulsive force applied to underwater push-off pads used by the swimmers. However, Payton and Bartlett (1995) suggested that this system was not suitable to be used during competitions due to its invasive nature.

A non-intrusive method of estimating propulsive hand forces during free swimming was proposed by Berger et al. (1995) and Sanders (1999). In their method, the instantaneous propulsive forces are estimated according to vector analysis of forces combined action on model hands in an open-water channel and the recording of underwater pulling action of a swimmer (Schleihauf, 1979). These data can be then used together with digitized kinematic data of the hand to estimate

the lift, drag and resultant force vectors produced during the swimming stroke cycle. Conversely, the calculation of the model hands in this method assumes that the water flow is steady, which is questionable because this kind of calculation may underestimate the outcomes (Kudo et al., 2008). Instead, Kudo et al. (2013) described that both positive and negative hand's acceleration promote an unsteady water flow in swimming.

2.2.6 Drag force

The drag force can be defined as an external force that acts parallel to the swimmer's body but in the opposite direction of movement. It is a resistive force that depends on the anthropometric characteristics of the swimmer in the water (i.e. buoyancy is a factor as well as flat-plate area of the swimmer's profile while swimming), on the characteristics of the equipment used by the swimmers, on the swimming velocity, and on the swimming technique.

The evaluation of the intensity of the hydrodynamic drag during swimming represents an important issue in swimming biomechanics. Drag can be determined passively by towing a non-swimming subject through the water, but this approach does not consider all the real drag created by a swimmer during the swimming motions. Thus, one of the most important parameters in swimming hydrodynamics is the drag of the swimmer's body during active swimming. In agreement with this concept, Kjendlie and Stallman (2008) found passive drag (i.e. non-swimming) values lower than active drag (i.e. during swimming) values in the same swimmer.

The first attempts to assess active drag were based on interpolation techniques that involved indirect calculations, considering the changes in oxygen consumption due to the attachment of additional loads to the swimmers' body (Di Prampero et al., 1974). Another technique was proposed by Hollander et al. (1986), and already mentioned, called the MAD-system which relies on the direct measurement of the push-off forces while swimming the front crawl stroke with arms alone. Kolmogorov and Duplishcheva (1992) designed another method to determine the active drag through velocity perturbations, also known as the method of small perturbations. In this approach, athletes must swim two 25-meters sprints at maximal effort, one ~~lap~~ with free swimming and the other while towing a hydrodynamic body that creates a known additional drag. For both the trials, the average velocity is calculated. Under the assumption that in both the swims the power output to overcome drag is maximal and constant, the drag force can be determined by considering the difference in swimming velocity. In contrast to the interpolation techniques and the MAD-system (which requires heavy and expensive experimental procedures), the velocity perturbation method to assess active drag just requires the use of the hydrodynamic drag device and a stopwatch (Kolmogorov and Duplishcheva, 1992). Additionally, this approach can be applied to measure

active drag in all four competitive strokes. Using this approach, several studies have been conducted to evaluate active drag in swimming (Kjendlie and Stallman, 2008; Marinho et al., 2010). Kjendlie and Stallman (2008) found that active drag in adults was significantly higher than in children. This difference between adults and children was mostly due to the larger size and higher velocity for adults during swimming. Marinho et al. (2010) reported no differences in the values of active drag between boys and girls.

The contribution of form, friction and wave drag components to total drag during swimming is an interesting topic in sports biomechanics (Pendergast et al., 2006). Data available from several experimental studies showed some difficulties involved in the evaluation of the contribution of each drag component (Bixler et al., 2007). It is widely recognized that frictional drag is the smallest component of total drag, especially at high swimming velocities, although this drag component should not be disregarded in elite level swimmers. Bixler et al. (2007), using numerical simulation techniques, found that friction drag represents about 25% of total drag when the swimmer is gliding underwater. Zaidi et al. (2008) also found an important contribution of friction drag to the total drag when the swimmer is passively gliding underwater. These authors found that friction drag represents about 20% of total drag. Thus, issues such as sports equipment, shaving and the decrease of immersed body surface area should be considered, since this drag component seems to influence the performance especially during the underwater gliding after starts and turns. In addition, form and wave drag represent the major parts of total hydrodynamic drag. Therefore, for maximal efficiency, swimmers must assume the most hydrodynamic position during swimming (Marinho et al., 2009; Toussaint et al., 2006). Although waveform represents a large part of total drag during swimming (Kjendlie and Stallman, 2008), when gliding underwater there is a major reduction of this drag component (which is why swimming rules control the amount of swimming underwater).

2.3 Biomechanical Analysis of Swimming

2.3.1 Video-based Analysis

Traditionally, the criterion method for motion analysis in swimming has been the analysis of video recordings (Seifert et al., 2005; Vezos et al., 2007). Indeed, the use of video cameras for recording, modeling, and examining swimming technique has become usual practice for elite swimmers (Bächlin et al., 2009). This kind of analysis is mostly performed by using underwater camcorders that record a raw video sequence (sometimes with markers attached to the swimmer) and by subsequently tracking the points of interest using specific software packages (Pansiot et al., 2010). The points tracked are typically anatomical landmarks that allow the kinematic modeling of

the body including the wrists, elbows, and shoulders for upper limbs, and the hips, knees, and ankles for lower limbs (Ohgi, 2002; Pansiot et al., 2010).

2.3.1.1 Marker Approach

Through the markers-tracking procedure, swimming motion has been analyzed by considering variables related to performance like the stroke rate, stroke length, body roll, and range of motion. The marker coordinates can be obtained using the direct linear transformation (DLT) method, an established algorithm that allows multiple images captured by at least two underwater cameras to be extracted on a frame-by-frame basis (Ohgi, 2002; Pourcelot et al., 2000), i.e. for each frame at least 2 images are used to estimate the 3D coordinates in a previously calibrated space. Thus, displacement versus time data can plotted with minimum error (Callaway et al., 2009) and the body segments paths during an entire stroke can be constructed (Ohgi, 2002).

The displacements of anthropometric data are usually measured using the DLT. Afterwards, other variables related to the swimming performance can be calculated. By using a marker fixed on the swimmer's center of mass, (Psycharakis and Sanders, 2008) measured the shoulder and hip roll changes during the crawl swimming. In a subsequent study, (Psycharakis et al., 2010) used the same method to calculate the variation of the swimmer's velocity during a stroke cycle, as this velocity is proposed to be linked to performance. These investigations are just two examples of how the DLT can be used in swimming motion analysis; however, in DLT all the points of interest must be manually digitized, well-known to be a time-consuming process.

Recently, efforts have been made toward the development of automated procedures in markers tracking in order to provide coaches, athletes and sports scientists with quick kinematic information. An automatic motion capture system similar to stereo-photogrammetry systems is available on the market (http://www.qualisys.com/products/hardware/oqus-underwater/, retrieved at 20/12/2013). It was specifically designed for the 3D analysis of swimming and it is composed of retro-reflective spherical markers and waterproofed cameras. Kjendlie and Olstad (2012) have tested this system with 6 cameras and reported an increase of 7% to 10% in the passive drag due to the resistance exerted by the 24 markers attached to the swimmer. Although further data are needed to support their findings, these findings may lead to the conclusion that the use of markers of non-negligible volume in the water is questionable. Indeed, an increased passive drag would negatively affect the performance of the swimmer.

A possible approach to avoid increasing passive drag consists in replacing the spherical markers with bi-adhesives placed on the swimsuit, or with markers drawn on the swimmer's skin (Ceccon et al., 2013; McCabe et al., 2011; McCabe and Sanders, 2012). When this setup is used, movements

are filmed through conventional underwater cameras, and the resulting video recordings are analyzed using specific software for the tracking of features. Manual tracking represents the least precise solution to analyze movements performed in the water. However, this tracking method requires an extensive amount of time. For example, the work of Psycharakis and Sanders (2008) used manual digitation to analyze 19 anatomical landmarks for 4 stroke cycles in 10 swimmers performing a 200-m front crawl trial. The mean stroke frequency was 0.74 Hz, involving a total duration of approximately 5.4 s for the examined fraction (4 cycles) of each swim. Six cameras at 50 frames per second were used, therefore, about 1620 frames were digitized for each swimmer. Although not all the markers had to be digitized in each frame (some were not visible by one or more cameras), a well-trained operator would have reasonably used no less than one minute per frame, involving a total digitation time of 27 hours for each swimmer.

With the aim of providing a quick feedback on the kinematic characteristics of swimming to swimmers and coaches from passive markers, Magalhães et al. (2013) assessed the degree of automation of software for automatic tracking calculated as the percentage of required manual interventions throughout the tracking process in 21 video recordings of different aquatic exercises (n=2940 marker positions). Cross, full black circle, full white circle and partial black circle were the types of marker used. The description of the software's algorithm was presented by Magalhães et al. (2012). The percentage of manual interventions in this software for the examined video recordings was up to 17%, while it reached higher values (up to 46%) for the commercial software (SIMI Reality Motion Systems GmbH, Germany) considered as reference, with significant difference between both systems (odds ratio lower than 1, $P < 0.05$). Hence, the authors stated that this tool can be used in research involving underwater motion analysis due to its good degree of automation and overall effectiveness in tracking different types of passive non-reflective markers when analyzing underwater exercises.

The software above assessed by Magalhães et al. (2013) has been already used by Ceccon et al. (2013) to automatically track passive markers in order to estimate the 3D joint kinematics of upper limbs during swimming by means of the calibration of anatomical system technique (CAST) proposed by Cappozzo et al. (1995). Fifteen front crawl trials were performed by an Italian national level swimmer and recorded using 6 conventional underwater color cameras. Comparing the automatic tracking mode of the referred software with the manual digitalization of commercial software (SIMI Reality Motion Systems GmbH), the authors found a good agreement between these two systems with a root mean difference lower than 20 mm in reconstructing the marker trajectories. Finally, the authors concluded that the automatic feature tracking technique is precise and accurate to estimate the anatomical landmark positions with a shorter processing time in

comparison with the manual tracking. Furthermore, the methodological contribution of this work was that it presented accurately the estimation of the three degrees of freedom of the shoulder and elbow joints through the method CAST during front crawl swimming.

Ceccon et al. (2013) and Magalhães et al. (2013) demonstrated that it is possible to achieve good precision and accuracy in marker tracking using an automated procedure with considerably less post-processing time than in the standard manual digitalization. Several commercial software packages are already available on the market, but none of them was specifically designed for swimming. Due to the characteristics of the aquatic environment where numerous hindrances can make accurate detection of the markers difficult, technologies able to provide accurate kinematic data of underwater motion are highly desirable, particularly if fully automated.

The underwater photogrammetry system tried by Kjendlie and Olstad (2012) seems to be a good option, due to its very high precision and rapid tracking, but the great expense, reduces its use to a few laboratories around the world. In addition, this system demonstrated an increase in passive drag due to use of spherical markers, which is definitely undesirable when performance enhancement is the goal.

The software presented by Ceccon et al. (2013) and Magalhães et al. (2013) is user-friendly, is easily accessible (free), is not extensively time-consuming, does not influence the performance, provides accurate kinematic data, and overcomes most of the difficulties in markers detection during underwater motion analysis. However, there is no fully automated system available in swimming, because these systems require constant human supervision and sometime some manual interventions are necessary to correct the cursor pointer position. In this sense, all these systems should be viewed as semi-automatic systems.

2.3.1.2 Markerless Approach

Marker tracking is not the only approach available in swimming motion video-based analysis. The markerless system has been suggested as an alternative method in the last years (Corazza et al., 2010; Corazza et al., 2006; Moeslund and Granum, 2001; Moeslund et al., 2006; Poppe, 2007). Using the markerless technology, it is possible to automatically estimate the position of body segments from conventional cameras, and no marker drawn nor attached to the subject skin is required. The background subtraction step is the most common approach, where the room's wall and floor are covered with blue or green panels (Jackman, 2007) and then the background is digitally removed to isolate only the exercising subject. In less controlled settings such as sports competitions, a background image is used as reference and this imagine is compared in all the subsequent video frames, in this way individualizing the subject in motion.

An underwater markerless motion capture technique was adapted by Ceseracciu (2011) and its accuracy was evaluated with respect to a commercial motion analysis system using manual markers tracking (SIMI Reality Motion Systems GmbH). To perform the 3D kinematics of front crawl swimming, 6 underwater cameras were positioned in order to maximize the view of the right upper limb. This markerless motion capture technique is based on 5 steps: videos uncompressing and de-interlacing, silhouette extraction, visual hull creation, model creation and model matching. For each front crawl trial, typically 2 to 3 hours were spent to process the data with the markerless method, which is much less than the 7 hours required by the traditional procedure of digitizing by an operator. The authors found good accuracy for the wrist joint in all directions but a relevant systematic error for the elbow and shoulder joints along the longitudinal direction, and their method was not able to reconstruct the joint trajectories during the in-sweep and up-sweep phases of the front crawl arm strokes. In the end, they concluded that the accuracy of the wrist joint measures seemed to be sufficient, a relevant aspect of the technical analysis of swimming strokes in which the hand trajectory is commonly used to identify and characterize stroke phases.

The underwater stroke video-based motion analysis has been carried out using both the marker-based and the markerless approaches. However, this method seems to have a number of drawbacks for swimming coaches because it depends on the work of highly qualified operators who need a long time and much effort for the digitizing process (Davey et al., 2008; Ohgi, 2002). In addition, air bubbles and the swimmer's own motion sometimes prevent observation of the full motion of the swimmers (Ohgi, 2002). Because of this, coaches cannot be provided with a real-time feedback about the swimming kinematics of their athletes (Ohgi, 2002).

2.3.2 Inertial and Magnetic Measurements Units

Recently, combinations of accelerometers, gyroscopes and magnetometers, also known as inertial and magnetic measurement units (IMMU) or sensor fusion, have been developed and miniaturized by micro-machining technology. They are becoming popular biomechanical methods applied to health and sporting activities. There is sufficient research in the field to show the validity of applications of IMMU for monitoring human movement in sport. Several authors have examined the discrimination of movement patterns and the evaluation of motion using data from accelerometers, gyroscopes and magnetometers, covering a large range of settings, including: ambulatory measurements, physical activity, gait analysis, orientation and movement, and improving athletic performance (Callaway et al., 2009; Davey et al., 2008). Hence, the use of IMMU is presented as a useful tool for monitoring human movement patterns.

Inertial and magnetic measurement units worn by the swimmers have been used as an

alternative in performance analyses to overcome the limitations of video-based methods. Wearable sensors do not require a complex setup and they can be considered swimmer-centric since the each swimmer wears his/her own sensors and is independent from the other swimmers (Pansiot et al., 2010). IMMU is an automated system that increases the reliability in data acquisition by reducing the sources of error (Davey, 2004).

Developing and testing specific protocols to perform a 3D kinematic analysis of swimming using IMMU has been the aim of several authors. Ohgi et al. (2000) presented the relationships between the wrist acceleration data and hand movement under the Maglischo's stroke pattern definition. Examining the tri-axial wrist acceleration of both front crawl stroke and breaststroke of 11 subjects, they showed the unique acceleration pattern characterizing each of the styles. In addition, Ohgi et al. (2003), using the same method of Ohgi et al. (2000), discriminated the stroke phase of the front crawl stroke (entry, down sweep, out sweep and in sweep), and also the three stroke phases of the breaststroke (recovery, in sweep and out sweep). By using the pattern recognition techniques, Slawson et al. (2008) stated that the four competitive swimming styles could be analyzed from signals of accelerometers worn on the wrist. Therefore, the recent practice of using IMMU in swimming training allows coaches and swimmers to assess how the swimming technique can be improved by assessing the characteristics of the swimmer's stroke motion during an entire swim (Ohgi and Ichikawa, 2002; Ohgi et al., 2002).

Although several authors have attempted to utilize IMMU in swimming, little data as well as few processing methods, have been presented to date. Classically, analyses of swimming data have been performed with a personal computer using off-line algorithms after the swimming exercise. Whilst this is a very useful procedure, an issue of post processing analyses is that coaches cannot provide immediate feedback to swimmers. This aspect is particularly relevant when a swimmer aims to correct specific movements related to performance. Furthermore, real-time feedback would provide coaches with individual indicators of swimming performance such as velocity, attitude, and position of the swimmer (Le Sage et al., 2010a).

Therefore, recent studies aimed to develop a real-time feedback method. Bächlin and co-workers have developed a method named “SwimMaster” wherein a real time feedback is obtained through online algorithm implementation (Bächlin et al., 2009; Bächlin and Tröster, 2009, 2012). Another real time feedback method is that proposed by Le Sage et al. (2010b), who developed a Kalman filter for using IMMU in swimming. The main advantage of both methods is the low computational power required, allowing a decrease in the gap between laboratory and training settings as the performance of a swimmer can be analyzed almost instantaneously after a swimming trial.

Magalhães et al. (In review) have performed a review on the applications of IMMU for swimming motion analysis. The research was based on a systematic search for publications in the following scientific databases: PubMed, ISI Web of Knowledge (Science Citation Index Expanded), IEEE Xplore, Google Scholar, Scopus and Scirus. The search included a time interval of 15 years from the period in which the search was carried out (late March 2013) and only articles published in that time window were included. The initial total number of articles identified from all databases was 62 (Medline 27, ISI 9, IEEExplore 16, Google Scholar 10, Scopus 4, Scirus 12), including journal articles, conference proceedings and book chapters. Considering the inclusion and exclusion criteria, out of the 62 full articles identified, only 23 articles were ultimately included in that review (Table 2.1). The following five main issues became the main topics of the review: 1) applications of inertial and magnetic sensing in swimming, 2) sensor specification and sealing, 3) sensor attachment location, 4) experimental designs, and 5) swimming performance assessment and monitoring applications.

2.3.2.1 Applications of inertial and magnetic sensing in swimming

The first attempts to use IMMU in swimming referred to the underwater phases discrimination (Ohgi et al., 2000), a fundamental prerequisite for any biomechanical analysis of swimming, as well as to discriminate the different swimming styles (Hou, 2012; Slawson et al., 2008; Vannozzi et al., 2010) and the characteristics of the swimmer's stroke motion (Ohgi and Ichikawa, 2002; Ohgi et al., 2002). Furthermore, various authors have focused their attention to the goal of providing coaches and swimmers with real-time feedback (Bächlin et al., 2009; Bächlin and Tröster, 2009, 2012; Le Sage et al., 2010b) about the swimmer's velocity, attitude and position with respect to the length of the swimming pool (Le Sage et al., 2010a).

2.3.2.2 Sensor specification and sealing

The most used sealing techniques for waterproofing found were hermetic sealing (Callaway et al., 2009), rubber latex skin (Pansiot et al., 2010) or aluminum alloy cylinder (Ohgi, 2002). Commercial systems often use IMMU inserted into a waterproof case (Dadashi et al., 2012; Fulton et al., 2011; Fulton et al., 2009a). Regarding data logging, storage and transmission, the majority of authors used flash memory and SD cards with a storage capacity ranging from128Mb to 1Gb (Ohgi, 2002; Stamm et al., 2011), reporting also acquisition duration up to 200 h, depending on the sampling frequency (James et al., 2011).

2.3.2.3 Sensor Attachment Location

The most popular sensor placements for swimming motion monitoring include the lower and upper back, head, wrist, and ankle. Pansiot et al. (2010) described the features that can be calculated from the sensor output depending on its placement for the four main swimming strokes (front crawl, backstroke, breaststroke, and butterfly) as synthetized in Table 2.

2.3.2.4 Experimental Designs

Most of the reviewed studies focused on experimental trials on trained or elite level swimmers, while Fulton and co-workers included in their experiments a group of paralympic athletes (Fulton et al., 2011; Fulton et al., 2009a, b). In several studies, the feasibility of using IMMUs for performance monitoring was tested using only one subject (Hagem et al., 2013; James et al., 2011; Le Sage et al., 2010a; Le Sage et al., 2011). Several authors aimed at describing the development of a swimmer-worn, wireless device capable of capturing real time acceleration data during the different phases of a swimming trial, i.e. the start, stroke phase, and turns (Slawson et al., 2011; Slawson et al., 2008). Only a few studies (Dadashi et al., 2012; Stamm et al., 2013; Stamm et al., 2011) utilized suitable experimental protocols; they evaluated a set of parameters that support the in-field application of the IMMU.

Table 2.1: List of the selected articles

Source	Type and Specification of sensors								Body Area	Stroke Type	Variables
	Units	Acc	Gyro	Mag	Sizes	Weight	Sample Frequency	Sealing			
Bächlin, M. and Tröster, G. (2012)	4	3-axial accelerometer 1GB of storage (flash memory)			36x42x12mm	34g	256Hz	Water-tightness: plastic foil. Wrist: inside a transparent plastic tube fixed using velcro fasteners.	Upper back Lower back Right wrist	Front crawl	Start (wall-push-off) Strokes End (wall-strike) Average velocity Time per stroke (TPS) Distance per stroke (DPS)
Chakravorti, N.*, et al.* (2013)	1	3-axial accelerometer			Not described				Lower back	All four stroke types	Stroke counts Stroke rates Lap counts
Dadashi, F., Aminian, K. and Millet, G.P. (2013)	1	3D accelerometer ± 11G 3D gyroscope ± 900°/s			Physilog®, BioAGM, CH		500Hz	Physilog®, BioAGM, CH	Lower back (sacrum)	Front crawl	Swimming velocity
Dadashi, F.*, et al.* (2012)	1	3D accelerometer ± 11G 3D gyroscope ± 900°/s			Physilog®, BioAGM, CH		500Hz	Physilog®, BioAGM, CH	Lower back (sacrum)	Front crawl	Instantaneous velocity
Dadashi, F.*, et al.* (2013)	3	3D accelerometer (± 10G) 3D gyroscope (± 1200°/s)			Physilog®, BioAGM, CH		500Hz	Hermetical sealing with plastic bags	Both forearms Lower back (sacrum)	Front crawl	Stroke phases Inter-arm coordination
Davey, N.P., Anderson, M. and James, D.A. (2008)	1	3D accelerometer			Cited: James DA, Davey N and Rice T. (2004).				Lower back (sacrum)	All four stroke types	Push-off Stroke type Stroke count metrics
Fulton, S.K., Pyne, D. and Burkett, B. (2011)	1	3D accelerometer (±2G) 1-D gyroscope (>600°/s) Storage: 256MB			MiniTraquaTM, Version 5				Dominant kicking leg	Flutter kick	Kick rate (kicks per minute)
Fulton, S.K., Pyne, D.B. and Burkett, B. (2009a)	4	3D accelerometer (±2G, Kionix; Model KMXM52, New York, USA); 1-D gyroscope (>600°/s) Storage: 256MB			52x33x11mm	20.7g ($18.9cm^3$)	100Hz	Plastic casing	Both thighs and shanks	Flutter kick	Kick patterns Kick detection

Fulton, S.K., Pyne, D.B. and Burkett, B. (2009b)	1	3D accelerometer (±2G) 1-D gyroscope (>600°/s) Storage: 256MB	Cited: Fulton, S.K., Pyne, D.B. and Burkett, B. (2009a)				Dominant kicking leg	Flutter kick	Kick count Kick rate Kick patterns
Hagem, R.M.*, et al.* (2013)	2	3D Accelerometer (nCore 2.0)	27×19mm	Not described			Both wrists	Front crawl	Total number of strokes Time (s) Stroke length (m/cycle) Stroke rate (s/stroke cycle) Velocity (m/s) Stroke duration Cycle/min
Hou, P. (2012)	2	3D accelerometer (MSR Electronics GmbH) Temperature sensor Humidity sensor Pressure sensor	Not described	18g	From 5Hz to 50Hz	Not described	Both wrists	Front crawl Backstroke Breaststroke	Swimming style recognition Intensity of swimming Number of turns Number of strokes Swimming speed Swim distance Energy expenditure estimation
James, D.A.*, et al.* (2011)	3	3D accelerometer (LIS331DLH, +- 8G) 3D gyroscope (LPR5150AL and LY5150AL, +- 1500°/s) 1GB micro SD card for data storage (up to 200h)	52x33x11mm	Not described	100Hz	In-house custom-built waterproof package	Forearm distal Lower back Lower leg	Front crawl	Arm stroke identification Effect of the kick on arm stroke timing.
Le Sage, T.*, et al.* (2010)	1	3D accelerometer 2D gyroscope	Not described		50Hz	Waterproofed package (AquaPac)	Lower back	All four styles	Real time: stroke rate, stroke duration and lap count
Le Sage, T.*, et al.* (2011)	1	3Daccelerometer (ADXL330) 2D gyroscope (IDG300)	15x9cm	110g	25Hz	Waterproofed package (AquaPac)	Lower back	All four styles	Real time: stroke rate, stroke duration and lap count
Le Sage, T.*, et al.* (2012a)	1	3D accelerometer	Not described					Front crawl	Real time: stroke rate, stroke duration, lap count, starts and turns
Le Sage, T.*, et al.* (2012b)	1	3D accelerometer	Not described				Lower back	Swimming start	Time to key occurrences Kick count Kick rate Stroke count Stroke rate

Lee, J., *et al.* (2012)	1	Cited: Davey et al., 2008				Lower back (sacrum)	Front crawl tumble turn	Different phases of the swimming turn
Lee, J.B., *et al.* (2011)	1	3D accelerometer 3D gyroscope	Not described		200Hz	Not described	Distal forearm	Front crawl swimming simulation on dry land	Arm-stroke phases
Nakashima, M., *et al.* (2010)	1	3 accelerometers (H48D) 3 gyroscopes (XV-3500CB)	Not described		190Hz	Waterproofed housing	Left wrist	Breaststroke Front crawl	Acceleration Angular velocity Wrist's motion reconstruction
Ohgi, Y., *et al.* (2003)	1	2D acceleration sensor ICs (ADXL250 Analog Devices, Inc.) up to 50G	Not described	62g	Not described		Wrist	Breaststroke	Stroke phase discrimination
Ohgi, Y., Ichikawa, H. and Miyaji, C. (2002)	1	Prototype I: 3D acceleration (ADXL210, +-10G), 32Mb internal memory Prototype II: 3D acceleration (ADXL210, +-10G); 3D gyroscope (ENC-03J, +- 1500°/s), 128Mb internal memory	Prototype I: 88x21mm Prototype II: 142x23mm	Prototype I: 50g Prototype II: 78g	128Hz	Capsulated by aluminum alloy cylinder	Wrist	Breaststroke Front crawl	Discrimination of stroke phases Fatigue estimation
Slawson, S.E., *et al.* (2008)	1	3D accelerometer (Freescale Semiconductors)	Not described		100Hz	Not described	Lower back	All four styles	Stroke count Stroke duration
Slawson, S.E., *et al.* (2010)	1	3D accelerometer	Not described		50Hz	Not described	Lower back	Front crawl	Turn phases: approach, rotation and glide
Slawson, S.E., *et al.* (2012)	1	3D accelerometer (Analog Devices, ADXL 330) 2D gyroscope (InvenSense, IDG300)	90x40mm	Not described	Not described		Lower back	Front crawl	Turn phases: approach, rotation and glide
Stamm, A., *et al.* (2011)	1	3D accelerometer (Cited: Davey et al., 2008)	Cited: Davey et al., 2008		100Hz	Not described	Lower back (sacrum)	Front crawl	Acceleration Absolute velocity
Stamm, A., James, D. and Thiel, D. (2013)	1	3D accelerometer (±8G, LIS331DLH 3D gyroscope (1.500°/s, LY5150 ALHTR & LPR5150ALTR) 1 GB micro SD Card	53x33x10mm	20g	100Hz	Waterproof casing	Lower back (sacrum)	Front crawl	Mean velocity Intra-stroke velocity variations Acceleration
Tella, V., *et al.* (2008)	1	Resistive sensor with a coiled cable (ISOcontrol, ATE Micro, Madrid, Spain)	Not described		1 kHz	Not described	Lower back (2nd and 3rd lumbar vertebrae)	Front crawl	Mean velocity Stroke frequency Stroke length Index of coordination

2.3.2.5 Swimming performance assessment and monitoring applications

The use of this technology in real-world performance assessment is still in its initial stages. Studies have shown the suitability of acceleration signals in providing useful timing information in the pool during training sessions (Daukantas et al., 2008; Ichikawa et al., 2003; Slawson et al., 2008). As additional biomechanical measures are introduced and validated using criterion measurement systems (e.g. video analysis and force sensors) and user-friendly interfaces are designed (Khoo et al., 2009), the acceptability of IMMU-based monitoring systems (Le Sage et al., 2012; Mullane et al., 2011) is expected to rapidly increase, meeting the expectations of both coaches and athletes.

The sensor fusion approach aims to combine the newer IMMU technology with the traditional video capture to exploit the advantages of both the systems (Lee et al., 2012; Stamm et al., 2011). Similar conceptual approaches of sensor fusion are progressively being used in different application of IMMU in several sports disciplines wherein the accurate orientation of the whole body or of single body segments can give important information for performance enhancement.

The body segments orientation represents one of the main critical point that calls for further studies in many IMMU applications in sports and specifically in swimming research. IMMU-based algorithms (e.g. Kalman or complementary filters) for estimating 3D body orientation are rarely used, while standardized approaches or commercial built-in algorithms don't fit well in all the practical situations. This issue will be further explored in the next chapters of this thesis.

Table 2.2: List of features from each sensor placement

Stroke	Feature	Head	Trunk	Arms	Leg
All	*Lap count & timing*	++	++	++	++
All	*Overall momentum*	++	++	-	-
FC	*Stroke count*	+	+	++	-
BaS	*Stroke count*	-	-	++	-
BrS, Bf	*Stroke count*	++	++	++	++
FC, BaS	*Body roll*	+	++	-	-
FC	*Breathing patterns*	++	+	-	-
FC, BaS	*Arm anti-symmetry*	-	-	++	-
BrS, Bf	*Arm symmetry*	-	-	++	-
FC, BaS	*Leg anti-symmetry*	-	-	-	++
BrS, Bf	*Leg symmetry*	-	-	-	++

Table reports the variables measured in each swim style according to the sensor placement. FC: front crawl, BrS: breaststroke, BaS: backstroke and Bf: butterfly.

2.4 Conclusion

With the advance of technology, assessing and monitoring swimmers not only in a laboratory setting but also training in the pool has become feasible. Valid kinematic data can be used to analyze movements in order to improve performance and prevent injuries.

The criterion standard in swimming has been the video-based methods using marker or markerless approaches. Both of these methods are accurate in providing kinematic data representative of the underwater motion, but they rely on a complex set-up and long post-processing time, making rapid field applications impossible. While efforts have been made to simplify and speed the set-up, the possibility of immediate feedback to coaches, athletes and biomechanists through video analysis has not been achieved. On the other hand, inertial and magnetic measurements units have gained great interest because they are light, user friendly, swimmer-centric, relatively cheap, and easily waterproofed. With the recent innovations of microelectronics, these IMMUs had presented good accuracy in measuring a wide array of biomechanical parameters and providing outputs very quickly. Due to the advantages of IMMU, the next chapters will focus in describing and evaluating a protocol to measure the 3D joint kinematic of upper limbs during swimming with IMMU.

CHAPTER 3

METHODS

3 Methods

This chapter describes the procedures developed during the thesis. It was divided into five main parts that describe: 1) the instruments and their accuracy; 2) the algorithm used for estimating the body segments orientation, 3) the protocol implemented to estimate the 3D joint kinematics of the upper limbs; 4) the data collected in laboratory and swimming pool; and 5) the statistical analyses.

3.1 Instruments

3.1.1 Inertial and Magnetic Measurement Units

Inertial and Magnetic Measurement Units (IMMU) are micro-electronic devices comprised of an accelerometer, a gyroscope and a magnetometer, developed to measure the tri-axial linear acceleration, the tri-axial angular velocity and the tri-axial components of the earth's magnetic field, respectively (Begg, 2006; Callaway et al., 2009). Further information on working and accuracy of the IMMU were described in the appendix I of this thesis.

There are many commercially available IMMU designed to perform 3D human kinematics measurements (Xsens, The Netherlands; APDM, U.S.A.; Intersense, U.S.A.; Trivisio, Germany; STT, Spain) and many others, but few commercial systems were built specifically to support measurement in the aquatic environment, e.g. MiniTraquaTM used by Fulton et al. (2011) and Physilog used by Dadashi et al. (2012). Therefore, some researchers have focused their efforts on designing IMMU devices suitable to swimming. In this section will be presented the IMMU chosen to acquire the linear acceleration and the angular velocity of the upper body segments and the local magnetic field during movements.

3.1.2 Device One

The first attempt was to develop two prototypes particularly adapted to perform underwater measurements (Figure 3.1) in partnership with the Micrel Lab of the University of Bologna. The prototypes were mini-sensors (44mm long x 24mm high x 10mm wide) composed of tri-axial accelerometers (±8g, 300Hz), tri-axial gyroscopes (±2000°/sec, 300Hz) and tri-axial magnetometers (±1000μT, 80Hz). In order to assess the viability of the prototypes for use in swimming, several tests were performed.

For the accelerometer, a static calibration method was implemented in MATLAB (version 2009b) according to the guidelines of the manufacturer. The prototypes were placed on a table aligned with the horizontal plane using a bubble inclinometer and held in a static position. For each of the six positions described in the calibration data sheet (i.e. axes Z, Y, X aligned with + or - g),

two 40-seconds static trials were performed. For each trial, the first 3s and the last 3s were discarded to eliminate incorrect values due to pressing the start/stop button. For the gyroscope, the offset for the axes X, Y, Z was calculated as the mean value of the twelve trials.

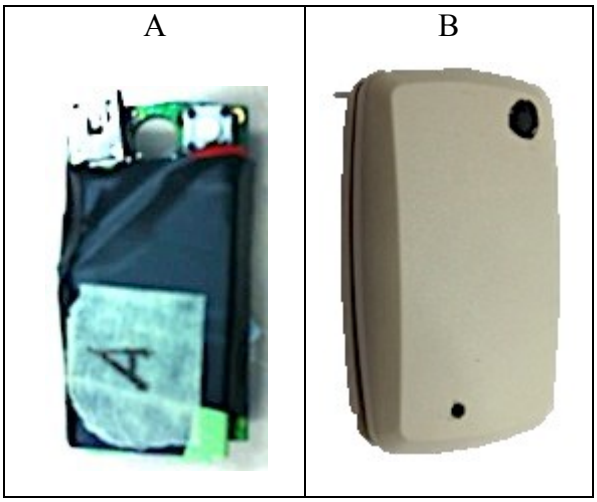

Figure 3.1: Prototypes uncovered (A) and covered (B).

After the calibration, the values were very close to zero indicating that the gyroscope offset was removed with reasonable accuracy. For the accelerometers, the calibration matrix described in the calibration data sheet was used to obtain the calibrated data from twelve trials. In absence of any error and noise, the values should be 0 m/s^2 for both the horizontal axis, and + or - 9.81 m/s^2 for the vertical axis aligned with gravity. The prototype estimated acceleration due to gravity to be 9.79 ± 0.22 m/s^2, ranging from 9.40 m/s^2 to 10.11 m/s^2. The average standard deviation of the three axes was 0.21 m/s^2. For the horizontal axis, the accelerometer values demonstrated an uncompensated cross talk. Probably this problem was related to the unstable fixation of the prototype to the external case during data acquisition.

This test demonstrated that the sensors of the prototypes seem to provide suitable measurements of linear accelerations in the static condition. However, during almost a year of testing, the prototypes continued to present numerous technical limitations, like: 1) no wireless synchronization between prototypes, and between the prototypes and the workstation; 2) low overall reliability; 3) short battery life limited to about two hours of acquisition; 4) low internal storage, limited to a 1 Gb; 5) no waterproofed housing provided; 6) no real-time monitoring; and 7) no dedicated software for data management. Subsequent prototypes could be developed to overcome these limitations, but the time necessary for developing and testing was too much for this research. Consequently, this system was considered unsuitable and thus was abandoned for the purposes of this study.

3.1.3 Device Two

In order to overcome the limitations of system one mentioned, 7 commercial IMMU devices were acquired (ADPM Movement Monitoring Solutions, model Opal, U.S.A.). The advantages of this system are: 1) wireless synchronization among the monitors (up to 24 monitors), and between each monitor and the access point; 2) good overall reliability; 3) battery life of over 16 hours with continuous monitoring and more than 8 hours while real-time streaming; 4) large internal storage (8 Gb); 5) easy to waterproof, 6) continuously stream data for real-time processing, then working as an instantaneous biofeedback; and 7) the software development kit supports the software used for the analysis (MATLAB, U.S.A.).

These IMMU were miniature (48.4mm long x 36.5mm high x 13.4mm wide), low power, and wireless (Figure 3.2). These monitors are composed of sensors for measuring the linear acceleration, the angular velocity, the magnetic field and the internal temperature, as presented in Table 3.1. Values lower than 6g and 2000deg/s of acceleration and angular velocity respectively, were expected in swimming. The frequency of 100Hz is the one of the most frequently used in studies with IMMU in swimming as reported by Magalhães et al. (In review), so an output rate of up to 128Hz is consistent with the literature. A major feature of this system is the possibility to keep the same output rate (i.e. 128Hz) up to 24 monitors during tests, unlike other commercially available systems. Generally, in those commercial systems the sample frequency is inversely proportional to the number of monitors, i.e. the output rate decreased while the number of monitor increased.

Figure 3.2: Monitor with body strap

Regarding to the hardware characteristics of the monitors, they had small dimensions, low weight (< 22g), high internal storage and long battery life. Together with the monitor, the company provided body straps to fix the monitors onto body segments (Figure 3.2). Therefore, with this

configuration it is possible to monitor the human movements naturally. The wireless radio is ultra-low power, with a frequency band of 2.40 – 2.48GHz ISM band, 2 Mbps on-air data-rate, latency of 30ms and 300ms with and without data buffer respectively, 30m line of sight and 10m indoors transmission range, about 720h of data buffer, and synchronization with a difference less than 1ms for up to 24 monitors. (Further information can be found at http://apdm.com/Wearable-Sensors/Opal, retrieved at 12/20/2013).

With the aim of verifying the precision of the sensors in measuring the linear acceleration, the angular velocity and the magnetic field, several trials were run together with another commercial IMMU (Xsens Motion Technologies, model MTx, The Netherlands), the most used for performing human motion analysis (Cutti et al., 2008; Ferrari et al., 2010b; Saber-Sheikh et al., 2010; Zhou and Hu, 2005). Three axes-aligned monitors of each type were fixed on each side of a wooden plate (width 8cm x length 15cm x depth 1cm), as shown in Figure 3.3.

Table 3.1: APDM Opal characteristics

	Accelerometer	***Gyroscope***	***Magnetometer***
Axes	3 axes	3 axes	3 axes
Range	± 2g or ± 6g	± 2000 deg/s	± 6 Gauss
Noise	0.0012 m/s²/√Hz	0.05 deg/s/√Hz	0.5 mGauss/√Hz
Sample Rate	1280 Hz	1280 Hz	1280 Hz
Output Rate[1]	20 to 128 Hz	20 to 128 Hz	20 to 128 Hz
Bandwidth	50 Hz	50 Hz	50 Hz
Resolution	14 bits	14 bits	14 bits

Twelve trials of rotations around the axes X, Y and Z, and free random movements were performed. A tester manually executed three trials for each axis, with each trial lasting about 1 min. The raw signals of both systems were compared by means of root mean square error (RMSE) and the agreement between systems tested with Pearson product-moment correlation coefficients (R). The output values of all sensors were averaged and presented in Table 3.2. There were low values of differences (< 1.2°) and high agreement ($r > 0.95$) between both systems. These results indicate that there was no significant difference between the systems in measuring raw signals. Figure 3.4 shows an example of plots across time of one trial during rotations around x-axis. Hence, it can be concluded that the two systems were similar in measuring linear acceleration, angular velocity and magnetic field in this test.

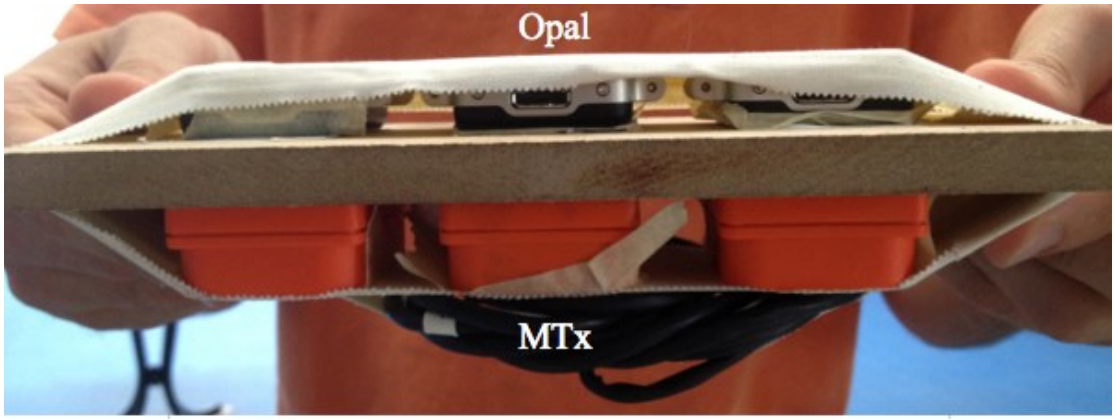

Figure 3.3: Monitors fixed on a wooden plate.

The reference system (Xsens) has been widely used for industrial applications, entertainment and movement science. Several studies have used this system to track human motion due its good performance (Berthouze and Mayston, 2011; Cutti et al., 2008; Ferrari et al., 2010b; Saber-Sheikh et al., 2010; Schepers et al., 2010). The model used in the present study (MTx) was similar to the system employed by Cutti et al. (2008) and Ferrari et al. (2010b). The monitors of which are attached to a portable device (named Xbus) through cables, and the Xbus transmit then the data wirelessly to the workstation. Due to the many cables fixed to the body together with the Xbus, this system may limit the natural movement assessment. Conversely, the Xsens also offers a model with similar features of the Opal (i.e. model MTw; further information at http://www.xsens.com/en/general/mtw, retrieved at 12/20/2013). However, the MTw system had 2 major limitations: 1) It did not have any internal memory (except a little buffer of a few seconds), thus data storage is through wireless connection, and 2) the wireless update rate decrease when monitors were added to the system. For example, 1 monitor works at 120Hz, 12 monitors at 50Hz and 32 monitors at 20Hz only. Considering that the wireless transmission does not work underwater and that the sampling frequency for the system could be set to a higher value, the Opal were used in this study.

Table 3.2: Comparing the two IMMU systems

	Accelerometer		**Gyroscope**		**Magnetometer**	
	RMSD (m/s^2)	**R**	**RMSD (°/s)**	**R**	**RMSD (G)**	**R**
Mean (min – max)	1.20 (0.49 – 3.39)	0.95 (0.75 - 1)	0.17 (0.05 - 0.83)	0.99 (0.85 - 1)	0.09 (0.01 - 0.13)	0.99 (0.96 - 1)

Table reports the mean of 12 trials. RMSD: Root Mean Square Difference. R: Pearson product-moment correlation coefficient.

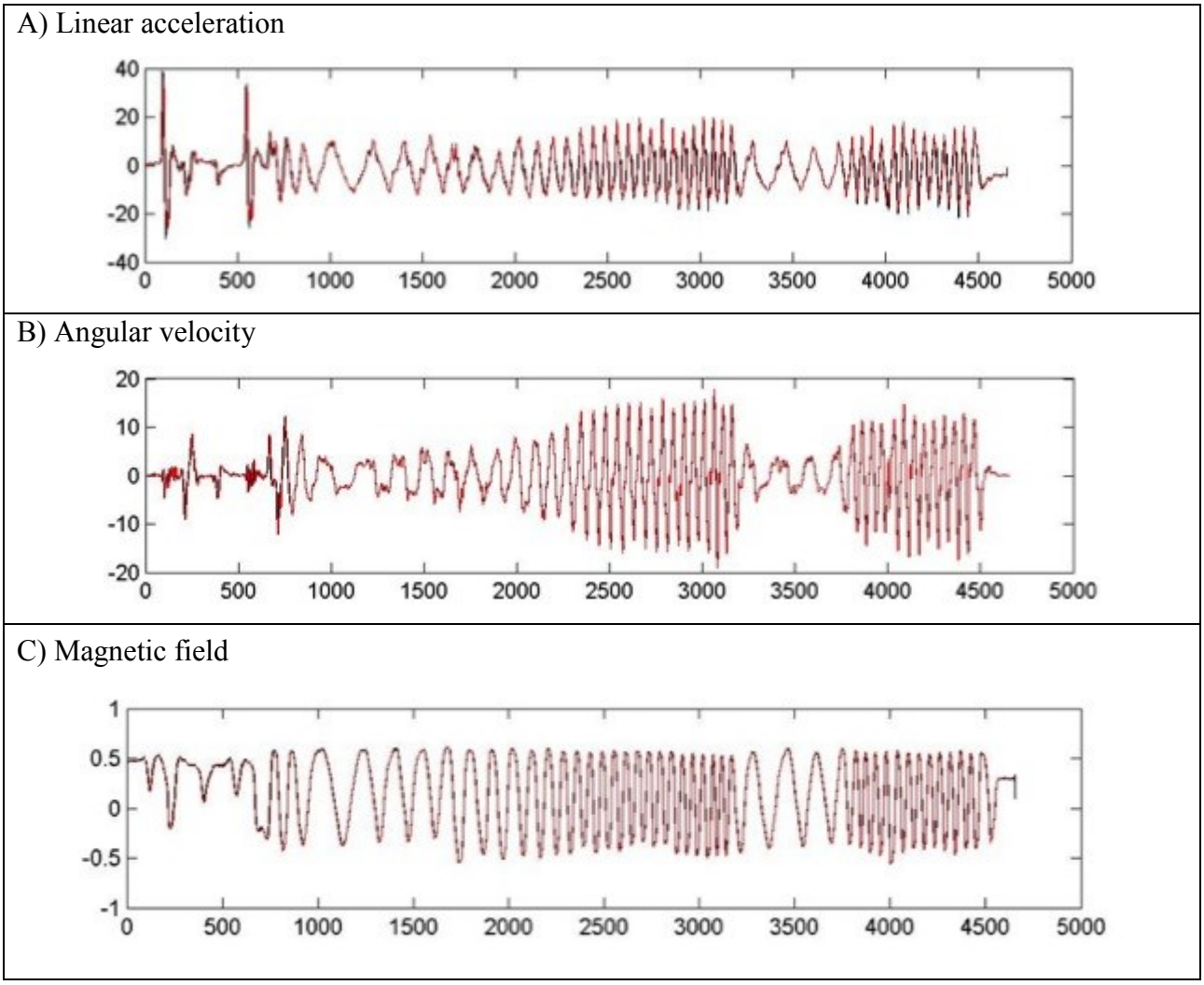

Figure 3.4: Comparison between the two IMMU Systems.
Linear acceleration (m/s^2), angular velocity (deg/s) and magnetic field (G) of one rotation trial. Values plotted along time (in frames). Black lines for the Opal and red lines for the MTx.

3.1.4 Stereo-Photogrammetric System

Human motion analysis has been performed chiefly through video analysis, as discussed in Chapter 2. Among all video systems available on the market, stereo-photogrammetry was chosen to be the criterion standard system during the simulated swimming in the laboratory. Several investigations have performed human kinematic analysis through a stereo-photogrammetric system (SPS) due to its high accuracy to measure the markers position in the calibrated space (Cutti et al., 2008; Ferrari et al., 2010b).

The system used in this study (Smart-DX 7000, BTS Bioengineering, Italy) is a high definition system (up to 4 Megapixels) supported up to 16 video cameras (Figure 3.5) with high frequency of acquisition (up to 2000Hz). The accompanying workstation came with managing software (BTS SMART-suite, Italy) including one for capture, one for tracking, and one for analysis, and also a MATLAB toolbox. After constructing a model in the software (SMART-Tracker, Italy), the retro-reflective passive markers can be automatically identified during the motor tasks. Further information can be found at http://www.btsbioengineering.com/products/kinematics/bts-smart-dx, retrieved at 12/20/2013.

The calibration set was composed of one stick (named wand) made of carbon fiber with 3 markers, and 2 other axes also made of carbon fiber with either 2 or 4 markers. To accomplish the 3D motion analysis, static and functional calibrations were done before the data acquisition. For the static calibration, a 5-second trial was acquired with the three sticks placed on the ground as shown in Figure 3.6. This procedure was to define the axes of the global system of reference (SOR). For the functional calibration, a 90-second trial was done by moving the wand randomly within the volume of calibration. At the end of both calibrations, the software (SMART-Capture, Italy) reported the mean errors for the reconstruction of the wand (3D in millimeters and 2D in pixels). For the set-up used in the laboratory, the overall accuracy for the wand's markers reconstruction was of 0.2 (±0.2) mm on a volume calibrated of about 5m (length) x 4.50m (height) x 2.50m (width).

Figure 3.5: SMART DX video cameras.

Figure 3.6: Calibration set.

3.2 Orientation Estimation Algorithm

Estimates of the 3D orientation of a rigid body by IMMU can be computed by integrating the signals from a tri-axial gyroscope over time. Unfortunately, due to the low-frequency gyro bias drifts, errors of measurement may grow unlimitedly over time, thus strongly limiting the direct application of the signal integration for this purpose. Nevertheless, gyros help achieving accurate orientation estimates for highly dynamic motions (Sabatini, 2011).

A tri-axial accelerometer is capable of providing drift-free inclination estimates by sensing the gravity vector, in static conditions. However, in dynamic conditions, it is not able to give accurate inclination estimates because the overall measured acceleration sensed is a combination of both the dynamic acceleration and the gravity acceleration. Therefore, sensor fusion between tri-axial gyro's, accelerometer's and magnetometer's signals should aid in a more accurately estimation of the 3D orientation through the IMMU (Daukantas et al., 2008).

Serious limitations affect sensor fusion. First, while moving, it is difficult to interpret the acceleration signals of an object in motion due to the gravity field (vertical reference). Hence, the vertical reference is reliable only for static or slowly moving objects (Veltink et al., 1996). Second, nearby ferromagnetic materials are disturbing to the magnetometers, and this problem becomes especially critical within indoor environments (Bachmann et al., 2004; De Vries et al., 2009), making difficult the correct use of the magnetometers' signals as a horizontal reference (heading) in laboratory/ambulatory settings. Regardless, sensor fusion is still the best technique when the aim is minimizing the gyro bias drift errors.

Ideally, an orientation filter should be capable of dealing with the gyro biases by overcoming the limitations regarding both acceleration and magnetic sensors. The task of an orientation filter is

to compute a single estimate of orientation through the optimal fusion of gyroscope, accelerometer, and magnetometer measurements. The filter proposed by Rudolph E. Kalman (1960) has become the accepted basis for the majority of orientation filter algorithms (Cooper et al., 2009; El-Gohary and McNames, 2011; Favre et al., 2007; Ferrari et al., 2010b; Ji-Hwan et al., 2009; Le Sage et al., 2010) that have been used in most of the commercial inertial sensors, as the one presented in the section 3.1.1.2. The widespread use of Kalman-based filters is an evidence of their accuracy and effectiveness.

The IMMU used in the present study came with software for data acquisition and managing (Motion Studio, U.S.A.) that outputs orientation data in the form of quaternions, which are easily converted in Euler angles. The IMMU's algorithm has been designed to estimate the 3D human motion orientation in general. Seeking for a solution adaptable to the sport context, the open source Kalman-based algorithm developed by Madgwick et al. (2011) was found in the literature. The innovative aspects of the this filter include: a low computational load; a single adjustable parameter defined by observable systems characteristics (named β); an analytically derived and optimized gradient descent algorithm enabling performance at low sampling rates; an on-line magnetic distortion compensation algorithm; and gyroscope bias drift compensation. The implications of the low computational load and ability to operate at low sampling rates as well significantly reduces the hardware and power necessary for wearable inertial movement tracking, enabling the creation of systems lightweight and inexpensive capable of functioning for extended periods of time. The diagram block representation of how it works is presented in Figure 3.7. The accelerometer's signals and the magnetometer's signals are combined to generate the settable value gain (β) that determines how much of this combination is desirable to compensate the gyro biases.

3.2.1 Beta Optimization Algorithm

With the intention of better dealing with the values of β, two procedures were executed. The β was tuned to find the best correspondence of the kinematic data estimated using the IMMU with respect to the criterion standard, which are the values estimated using the stereo-photogrammetric system. The relative kinematic orientation of the actual frame with respect to the first frame was computed and compared between the IMMU system and the criterion standard using the RMSE. The relative orientation was computed using the eta value of the quaternion representation.

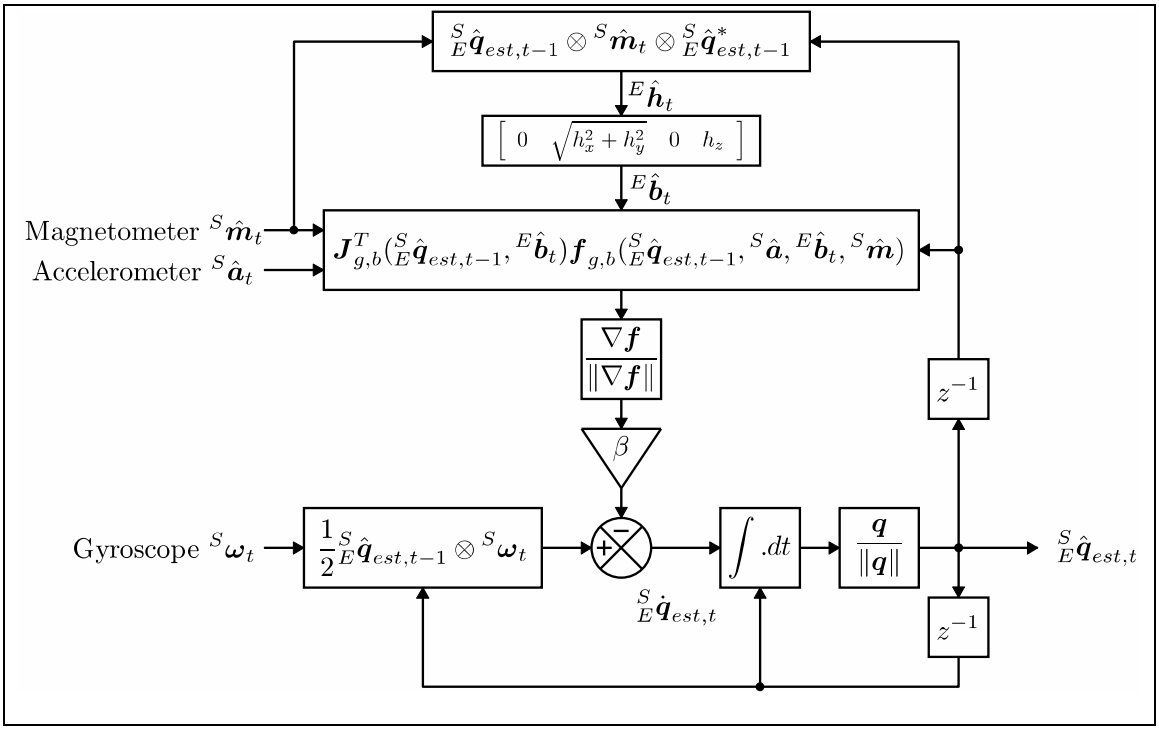

Figure 3.7: Block diagram representation of the orientation estimation algorithm. m: normalized magnetometer measurement , a: normalized accelerometer measurement, ω: angular rate (rad.s^{-1}), q: quaternion derivative describing rate of change of the earth frame relative to the sensor frame, *f*: objective function, J: Jacobean, d: measured field in the sensor frame, t: time. Source: Madgwick et al. (2011).

The first procedure was to achieve an optimal value of β considering all trials together (labeled KMA) by maximizing the correlation between the orientations estimated using the two instruments. In sequence, a second procedure was performed differentiating the optimization value patterns. Different criteria were for the dynamic (front crawl and breaststroke) and for the calibration trials. In both cases, the RMSE was averaged among the trials for all the monitors/clusters. The first 8s were always discarded in order to eliminate the initial transient of the Kalman filter.

A first exploration of β was performed from a minimum of 0.5 to a maximum of 10 with a step of 0.5 to find the better correspondence with the criterion standard (minimum average RMSE for all sensors). Then, iteratively, the exploration was refined with a halved step around the optimal value found in the previous phase. The iteration ended when the RMSE reached a mean value less than 2.5° or when the maximum number of iterations fixed by the user (7) was reached.

3.3 Protocol

A motion analysis protocol is a procedure that accurately describes how to measure the kinematics/kinetics parameters required to test the hypotheses underlying one or more research questions. According to Kontaxis et al. (2009), a protocol must address this aim by describing: 1) which joints and segments are of interest; 2) which mechanical model is assumed to represent these

joints or segments; 3) the definition of the embedded coordinate systems and of the joint angles; 4) the markers and or IMMUs placement on the human body; 5) the number of tasks to be measured, and 6) possible kinematic refinements.

Two different approaches are commonly used: A) anatomical axes are defined using information on anatomical landmarks; or B) anatomical axes are defined estimating the functional axes of rotation of the joints. Unfortunately, at the current state of the art, IMMU cannot allow an estimation of the position of anatomical landmarks accurately enough for the purposes of human motion analysis. However, Picerno et al. (2008) described an IMMU-based protocol wherein the position of anatomical landmarks that defined an axis of rotation was used in the calibration phase by means of a specifically designed device. Since this approach is time consuming, it was considered not very suitable for application in the sport context.

Therefore, the protocol described by Cutti et al. (2008) that benefits of the approach B was chosen for the main following reasons:

1) It was specifically designed for implementation with IMMU;
2) It was suitable and as accurate as a SPS for the estimation of the 3D joint angles kinematics of the upper limb (shoulder, scapula, elbow) in a clinical context;
3) It could be adapted for the use of different IMMU systems (that are) able to compute the orientation of the IMMUs with respect to a fixed global system of reference;
4) It could be adapted for the use in sports context.

However, Cutti et al.'s protocol did not model the wrist joint, one of major interest for swimming kinematic analysis. Thus, the mechanical model and definition of the wrist joint and of the hand segment are hereinafter introduced. In contrast, the scapular-thoracic joint, included in the Cutti et al.'s protocol, was not considered because the IMMU were not easily fixed on the scapula, thus giving measurement artifacts. When a specific waterproofed swimsuit with dedicated pockets for the IMMUs is developed, the scapular-thoracic joint also will be analyzed.

3.3.1 Protocol Description

3.3.2 Joints and Segments

The joints considered in the protocol were the shoulder, elbow and wrist. Since each joint is supposed to be constituted by adjacent segments, thorax, left and right upper-arms, left and right forearm, and left and right hands were considered the rigid segments for the model.

From a biomechanical point of view, each side was modeled as an open kinematic chain constituted by thorax, upper-arm, forearm and hand. Similarly to the representation described by Cutti et al. (2008), the shoulder was considered as the ball-and-socket joint between thorax and arm,

whereas the elbow was considered as the double-hinge joint (with non-intersecting axes) between arm and forearm. Similarly to the elbow, the newly introduced wrist joint was modeled as the double-hinge joint formed by forearm and hand. Specifically, the shoulder joint kinematics were described by 3 degrees of freedom (flexion-extension, abduction-adduction, and internal-external rotation), while the elbow joint kinematics were described by 2 degrees of freedom (flexion-extension and pronation-supination), and a constant, subject-specific parameter: the carrying angle. The wrist joint kinematics, as well as that of the elbow, were described by 2 degrees of freedom (flexion-extension and radial-ulnar deviation) and a further parameter (not considered in the further analyses) that would correspond to the internal-external rotation; however, this is physiologically constrained.

3.3.3 Anatomical System of Reference Definition

According to Kontaxis et al. (2009), for each segment that formed 2 joints, both a proximal and a distal embedded anatomical systems of reference (ASOR) were defined. Thus, only the thorax and the hand were represented by only one ASOR. Wherever possible, ASOR definitions adopted in this study were introduced by Cutti et al. (2008).

The ASOR of the thorax (THX) requires a static calibration trial of 10 seconds for computation. Since the IMMU's orientation estimation was more reliable when the subject is lying still (IMMU z axis pointing up[1]), the definition of the thorax ASOR given by Cutti et al. (2008), who assumed the subject being standing, needed to be changed. However, the International Society of Biomechanics and the International Shoulder Group recommendations were followed (Wu et al., 2005). The Z axis was defined as opposed to gravity, the X axis was orthogonal to the Z axis, and the X axis of the IMMU was pointing toward the right side of the subject, and the Y axis orthogonal to the X and Z axes, pointing cranially.

The ASORs of proximal and distal humerus were assumed as the same as those of Cutti et al. (2008). Thus, both the proximal humerus ASOR (H1) and the distal humerus ASOR (HF1[2]) of Cutti et al. (2008) were replicated. The H1 ASOR was assumed aligned with the thorax ASOR during the static calibration trial, whereas the HF1 ASOR was computed estimating the flexion-extension axis of rotation of the elbow, that required the subject to perform a pure elbow flexion-extension trial. For HF1, the X axis was defined in the direction of that estimated axis of rotation,

[1] For the definition of the ASORs, data relative to the orientation of the technical system of reference of the IMMU have to be used. For that reason, the IMMU must be fixed on the body in a standardized way, which will be described in details in the section 3.3.1.3.

[2] The HF1 is referred by Cutti's protocol as HD. However, the convention HF1 was adopted to underline the fact that is computed using a functional approach.

pointing laterally, the Z axis orthogonal to that X axis and the Y axis of H1, pointing posteriorly, the Y axis orthogonal to the X and the Z axis, pointing cranially.

The forearm (F) ASOR defined by Cutti et al. (2008) was used with a little modification for the proximal forearm (PF), and "as it was" for the distal forearm (DF). More in detail, the DF ASOR was computed by estimating the elbow pronation-supination axis of rotation, which required the subject to perform a pure elbow pronation-supination. In agreement with Cutti et al. (2008), for DF the Y axis was defined in the direction of this estimated axis of rotation, pointing to the elbow, the X axis orthogonal to that Y axis and the Z axis of the IMMU, pointing laterally, the Z axis orthogonal to the X and the Y axis, pointing away from the wrist. This definition of the forearm ASOR considers the elbow joint completely supinated when the subject assumes the anatomical position. Unfortunately, since in swimming the elbow is almost completely pronated in many phases of arm stroke, that definition led to possible gimbal locks or numeric singularity problems when computing the elbow joint angles. In order to avoid these problems and to have a better representation of the kinematics of the swimming, the PF ASOR was computed as the DF ASOR but rotated -90° along the Y axis. With that definition, 90° of pronation using the DF equals 0° when using the new PF ASOR.

The hand (HND) ASOR definition was introduced to allow the estimation of the wrist joint angles. Following the approach used to compute the humerus H1 ASOR from the thorax ASOR, the hand ASOR was assumed to align with the distal forearm ASOR, during the static calibration trial. From a theoretical and mechanical point of view, the estimation of the wrist flexion-extension axis of rotation should give a more correct and accurate representation of this double hinge joint. As a consequence of that, it would have been more appropriate to use a definition of both the distal forearm and the hand ASORs that included the estimated axis of rotation. Unfortunately, the limited joint range of motion and the difficulties of a subject to perform a pure wrist flexion-extension keeping a constant radial-ulnar deviation, might lead to increased errors and an overall low accuracy. For that reason and for the definition of the distal forearm and hand ASOR, the approach used by Cutti et al. (2008) for the elbow joint was followed.

All the definitions given in this section were intended for the right side only. However, a technical summary of the definition of all the ASORs of the protocol is reported both for the right and the left side in Table 3.3. Further details on positioning the IMMU on the body segments and the calibration trials required for computing the ASORs will be described in the following sections.

3.3.4 Inertial and Magnetic Measurement Units Positioning on Body Segments

The definition of the ASORs illustrated in Table 3.3, requires a specific positioning of the IMMU on human body segments. IMMU can be fixed using hypoallergenic double-sided tape directly on the skin. With reference to Figure 3.8, the IMMU on the thorax has to be fixed by aligning the X-axis to the longitudinal axis of the flat portion of the sternum, since the X-axis orientation of the IMMU is directly used for the computation of the thorax ASOR. This positioning is recommended when the static calibration is performed with the subject lying down. On the contrary, if the static calibration is performed with the subject standing, it is advisable to follow the indications described by Cutti et al. (2008), and to define the thorax ASOR accordingly. The IMMU on the humerus can be fixed laterally to allow the swimmer both a natural "swim style" and to maximally reduce the soft tissue artifacts. The suggested position is "over the central third of the humerus, slightly posterior" (Cutti et al., 2008).

As described by Cutti et al. (2008), the IMMU on the forearm has to be fixed over the "distal flat surface of radius and ulna, with the IMMU Z axis pointing away from the wrist." The IMMU on the hand was fixed over its dorsum, with the IMMU Z axis pointing away from the hand. Since the IMMU is not much smaller than the dorsum of a hand, it is advisable to ask the subject for a positioning that should not be annoying or limit the wrist range of motion.

It should be noticed that the Opals are not waterproofed. As a consequence, if the data acquisition is to be performed in the swimming pool, they necessarily must be waterproofed before positioning them on the body segments.

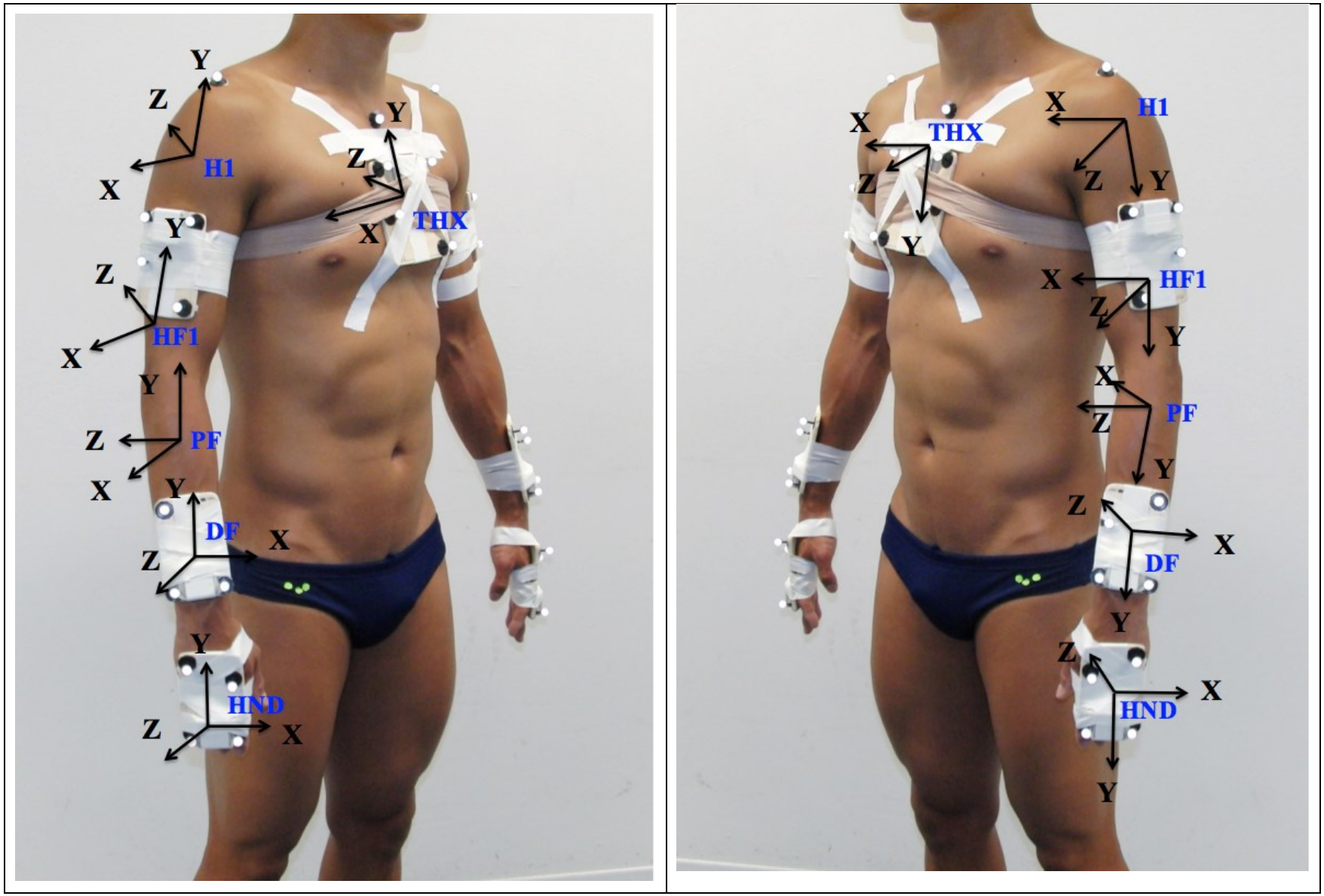

Figure 3.8: Inertial and magnetic measurement units positioning.
THX: thorax. H1: proximal humerus. HF1: distal humerus. PF: proximal forearm. DF: distal forearm. HND: hand.

Table 3.3: Definition of the anatomical system of reference

Body segment / Rot. matrix	Right side - Axes definition	Direction	Left side - Axes definition	Direction
Thorax - ${}^{THX\text{-}IU}R_{THX}$	${}^{THX\text{-}IU}Z_{THX} = -\,{}^{THX\text{-}IU}Z_{G}$	Posterior	${}^{THX\text{-}IU}Z_{THX} = {}^{THX\text{-}IU}Z_{G}$	Anterior
	${}^{THX\text{-}IU}X_{THX} = {}^{THX\text{-}IU}Z_{THX} \wedge [1\ 0\ 0]$	Right	${}^{THX\text{-}IU}X_{THX} = [1\ 0\ 0] \wedge {}^{THX\text{-}IU}Z_{THX}$	Right
	${}^{THX\text{-}IU}Y_{THX} = {}^{THX\text{-}IU}Z_{THX} \wedge {}^{THX\text{-}IU}X_{THX}$	Cranial	${}^{THX\text{-}IU}Y_{THX} = {}^{THX\text{-}IU}Z_{THX} \wedge {}^{THX\text{-}IU}X_{THX}$	Caudal
Proximal Humerus - ${}^{H\text{-}IU}R_{H1}$	${}^{H\text{-}IU}R_{H1} = {}^{H\text{-}IU}R_{THX}$		${}^{H\text{-}IU}R_{H1} = {}^{H\text{-}IU}R_{THX}$	
Distal Humerus - ${}^{H\text{-}IU}R_{HF1}$	${}^{H\text{-}IU}X_{HF1} = {}^{H\text{-}IU}MHA_{FLEX}$	Right	${}^{H\text{-}IU}X_{HF1} = -\,{}^{H\text{-}IU}MHA_{FLEX}$	Right
	${}^{H\text{-}IU}Z_{HF1} = {}^{H\text{-}IU}X_{HF1} \wedge {}^{H\text{-}IU}Y_{H1}$	Posterior	${}^{H\text{-}IU}Z_{HF1} = {}^{H\text{-}IU}X_{HF1} \wedge {}^{H\text{-}IU}Y_{H1}$	Anterior
	${}^{H\text{-}IU}Y_{HF1} = {}^{H\text{-}IU}Z_{HF1} \wedge {}^{H\text{-}IU}X_{HF1}$	Cranial	${}^{H\text{-}IU}Y_{HF1} = {}^{H\text{-}IU}Z_{HF1} \wedge {}^{H\text{-}IU}X_{HF1}$	Caudal
Proximal Forearm - ${}^{F\text{-}IU}R_{PF}$	${}^{F\text{-}IU}X_{PF} = {}^{F\text{-}IU}Z_{DF}$, ${}^{F\text{-}IU}Y_{PF} = {}^{F\text{-}IU}Y_{DF}$, ${}^{F\text{-}IU}Z_{PF} = -\,{}^{F\text{-}IU}X_{DF}$		${}^{F\text{-}IU}X_{PF} = {}^{F\text{-}IU}Z_{DF}$, ${}^{F\text{-}IU}Y_{PF} = {}^{F\text{-}IU}Y_{DF}$, ${}^{F\text{-}IU}Z_{PF} = -\,{}^{F\text{-}IU}X_{DF}$	
Distal Forearm - ${}^{F\text{-}IU}R_{DF}$	${}^{F\text{-}IU}Y_{DF} = {}^{F\text{-}IU}MHA_{PS}$	Cranial	${}^{F\text{-}IU}Y_{DF} = -\,{}^{F\text{-}IU}MHA_{PS}$	Caudal
	${}^{F\text{-}IU}X_{DF} = {}^{F\text{-}IU}Y_{DF} \wedge [0\ 0\ 1]$	Right	${}^{F\text{-}IU}X_{DF} = [0\ 0\ 1] \wedge {}^{F\text{-}IU}Y_{DF}$	Right
	${}^{F\text{-}IU}Z_{DF} = {}^{F\text{-}IU}X_{DF} \wedge {}^{F\text{-}IU}Y_{DF}$	Posterior	${}^{F\text{-}IU}Z_{DF} = {}^{F\text{-}IU}X_{DF} \wedge {}^{F\text{-}IU}Y_{DF}$	Anterior
Hand - ${}^{HND\text{-}IU}R_{HND}$	${}^{HND\text{-}IU}R_{HND} = {}^{HND\text{-}IU}R_{DF}$		${}^{HND\text{-}IU}R_{HND} = {}^{HND\text{-}IU}R_{DF}$	

${}^{A}X_{B}$ indicates the unit vector X orientation of the system of reference B represented in the system of reference A, whereas ${}^{A\text{-}IU}X_{B}$ indicates the unit vector X orientation of the system of reference B represented in the system of reference of the IMMU fixed in A. ${}^{A}R_{B}$ indicates the rotational matrix that describes the orientation of the system of reference B with respect to the system of reference A. Where "G" is in place of A or B, "G" indicates the global fixed system of reference. ${}^{H\text{-}IU}MHA_{FLEX}$ indicates the estimated flexion-extension axis of rotation of the elbow (unitary), pointing laterally both for the right and the left side. ${}^{H\text{-}IF}MHA_{PS}$ indicates the estimated pronation-supination axis of rotation of the elbow (unitary), pointing towards the elbow both for the right and the left side. Directions of the axes are to be intended when facing a subject standing still.

3.3.5 Inertial and Magnetic Measurement Units Output Data

The target of the overall computation is an accurate measure of the joint angles of the shoulders, elbows, and wrists. The output provided by the IMMUs is also the starting input that can be used for this purpose. Usually an IMMU outputs the orientation of the technical system of reference for each monitor used, with respect to a fixed global system of reference. In addition, raw signals of the accelerometers, gyroscopes and magnetometers can be available. The orientation of each IMMU is commonly provided applying an embedded Kalman Filter, using one of the following mathematical representations: quaternions, matrices of rotations, roll, pitch and yaw angles. The output of the ADPM system was in the form of quaternions that were the starting input of the computation of this protocol. Quaternions were converted in matrices of rotational representations, first. Thus, a matrix of rotation in the form ${}^{G}R_{IU}$ was computed for each IMMU. These matrices were used for the computation as described in the following 2 sections.

3.3.6 Calibration Tasks and Computation of the Anatomical Systems of Reference

The ASORs previously defined are required to perform 3 calibration tasks: 1) static, 2) elbow flexion-extension and 3) elbow prono-supination. Each calibration is needed to compute specific calibration data that is represented in the flow chart below, and will be hereinafter explained. In the static trial, the subject had to lie on a table keeping his arms alongside the body, and at the same time holding the dorsum of the hands aligned to the upper side of the forearms. The subject was asked to hold breath during this 10-second test, as breathing may add measurement noise.

As described in the Table 3.3, the position assumed by the subject during this task allows investigators to:

- Compute the ASOR of the thorax and its relative orientation with respect to the IMMU (${}^{THX\text{-}IU}R_{THX}$);
- Compute the ASOR of the proximal humerus (H1) and its relative orientation with respect to the IMMU (${}^{H\text{-}IU}R_{H1}$). The ASOR of the proximal humerus is intended to be aligned to the ASOR of the thorax;
- Assume that the ASORs of the hands are aligned to those of the distal forearms. As the ASOR of the distal forearm can be defined only after the second and third calibrations, ${}^{G}R_{F\text{-}IU}$, ${}^{G}R_{HND\text{-}IU}$ are just outputs given as input to the third calibration. As a consequence, the correct execution of this task is essential for an accurate estimation of the ASOR of the thorax, the humerus, and the hands.

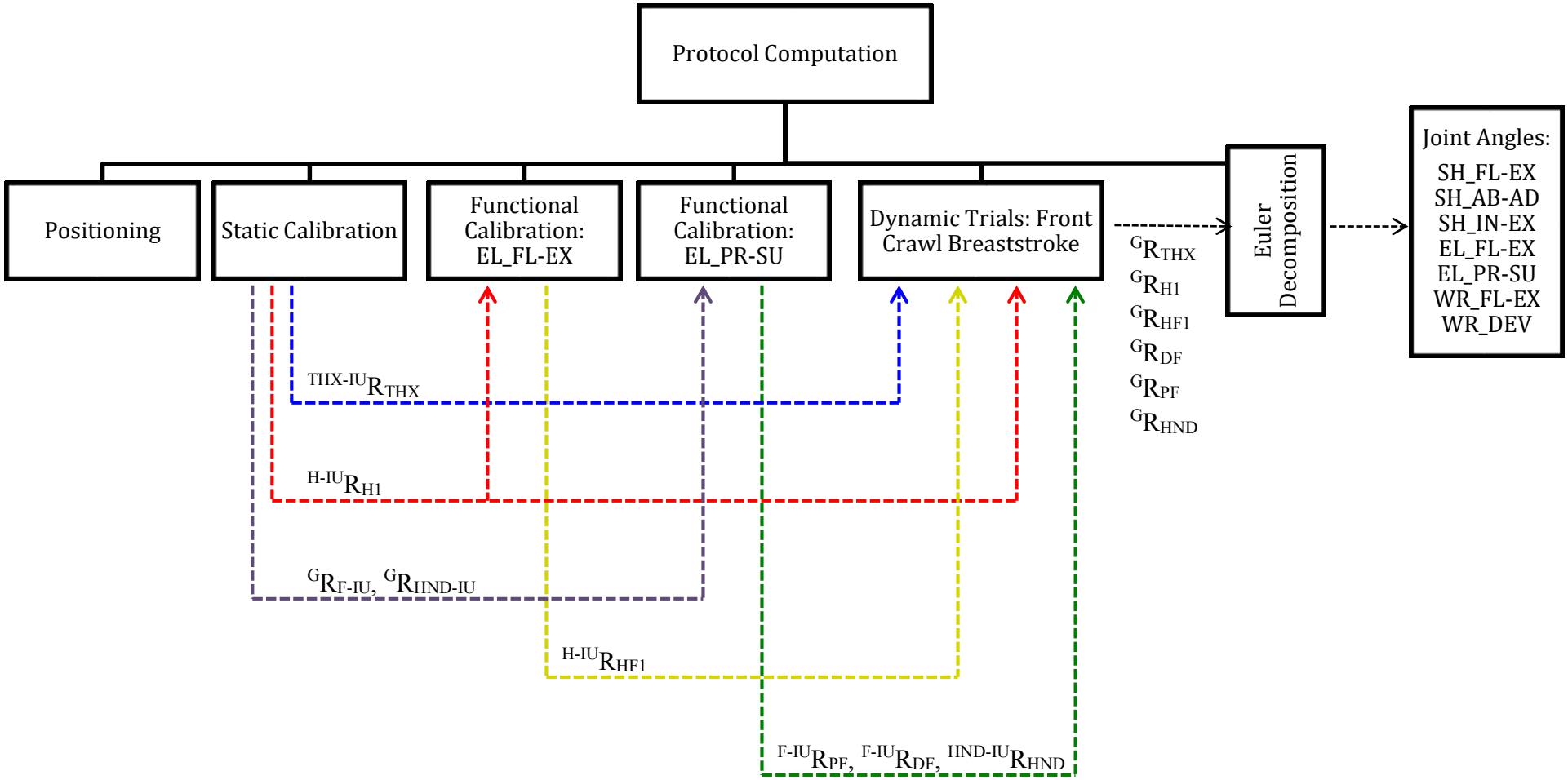

Figure 3.9: Flow chart of the protocol computation.
$^{A}R_{B}$: rotational matrix of B with respect to A (see also Table 3.3). IU: inertial unit. THX: thorax. H: humerus. H1: proximal humerus. HF1: distal humerus. F: forearm. PF: proximal forearm. DF: distal forearm. HND: hand. G: global. SH_FL-EX: shoulder flexion-extension. SH_AB-AD: shoulder abduction-adduction. SH_IN-EX: shoulder internal-external rotation. EL_FL-EX: elbow flexion-extension. EL_PR-SU: elbow pronation-supination. WR_FL-EX: wrist flexion-extension. WR_DEV: wrist radial-ulnar deviation.

The second calibration task is a functional trial in which the subject is standing, and has to perform a flexion-extension of the elbow, from about 10° to 130° of flexion, keeping a constant pronation-supination angle. The number of cycles of the movement to collect for each task was 5, and the suggested number of tasks to acquire was 3. The subject could perform the trial at a self-selected speed. However, very fast or very slow movements are not advisable for an accurate estimation of the elbow flexion-extension axis of rotation (Woltring et al., 1994). With reference to Table 3.3, this trial allows computation of the elbow flex-extension axis of rotation, used as an anatomical axis to compute the ASOR of the distal humerus with respect to the IMMU ($^{H\text{-}IU}R_{HF1}$).

The third calibration task was a functional trial in which the subject was standing, and performed a full-range pronation-supination of the elbow, keeping a constant flexion-extension. Similarly to the second calibration, the number of cycles of the movement to collect for each task was 5 and 3 of them were taken, and very fast or very slow movement are not advisable for an accurate estimation of the elbow pronation-supination axis. According to Table 3.3, this trial allowed computation of the prono-supination axis of rotation of the elbow, used as an anatomical axis to compute the ASOR of the proximal and distal forearm with respect to the IMMU ($^{F\text{-}IU}R_{PF}$, $^{F\text{-}IU}R_{DF}$). Since this calibration allowed the computation of the distal forearm ASOR, and that the assumption of the static trial was that the hand ASOR was aligned with the distal forearm ASOR, the hand ASOR was here computed with respect to the IMMU ($^{HND\text{-}IU}R_{HND}$). Calibrations 2 and 3 must be performed for both sides, if considered.

3.3.7 Joint angles computation

At the end of the calibration procedure, every ASOR is known with respect to the corresponding IMMU technical system of reference. The outputs of each functional trial are the orientation matrices of each IMMU with the respect to the global fixed SOR. As a consequence, the orientation of each ASOR with respect to the global SOR was computed using the equation:

$$^{G}R_{XXX} = {}^{G}R_{XXX\text{-}IU} * {}^{XXX\text{-}IU}R_{XXX}$$

where G is the global SoR, and XXX is the acronym of the segment. Joint angles were then calculated through the decomposition of the relative orientation of adjacent segments. The shoulder flexion-extension, intra-extra rotation and abduction-adduction were calculated using the XY'Z'' Euler sequence; the elbow flexion-extension and pronation-supination were calculated using the XZ'Y'' Euler sequence; the wrist flexion-extension and radial-ulnar deviation were calculated using the XY'Z'' Euler sequence.

The Euler sequence used for the shoulders was different from the one proposed by Cutti et al. (2008). The XY'Z'' sequence was chosen because it better represents the kinematics of the

shoulder when it performs wide range movements, and when these movements are not performed mainly around just one axis of rotation (i.e. pure flexion-extension), as usually happens in clinical context. On the other hand, the Euler sequence used for the elbow is consistent with that proposed by Cutti et al. (2008).

The definition of the ASORs described in the Table 3.3 would represent an anatomical 0° of pronation as -90°. This offset was balanced by adding +90° to the pronation-supination angle of the elbow, once computed, in order to be consistent with the representation of the joint angles of the elbow currently used by the scientific community and in clinical settings. The carrying angle of the elbow (rotation around Z' axis) and the hypothetic internal-external rotation angle of the wrist (rotation around Y' axis) were not considered, according to the joint model adopted. For the definition of the ASORs illustrated in Table 3.3, the specified Euler sequences can be used without changing any sign of the joint angles both for the right and the left side.

3.3.8 Swim Strokes Segmentation

An algorithm was developed to semi-automatically performed the swim strokes segmentation. For both front crawl and breaststroke swims, the identification of the beginning of the stroke cycles were carried out in the recovery phase (also known as aerial phase), as proposed by Takagi et al. (2004). Thus, the maxima of the elbow flexion/extension angles were used for the segmentation of the breaststroke, whereas the minima of the shoulder flexion/extension angles were used for segmentation of front crawl (Figure 3.9). The same expert operator supervised the automatic extraction of the features. The algorithm was performed first on the right side and then on the left side.

With the purpose of avoid small peaks detection, the data were first filtered using a moving average filter with a 3 frames window. Then, the algorithm identified the local maxima/minima of the flexion/extension angles and allowed the operator to set a threshold to discard all the values below/above the threshold. Furthermore, the operator could select a time-window for manual identification of values not previously detected by the algorithm. Finally, the arm stroke cycles were automatically timely rescaled to have the first frame at the beginning of the cycle. Average and standard deviation of the frame at which the maximum/minimum occurred were calculated. Cycles with a maximum/minimum position higher or lower than the average plus and minus one standard deviation were automatically discarded. As last supervision check, the operator could manually identify additional cycles not properly segmented to exclude those cycles.

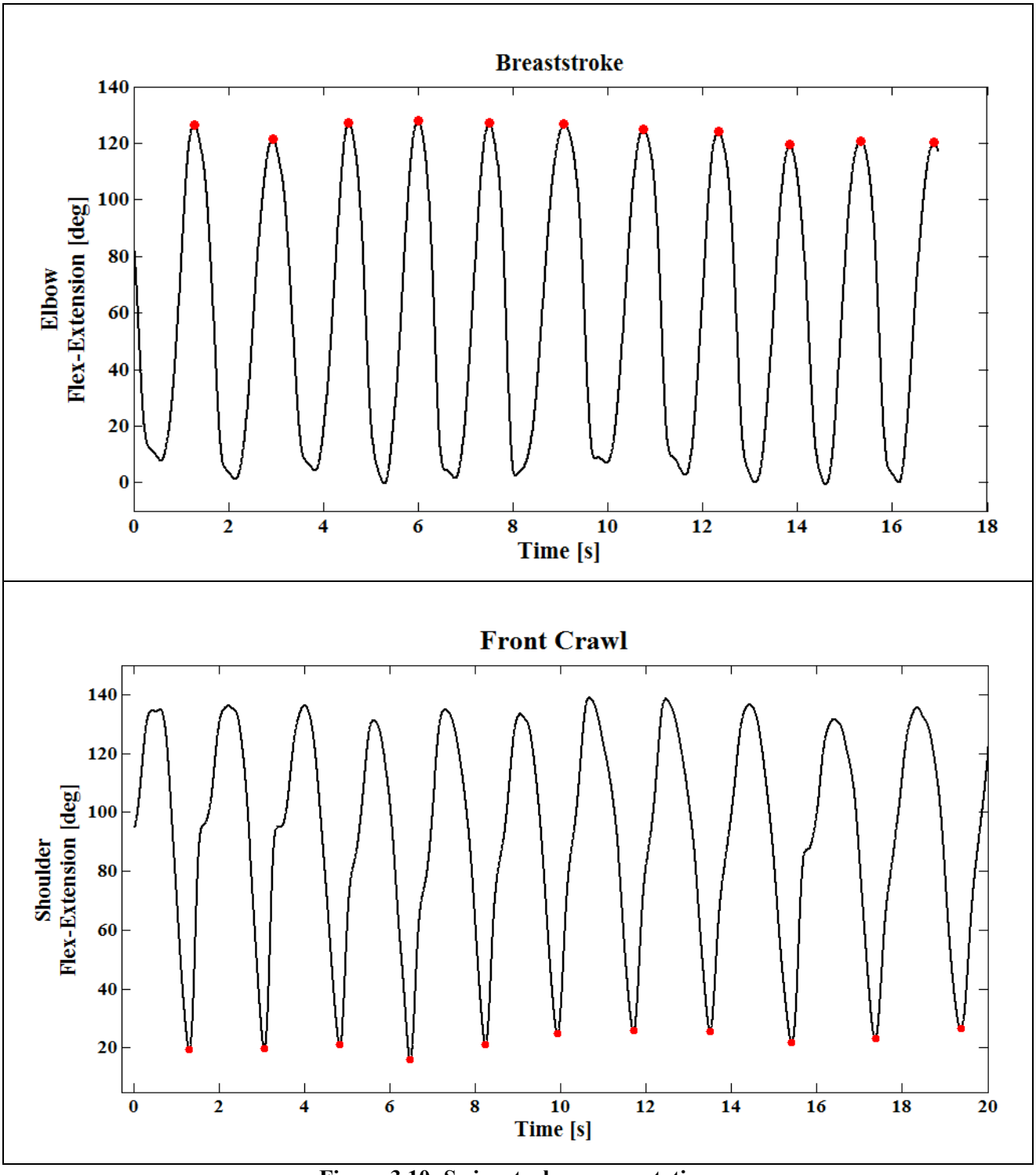

Figure 3.10: Swim strokes segmentation.
Examples of one simulated breaststroke trial (top) and one simulated front crawl trial (bottom). Red circles are the indices used for segmentation, i.e. two successive indices defined the beginning and the end of a swim stroke cycle.

3.3.9 Data Collection

The 3D joint kinematics analysis was accomplished in 2 situations. In a first phase, simulated swimming trials were carried out in laboratory in dry conditions and, afterwards, real swimming trials were performed in the swimming pool.

Eight male current or former sports sciences students agreed to participate and freely signed the informed consent. The characteristics of the participants are presented in Table 3.4. To be considered eligible, participants should have had: 1) swimming experience in at least regional swim competitions; 2) no recent musculoskeletal pathologies; and 3) no pain before or during the tests. They were informed that they could abandon the tests at any moment with no justifications required. Regarding the swimming style, 57% of the participants were specialized in the front crawl, 29% in the breaststroke and 14% in the butterfly. Concerning the swimming level, 71% of the participants were either current or former professionals, whilst 29% were amateurs.

Table 3.4: Characteristics of the participants

Age (years)	Height (cm)	Weight (kg)	Years of Training
27.1 ± 0.6	180.4 ± 5.2	76.4 ± 6.21	10.7 ± 3.6

Table reports the values in mean ± standard deviation.

3.3.10 Swimming Test in Laboratory

This test aimed to validate the 3D joint kinematic estimation using an IMMU during swimming simulations. For that, a SPS was used as the criterion standard reference system. Validating new instruments in the laboratory is a common practice, wherein an accurate criterion standard procedure is available and the data collection can be controlled thus minimizing sources of errors. Specifically for swimming, some authors have already used arm stroke simulations in dry land to measure biomechanical variables (Kimura et al., 1990; Spigelman, 2009; Spigelman et al., 2008). Furthermore, in laboratory not only the underwater phases but the entire stroke cycles can be easily validated including the aerial phase.

The test in dry conditions was carried out in the Biomechanics Laboratory of the Sport Sciences School of the University of Bologna (UNIBO). Seven SMART-DX 7000 cameras were positioned in a semi-circular set-up around a bench with the aim of maximizing the view of the markers placed on both upper limbs and thorax (figure 3.10).

Figure 3.11: Cameras set-up.

In order to be able to compare kinematic data estimated from both IMMU and SPS, seven reflective clusters were built and firmly fixed onto swimmers' body. Each cluster was made of a rigid light-weighted wooden plate containing one monitor and 4 retro-reflective passive markers (Figure 3.11A). The monitors axes were manually aligned with the axes formed by the markers in a way to correspond both systems of reference, i.e. the X-axis was pointing down, the Y-axis was pointing left and the Z-axis was pointing out (Figure 3.11A). The clusters were visually aligned with the mean line of the segments and firmly taped onto it. The athletes were asked to report pain or whether the strappings were blocking their movements. All adjustments on the clusters' placement were made immediately before the data acquisition.

The clusters were placed on the chest, arms, forearms and hands (Figure 3.11B). As the movements of a cluster represented the movements of the segment to which the cluster was attached, it can be said that both systems recorded the same upper-limb motion during the simulated swimming. Once a subject was outfitted with the clusters, the simulated swimming test was ready to start.

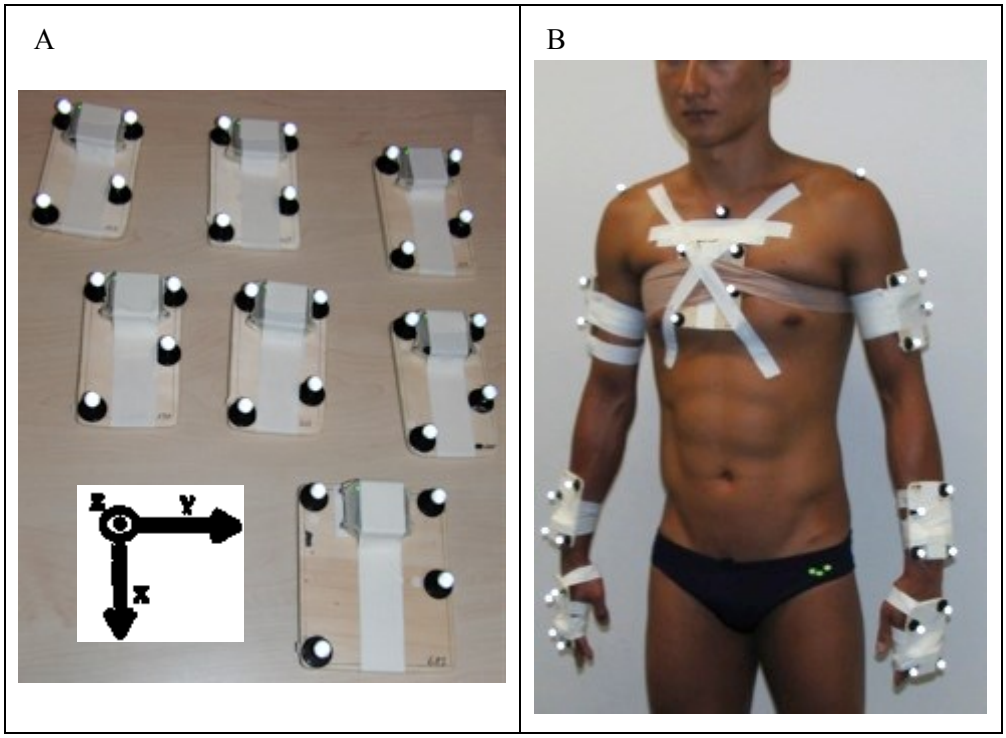

Figure 3.12: Clusters mounting (A) and placement (B).

The first step was the 5-second static calibration. Two different positions were acquired: 1) orthostatic position with the upper limbs resting along the torso and the hand's palm toward the thigh; and 2) lying position with the upper limbs extended along the torso and the palm of hand toward the thigh. This second position was added to the original protocol developed by Cutti et al. (2008) because, in pilot tests, it was observed a better performance of the sensors in correcting the gyroscope drift was observed, so this was the elected position for the static calibration.

In sequence, the functional calibrations were performed with the aim of calculating the mean helical axis (MHA) that defines the joint axes (Woltring et al., 1994). To calculate the medio-lateral MHA, the subject performed 10 cycles of elbow flexion-extension (ranging from about 10° to 100°) with the thumb pointing up (Figure 3.12). Both right and left sides were measured independently. Similarly, to calculate the longitudinal axis of the forearms, the elbow was flexed at 90° and 10 cycles of pronation-supination ranging from 90° of pronation to 90° of supination (considering the 0° the neutral position of the distal radio-ulnar joint) were performed (Figure 3.13). The protocol required two trials for each upper limb, one of flexion-extension and one of pronation-supination, totalizing 4 trials for this type of calibration.

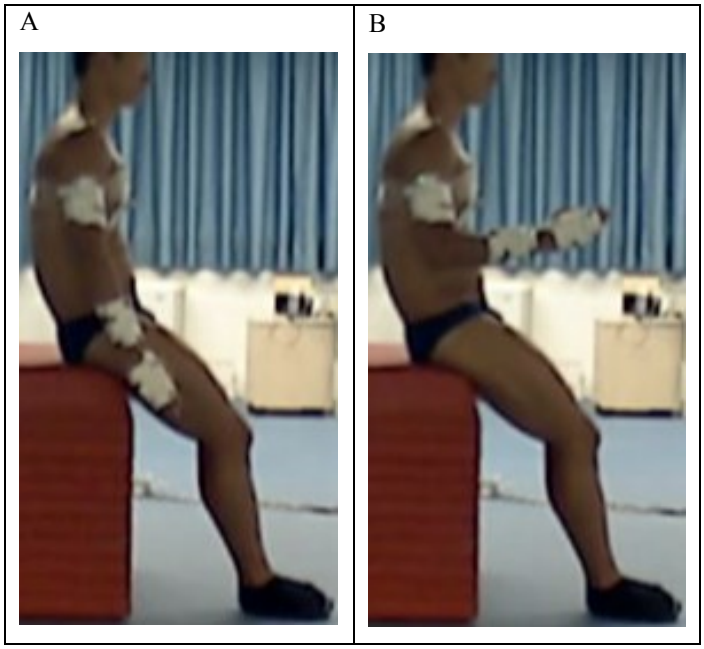

Figure 3.13: Elbow extension (A) and flexion (B).

Subsequently, the athlete executed the dynamic trials, i.e. the swim simulation in dry condition. He was requested to lie on a bench in prone position. Along the simulated swim trials, an assistant person pressed both lower limbs down against the bench at the ankle level to support his inferior half of the body. In this way, the torso, head, and upper limbs were free to move. Twelve swimming simulations were performed, 6 simulating the front-crawl (Figure 3.14) and 6 simulating the breaststroke (Figure 3.15).

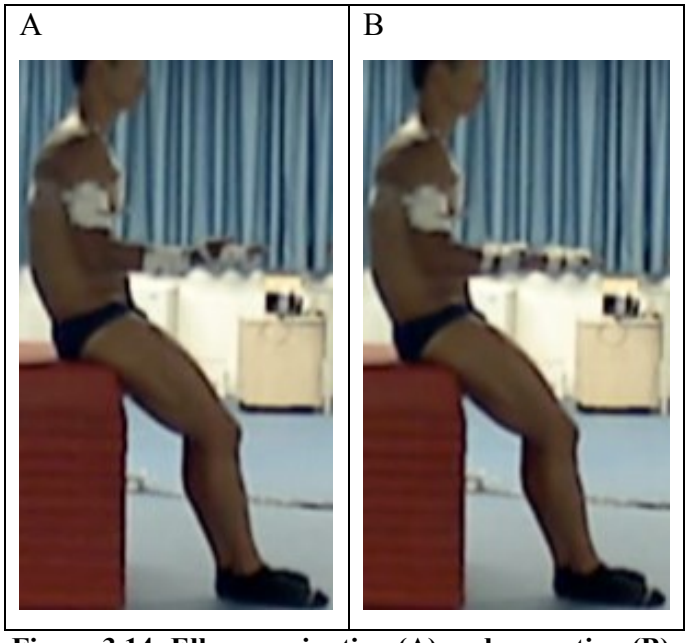

Figure 3.14: Elbow supination (A) and pronation (B).

The swimmers were asked to swim in the same way they would have done in a swimming pool. For each trial, 10 arm-strokes cycles were requested but they could stop the test if there felt pain or tiredness. The average number of arm-strokes cycles in each trial was 7, so totaling about 50 complete arm-strokes cycles for each swim style and for each athlete.

Figure 3.15: Simulated front crawl.

Figure 3.16: Simulated breaststroke.

3.3.11 Swimming Test in the Pool

This test aimed to verify whether the IMMU system evaluated previously in laboratory dry tests was able to estimate adequately the angles of the shoulders, elbows and hands during real

swimming in the pool. The test was carried out in the 25-meter swimming pool of the Record Center of the UNIBO and was quite similar to that in the laboratory but with two main differences. First, as there was no reference system, clusters were unnecessary and the monitors were fixed directly on the body (Figure 3.16). Second, as the IMMU was not a waterproofed system, its waterproofing was achieved by sealing each monitor within 2 plastic bags through a vacuum machine (Magic Vac^{TM}, Genius V402PK2, Italy).

Before the swimming tests, a sequence of tests was performed to verify whether the raw signals of the sensors remained stable during static trials underwater and in the pool's border. In this environment, the vacuum machine used to seal the monitors and swimming pool water pumps create a magnetic field that can interfere with the magnetic sensors. In addition, the underwater buoyant force might impact the acceleration sensing, so it was examined in different depths. By using the laboratory data as baseline, the results showed no alterations in the raw signals of the magnetometers and accelerometers during the static tests. Thus, the IMMU were eligible to be used for the swimming tests.

Figure 3.17: Monitors fixation for pool swimming.

Afterwards, the joint angles of 6 swimmers during pool swimming were measured using the IMMU. Among the 8 total participants, 2 could not be tested in water due to personal problems or injuries. The calibration trials were performed at the poolside following the same procedures of the dry land collection session. Since there was no wireless transmission underwater, the acquisition was started in dry land just few seconds before the swim start and data were stored in the IMMU.

Each swimmer performed 4 different types of swimming trials: free front-crawl, tethered front-crawl, free breaststroke and tethered breaststroke. Tethered swimming was examined because the movements executed are closer to those simulated in laboratory. Three trials were performed for each type of swimming. For free-swimming trials, the athletes were asked to swim 150 m (3 trials of 50 m) and for the tethered-swimming trials, they were asked to perform 3 trials of 10 complete arm-stroke cycles. At the end of each trial, the subject went out of the swimming pool to download wirelessly the data to the workstation.

3.4 Effect of the Drag Force

A multi-part test was designed to estimate the influence of the drag force of a viscous fluid like the water on the measures of the inertial sensors. After having waterproofed 6 monitors, they were firmly attached to a wooden bar in 3 different positions: at the extremes and at the centre of the bar. In each position, 2 units were fixed one on the other with the same axes alignment. Successively, the bar was submerged in the swimming pool until have 4 monitor underwater at 2 different depths and 2 monitors out of the water. Then, the bar was manually moved trying to have only translations along the 3 axes with movements at different velocities. Only translation along one axis was executed for each trial. Three trials were conducted for each axis. Finally, the same operator out of the water performed the same test with all 6 units in dry-land condition. The figure 3.17 illustrates an operator manoeuvring the wooden bar in both in-water and dry-land conditions.

After having verified through the gyroscope measurements, that negligible rotations were performed, only the measures of the accelerometer axes in the direction of movement were taken into account. All the possible combinations among the 6 units were analysed and compared, differentiating among monitors at the same, close or distant position. RMSE and R were estimated in dry land and water condition and statistically compared.

The monitors at the same position showed the same values ($R > 0.99$), thus repetitive results were not reported here in detail. The monitors attached at close positions reported higher R and lower RMSE with respect to the units attached at distant positions that was at the extremes of the bar (see Figure 3.18). This result was the same in water and in dry-land condition, and can be attributed mostly to the non-perfect translation performed by the operator. No difference was found between the water and the dry-land condition regarding the value of R. A slightly better result, statistically significant, was found in the water regarding the RMSE. But from the point of view of the measurement, they can be considered negligible.

A

B

Figure 3.18: Drag test in dry land (A) and in water (B).

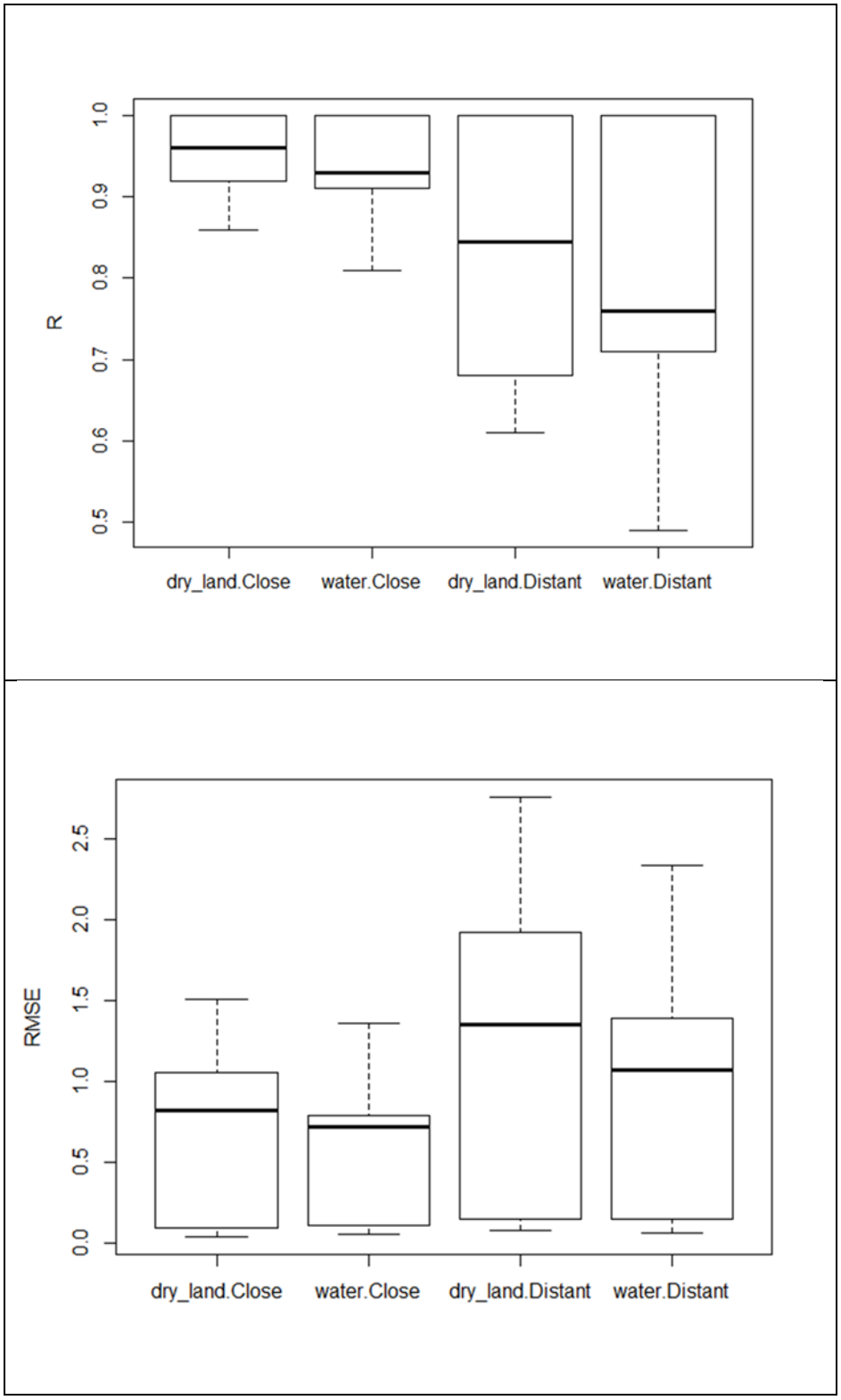

Figure 3.19: Comparative box-plots of the drag test.
Close and distant terms refer to the position between the monitors. R: Pearson product-moment correlation coefficient (top). RMSE: root mean square error (bottom).

3.5 Statistical Analyses

Descriptive statistics were used to summarize the characteristics of the participants. The performance of the IMMU and the SPS during simulated swimming in laboratory were compared by means of root mean square error (RMSE), Pearson product-moment correlation coefficient (R), coefficient of multiple correlation (CMC), regression coefficient (m) and absolute value of the error term of a linear regression (abs(q)). Since joint angles were segmented in stroke cycles and time-normalized, the statistical analysis was conducted on the cycles for each subject and for each joint angles.

The CMC adopted in the analyses was the one proposed by Ferrari et al. (2010a), which measures the overall similarity of cyclical waveforms taking into account the concurrent effects of differences in offset, correlation, and gain. The CMC was computed using as cyclical waveforms the stroke cycles. The RMSE is a measure of the differences between values predicted by 2 instruments and it represents the sample standard deviation of the differences between predicted values and observed values. The RMSE is considered as a good measure of accuracy (Hyndman and Koehler, 2006). R is a measure of the degree of linear dependence between two variables. The m and abs(q) are those indices normally computed in linear regression, where m is the an estimate of the regression coefficient, and abs(q) is a parameter that captures all factors which affects the dependent variable.

For the computation of the overall RMSE, r, m and abs(q), all the stroke cycles for each swim style, for each subject and each joint angles were merged together. Likewise, the "relative RMSE" was calculated by normalizing and expressing the RMSE as percentage of the joint range of motion performed by the subject, differentiating for each joint angle. The analyses were performed using 2 statistical software: the MATLAB (version 2009b) and the R statistical software (version 2.15.3).

CHAPTER 4

RESULTS AND DISCUSSION

4 Results and Discussion

The aim of the thesis was to experiment a protocol originally designed to estimate the joint angles of the upper limbs during one-degree-of-freedom movements in ambulatory settings and here modified to perform 3D kinematics analysis of shoulders, elbows and wrists during swimming. Eight high-level swimmers were first assessed in a laboratory by means of an inertial and magnetic measurement units system (IMMU) while simulating the swimming movements. A stereo-photogrammetric system (SPS) was used as reference. The joint angles estimated with the two systems were compared using the RMSE, relative RMSE, R, CMC, m and abs(q) indices. Subsequently, the athletes were assessed in the swimming pool during real swimming through the IMMU. The results of both laboratory and swimming pool assessments are presented and discussed in this Chapter.

4.1 Swimming Test in Laboratory

4.1.1 Comparing the Orientation Algorithms

The performance of three orientation algorithms was compared using the coefficient of multiple correlation (CMC). The first examined algorithm was the one provided by APDM (Motion Studio, U.S.A., updated in 10/22/2013) and labeled KBE. The second was the algorithm presented by Madgwick et al. (2011) with a value of β fixed at 0.844 considering all dynamic and calibration trials (KMA). And the third and last algorithm was the one presented by Madgwick et al. (2011) with different values of β optimized for three different category of trials (KMB): calibration (β = 0.625), front crawl (β = 0.875) and breaststroke (β = 0.8125). The CMC values were expressed as the median and interquartile range (IQR) and presented in Figure 4.1. For the front crawl, the CMC was 0.94 (0.07) for KMA, 0.965 (0.0675) for KMB and 0.94 (0.23) for KBE; for the breaststroke, the CMC was 0.98 (0.04), 0.99 (0.03) and 0.96 (0.145) for KMA, KMB and KBE, respectively. In both front crawl and breaststroke, as expected, the KMB showed slightly higher CMC values than the KMA, and definitely higher CMC values than the KBE. Therefore, this optimized algorithm (KMB) was used for further analyses.

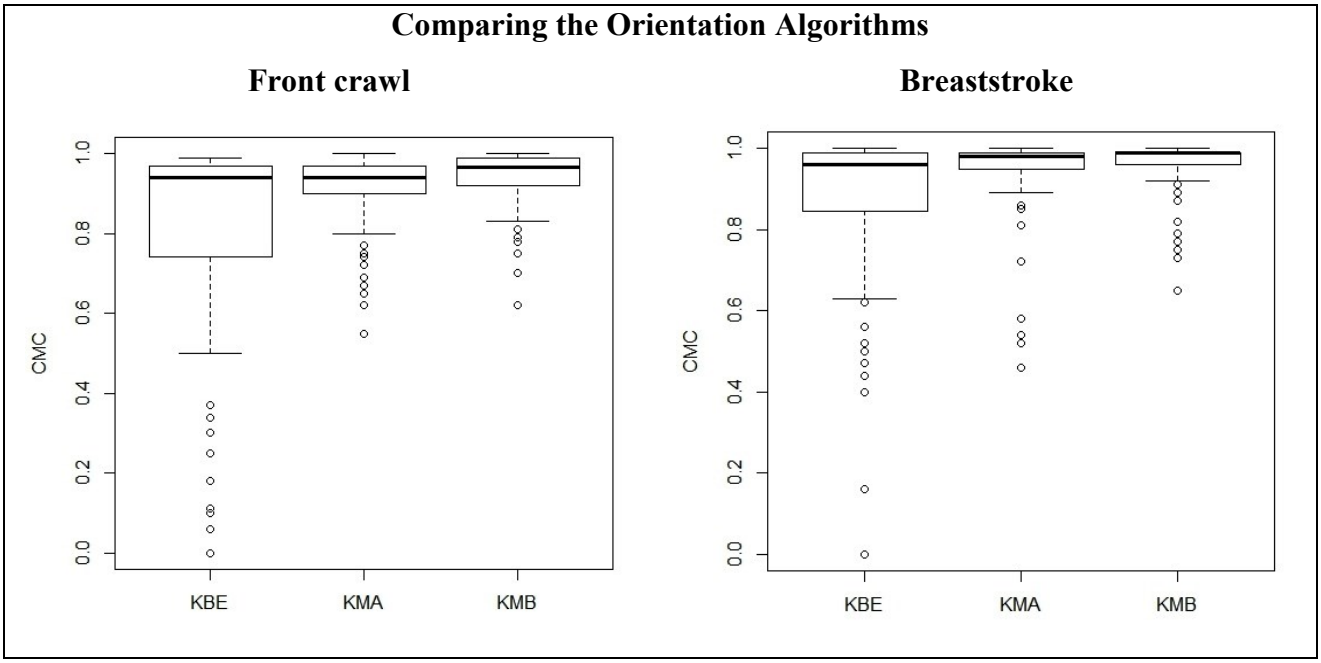

Figure 4.1: Comparing the Orientation Algorithms.
Comparative box-plots among the orientation algorithms. KBE: algorithm from APDM, KMA: algorithm from Madgwick et al. (2011) with fixed value of β and KMB: algorithm from Madgwick et al. (2011) with varying value of β. CMC: coefficient of multiple correlation.

4.1.2 Comparing the body sides

Considering possible bilateral asymmetries of the swimmers and possible protocol measurement errors, the IMMU performance referred to the left versus right upper limbs was compared through CMC, RMSE and relative RMSE (Table 4.1). Figure 4.2 displays the comparative box-plots for the front crawl and breaststroke. Overall, there were no significant differences between the left and right sides in both front crawl and breaststroke for any examined indices.

In addition, the Wilcoxon test revealed the following values: W = 1361 (p = 0.7664) for CMC, W = 1132.5 (p = 0.2256) for RMSE and W = 1246 (p = 0.6436) considering the front crawl, and W = 1383 (p = 0.7648) for CMC, W = 1423 (p = 0.9677) for RMSE and W = 1489 (p = 0.7127) considering the breaststroke. These values show no statistical difference between the left and right sides. Consequently, the data of both sides were grouped together for the further analyses.

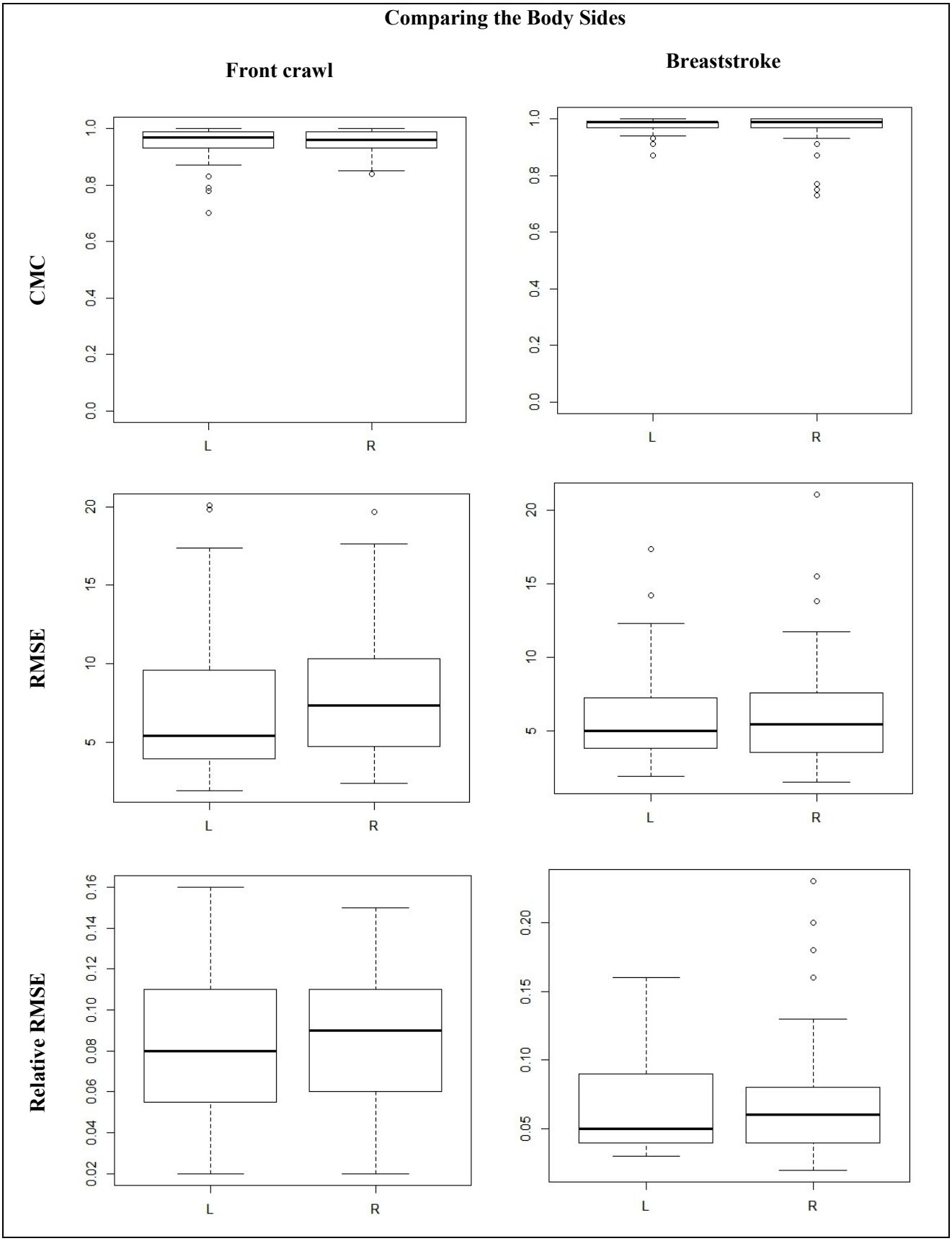

Figure 4.2: Comparing the Body Sides.
Comparative box-plots between the left (L) and the right (R) body sides. CMC: coefficient of multiple correlation, RMSE: root mean square error in degrees, and relative RMSE: ratio between RMSE and range of motion.

Table 4.1: Comparing the body sides

	CMC		RMSE		Relative RMSE	
	Left	**Right**	**Left**	**Right**	**Left**	**Right**
Front crawl	0.97 (0.06)	0.96 (0.06)	5.42 (5.52)	7.34 (5.58)	0.08 (0.05)	0.09 (0.05)
Breaststroke	0.99 (0.02)	0.99 (0.03)	5.01 (3.44)	5.46 (3.94)	0.05 (0.05)	0.06 (0.04)

Table reports the comparison between the body sides (median and IQR). CMC: coefficient of multiple correlation, RMSE: root mean square error, and Relative RMSE: ratio between RMSE and range of motion.

4.1.3 Calibration trials

The protocol follows the dynamic approach of determining the anatomical system of reference (SoR) of distal humerus and forearm during elbow flexion-extension and pronation-supination motor tasks. In those trials, the agreement between IMMU and the reference system were analyzed by means of RMSE, R, m and abs(q) and the results presented in the Table 4.2 and Figure 4.3.

Table 4.2: Comparing the calibration trials

	RMSE	R	m	abs(q)
Elbow flexion-extension	3.77 (1.44)	1.00 (0.01)	1.01 (0.04)	1.45 (2.67)
Elbow prono-supination	3.75 (2.06)	1.00 (0.00)	0.97 (0.02)	3.43 (2.69)

Table reports the comparison between the calibration trials (median and IQR). RMSE: root mean square error, R: Pearson product-moment correlation coefficient, m: regression coefficient, and abs(q): absolute intercept value.

4.1.4 Dynamic trials

The performance of the IMMU in estimating the joint angles was compared with the data from the SPS by means of the CMC, RMSE, relative RMSE, r, m and abs(q) indices. Movements with 3 degrees of freedom (DOF) for shoulders (flexion-extension, abduction-adduction and internal-external rotation), 2 DOF for elbows (flexion-extension and pronation-supination) and 2 DOF for wrists (flexion-extension and radial-ulnar deviation) were considered. Yet, as shown in the section 4.2.2, it is important to remember that no substantial difference existed between left and right body sides. Table 4.3 shows the median (IQR) values of the examined indices for all joint angles, which are also illustrated in box-plots (Figures 4.4 to 4.5).

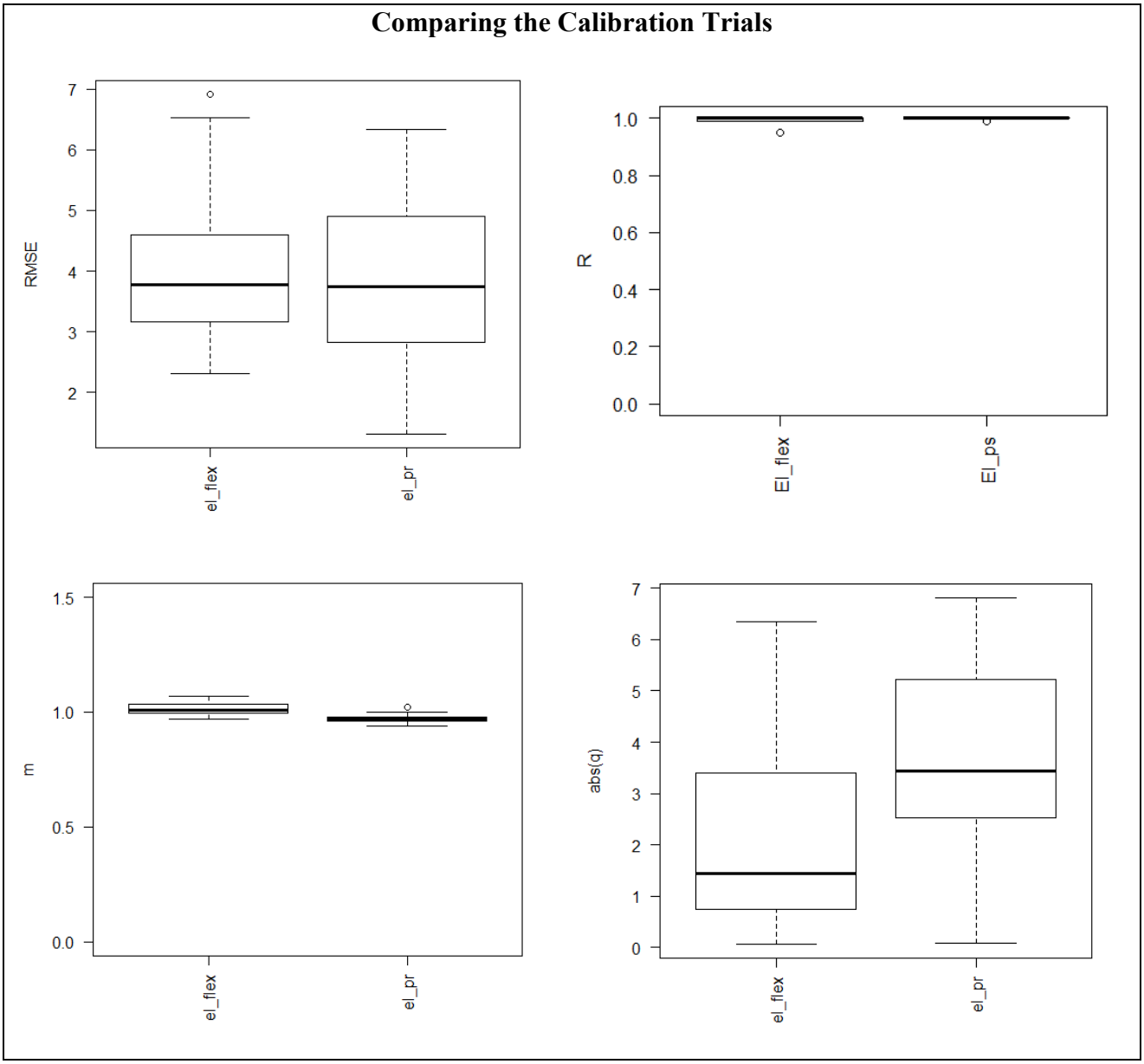

Figure 4.3: Comparing the calibration trials.
Comparative box-plots between the calibration trials. RMSE: root mean square error, R: Pearson product-moment correlation coefficient, m: regression coefficient, and abs(q): absolute intercept value. El_flex: elbow flexion-extension and El_pr: elbow pronation-supination.

The analysis of the front crawl showed the following results: 1) the median value of RMSE was equal to 7.3 degrees, ranging from 3.2 degrees for the wrist radial-ulnar deviation to 14.8 degrees for the elbow flexion-extension; 2) the median value of relative RMSE was equal to 0,10 (i.e. the median value of RMSE represents 10% of total range of motion), ranging from 0.05 for the shoulder flexion-extension to 0.11 for the elbow flexion-extension; 3) the median value of CMC was equal to 0.95, ranging from 0.90 for the wrist radial-ulnar deviation to 0.99 for the shoulder flexion-extension, and for the internal and external rotation; 4) the median value of R was equal to 0.96, ranging from 0.91 for the wrist radial-ulnar deviation to 0.99 for the shoulder flexion-extension; 5) the median value of m was equal to 0.905, ranging from 0.75 for the wrist radial-ulnar deviation to 1.03 for the shoulder internal-external rotation; 6) the median value of abs(q) was equal to 3.46, ranging from 1.47 for the wrist radial-ulnar deviation to 17.43 for the elbow pronation-supination.

Concerning the breaststroke style, the following results were found: 1) the median value of RMSE was equal to 5.3 degrees, ranging from 3.4 degrees for the shoulder internal-external rotation to 7.5 degrees for the elbow flexion-extension; 2) the median value of relative RMSE was equal to 0.06 (i.e. the median value of RMSE represents 6% of total range of motion), ranging from 0.045 for the shoulder flexion-extension to 0.1 for the wrist radial-ulnar deviation; 3) the median value of CMC was equal to 0.99, ranging from 0.93 for the wrist radial-ulnar deviation to 0.995 for the shoulder internal-external rotation; 4) the median value of R was equal to 0.99, ranging from 0.93 for the wrist radial-ulnar deviation to 1.00 for the shoulder flexion-extension; 5) the median value of m was equal to 0.985, ranging from 0.87 for the wrist radial-ulnar deviation to 0.995 for the shoulder flexion-extension; 6) the median value of abs(q) was equal to 3.31, ranging from 1.52 for the shoulder internal-external rotation to 6.28 for the elbow pronation-supination.

Table 4.3: Comparing the joint angles

	Front Crawl						Breaststroke					
	CMC	**RMSE**	**Rel. RMSE**	**R**	**m**	**abs(q)**	**CMC**	**RMSE**	**Rel. RMSE**	**R**	**m**	**abs(q)**
Sh_Fl-Ex	0.99 (0.01)	5.06 (3.90)	0.05 (0.02)	0.99 (0.002)	0.99 (0.03)	2.44 (2.24)	0.99 (0.01)	5.72 (2.84)	0.045 (0.01)	1.00 (0.01)	0.995 (0.03)	4.59 (2.41)
Sh_Ab-Ad	0.97 (0.02)	9.60 (3.64)	0.10 (0.04)	0.95 (0.03)	0.90 (0.07)	5.63 (7.80)	0.99 (0.002)	4.9 (3.25)	0.05 (0.02)	0.995 (0.01)	0.985 (0.04)	2.88 (5.53)
Sh_In-Ex	0.99 (0.01)	7.31 (2.98)	0.06 (0.01)	0.98 (0.02)	1.03 (0.04)	2.13 (1.68)	0.995 (0.01)	3.37 (1.08)	0.04 (0.002)	0.99 (0.002)	0.98 (0.06)	1.52 (1.61)
El_Fl-Ex	0.95 (0.04)	14.76 (5.12)	0.11 (0.04)	0.96 (0.03)	0.77 (0.10)	12.27 (10.18)	0.99 (0.02)	7.54 (5.15)	0.06 (0.05)	0.99 (0.01)	0.99 (0.03)	5.24 (7.01)
El_Pr-Su	0.93 (0.03)	9.70 (3.67)	0.10 (0.04)	0.92 (0.02)	0.83 (0.13)	17.43 (17.59)	0.98 (0.02)	5.91 (4.43)	0.06 (0.04)	0.99 (0.02)	0.92 (0.07)	6.28 (6.08)
Wr_Fl-Ex	0.94 (0.1)	4.60 (1.09)	0.08 (0.05)	0.96 (0.04)	0.97 (0.10)	3.46 (1.71)	0.975 (0.03)	5.26 (3.22)	0.75 (0.05)	0.975 (0.01)	0.99 (0.09)	3.31 (3.17)
Wr_Dev	0.90 (0.08)	3.22 (1.32)	0.10 (0.04)	0.91 (0.07)	0.75 (0.18)	1.47 (1.14)	0.93 (0.05)	4.42 (1.98)	0.1 (0.02)	0.93 (0.05)	0.87 (0.22)	1.98 (1.92)

Table reports the comparison between the joint angles (median and IQR) estimated by the IMMU and by the SPS. Sh_Fl-Ex: shoulder flexion-extension, Sh_Ab-Ad: shoulder abduction-adduction, Sh_In-Ex: shoulder internal-external rotation, El_Fl-Ex: elbow flexion-extension, El_Pr-Su: elbow pronation-supination, Wr_Fl-Ex: wrist flexion-extension, and Wr_Rad: wrist radial-ulnar deviation. CMC: coefficient of multiple correlation, RMSE: root mean square error, Rel. RMSE: ratio between RMSE and range of motion, R: Pearson product-moment correlation coefficient, m: regression coefficient, and abs(q): absolute intercept value.

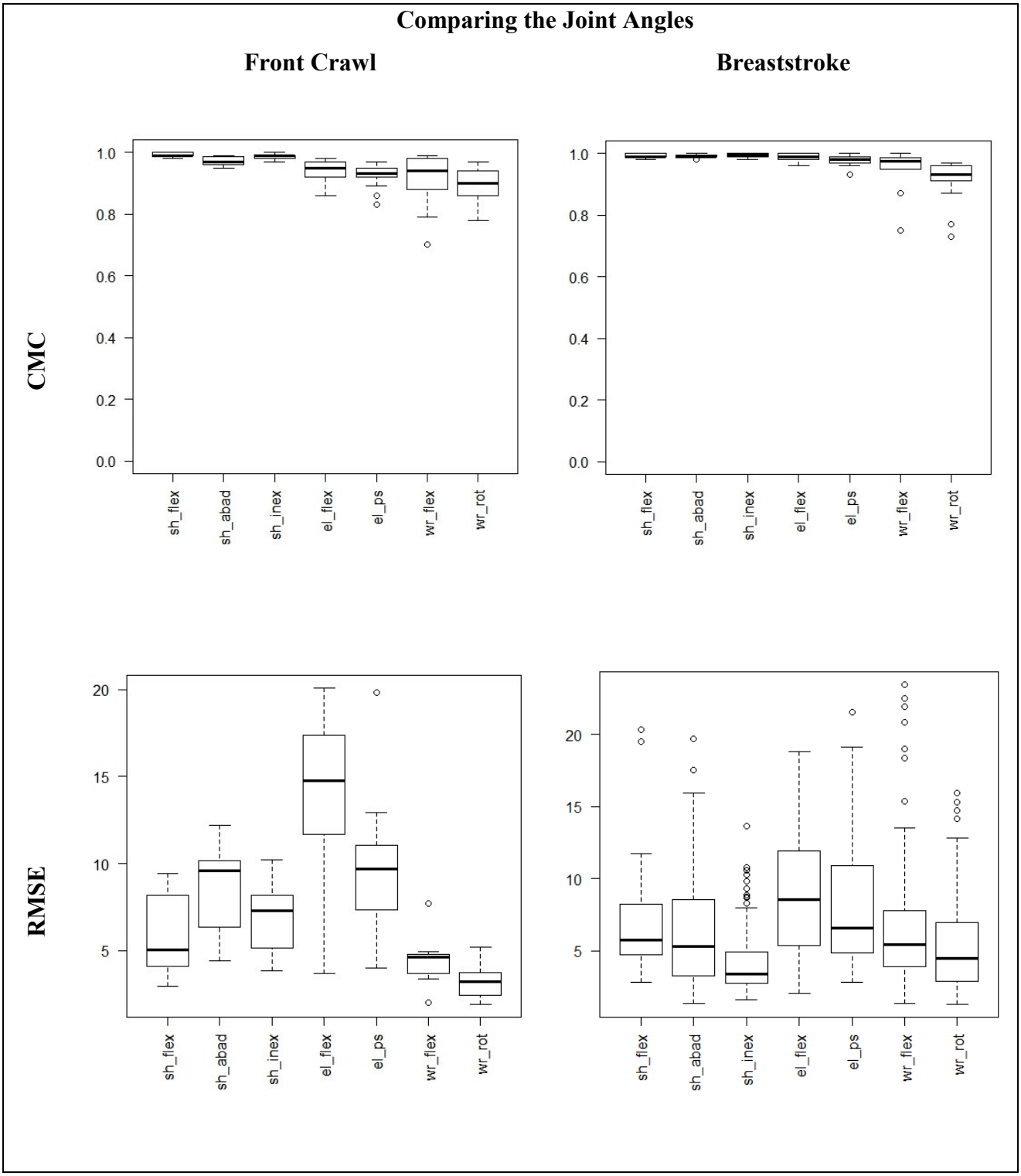

Figure 4.4: Comparing the joint angles.
Comparative box-plots among all joint degrees of freedom. Sh_Fl-Ex: shoulder flexion-extension, Sh_Ab-Ad: shoulder abduction-adduction, Sh_In-Ex: shoulder internal-external rotation, El_Fl_Ex: elbow flexion-extension, El_Pr-Su: elbow pronation-supination, Wr_Fl-Ex: wrist flexion-extension, and Wr_Rot: wrist radial-ulnar deviation. CMC: coefficient of multiple correlation, and RMSE: root mean square error.

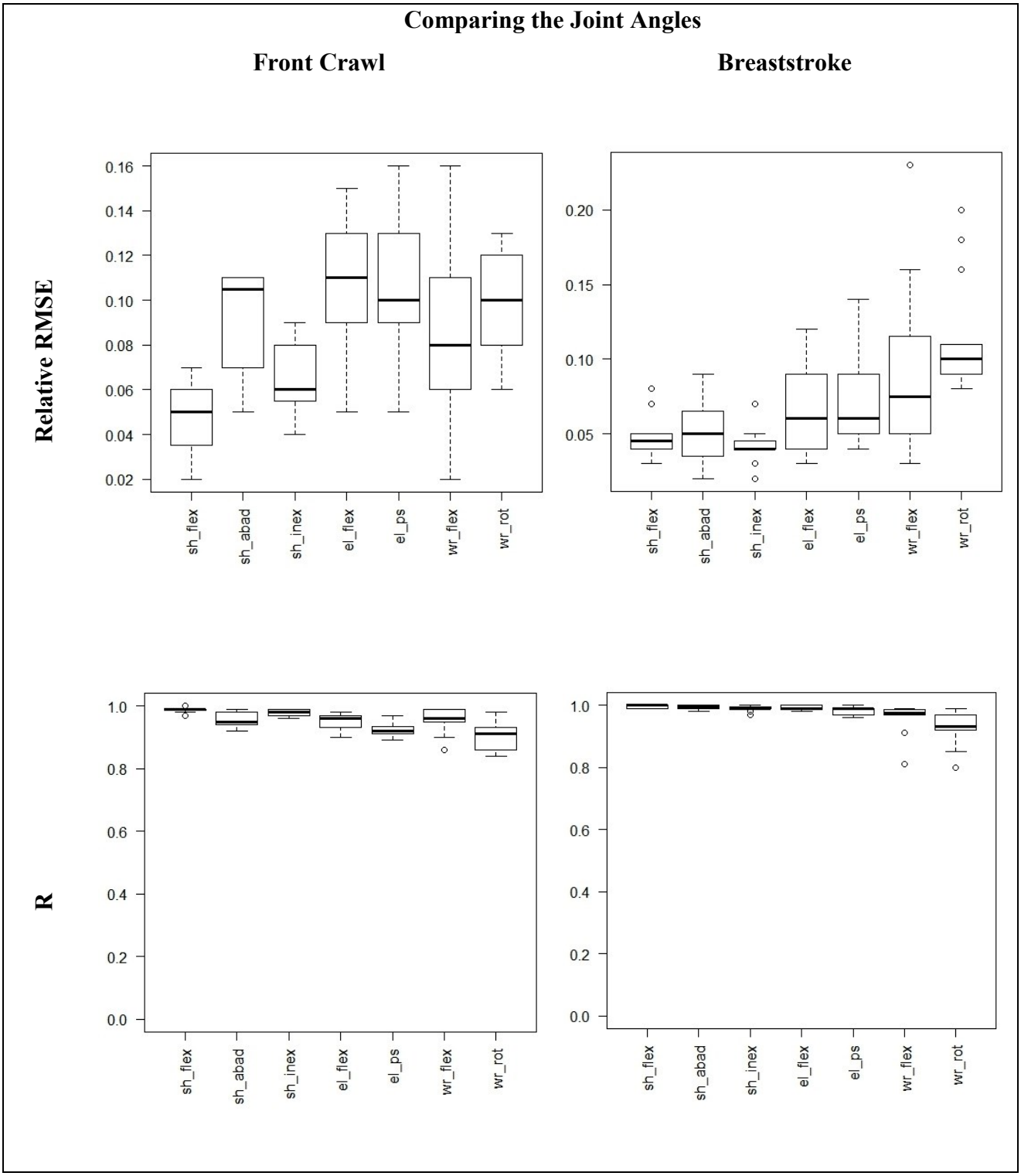

Figure 4.5: Comparing the joint angles.
Comparative box-plots among all joint degrees of freedom. Sh_Fl-Ex: shoulder flexion-extension, Sh_Ab-Ad: shoulder abduction-adduction, Sh_In-Ex: shoulder internal-external rotation, El_Fl_Ex: elbow flexion-extension, El_Pr-Su: elbow pronation-supination, Wr_Fl-Ex: wrist flexion-extension, and Wr_Rot: wrist radial-ulnar deviation. R: Pearson product-moment correlation coefficient, and Relative RMSE: ratio between RMSE and range of motion.

4.1.5 Individual results

The comparison between the joint angles values of each participant estimated by the IMMU and by the SPS is presented in Table 4.4. The median results of all swimmers for the front crawl style are: 1) CMC of 0.97 (ranging from 0.95 to 0.99), 2) RMSE of 7.7 degrees (ranging from 4.5 to 8.9 degrees), 3) Relative RMSE of 10% (ranging from 6% to 11%), and 4) R of 0.96 (ranging from 0.93 to 0.99). For breaststroke, the following median values were calculated: 1) CMC of 0.99 (ranging from 0.98 to 0.99), 2) RMSE of 5.6 degrees (ranging from 4.0 to 7.9 degrees), 3) Relative RMSE of 6% (ranging from 4% to 8%), and 4) R of 0.99 (ranging from 0.98 to 1.00).

For each simulated swimming trial, the athletes performed about seven arm stroke cycles totaling about 50 arm stroke cycles after the 12 trials proposed. Afterwards, all cycles of the same athlete were averaged according to the swim style and to the joint. In this way, with the intention of show different patterns of motion during the same motor task, the 3D joint kinematics of two swimmers were grouped in six conditions. For the simulated front crawl, the joint ranges of motion in the sagittal, frontal and transverse planes are shown in the Figures 4.7, 4.8 and 4.9, respectively. While for the simulated breaststroke, the joint ranges of motion in the sagittal, frontal and transverse planes are shown in the Figures 4.10, 4.11 and 4.12, respectively.

Different patterns of movement could be found when comparing the left versus right body sides of a same athlete, as visualized in the Figure 4.13. In Figures 4.7 to 4.13, the joint angles (in degrees) estimated by the IMMU and by the SPS were plotted over the percentage of swim cycles duration (ranging from 0 to 100%); the lines represent the mean data of the eight swimmers tested.

Table 4.4: Comparing the swimmers

Swimmer		1	2	3	4	5	6	7	8	ALL
Front crawl	**CMC**	0.96 (0.03)	0.96 (0.07)	0.99 (0.07)	0.99 (0.02)	0.97 (0.06)	0.95 (0.04)	0.97 (0.07)	0.96 (0.06)	0.97 (0.02)
	RMSE	8.09 (5.37)	7.36 (5.51)	4.52 (1.07)	4.91 (1.24)	8.26 (2.96)	8.76 (7.00)	8.86 (5.41)	7.34 (6.90)	7.73 (1.65)
	Rel. RMSE	0.10 (0.03)	0.08 (0.05)	0.06 (0.05)	0.06 (0.01)	0.09 (0.04)	0.11 (0.02)	0.10 (0.06)	0.10 (0.04)	0.10 (0.03)
	R	0.96 (0.03)	0.97 (0.05)	0.99 (0.05)	0.99 (0.02)	0.96 (0.04)	0.93 (0.07)	0.95 (0.05)	0.95 (0.05)	0.96 (0.03)
Breaststroke	**CMC**	0.98 (0.02)	0.98 (0.04)	0.98 (0.02)	0.99 (0.01)	0.99 (0.02)	0.99 (0.03)	0.99 (0.03)	0.99 (0.01)	0.99 (0.02)
	RMSE	6.03 (4.04)	7.88 (5.80)	5.91 (2.96)	5.17 (2.35)	3.95 (1.19)	5.33 (2.30)	6.25 (4.17)	4.18 (2.47)	5.62 (1.16)
	Rel. RMSE	0.07 (0.04)	0.08 (0.05)	0.07 (0.03)	0.04 (0.01)	0.05 (0.03)	0.06 (0.05)	0.06 (0.07)	0.04 (0.03)	0.06 (0.02)
	R	0.98 (0.02)	0.99 (0.03)	0.98 (0.01)	0.99 (0.01)	1.00 (0.01)	0.99 (0.01)	0.99 (0.01)	1.00 (0.01)	0.99 (0.01)

Table reports the comparison between the IMMU and the SPS considering the performance of each swimmer. Columns 1 to 9 refer to the swimmers' individual data and the column ALL reports the median values of all swimmers. CMC: coefficient of multiple correlation, RMSE: root mean square error, Relative RMSE: ratio between RMSE and range of motion, and R: Pearson product-moment correlation coefficient.

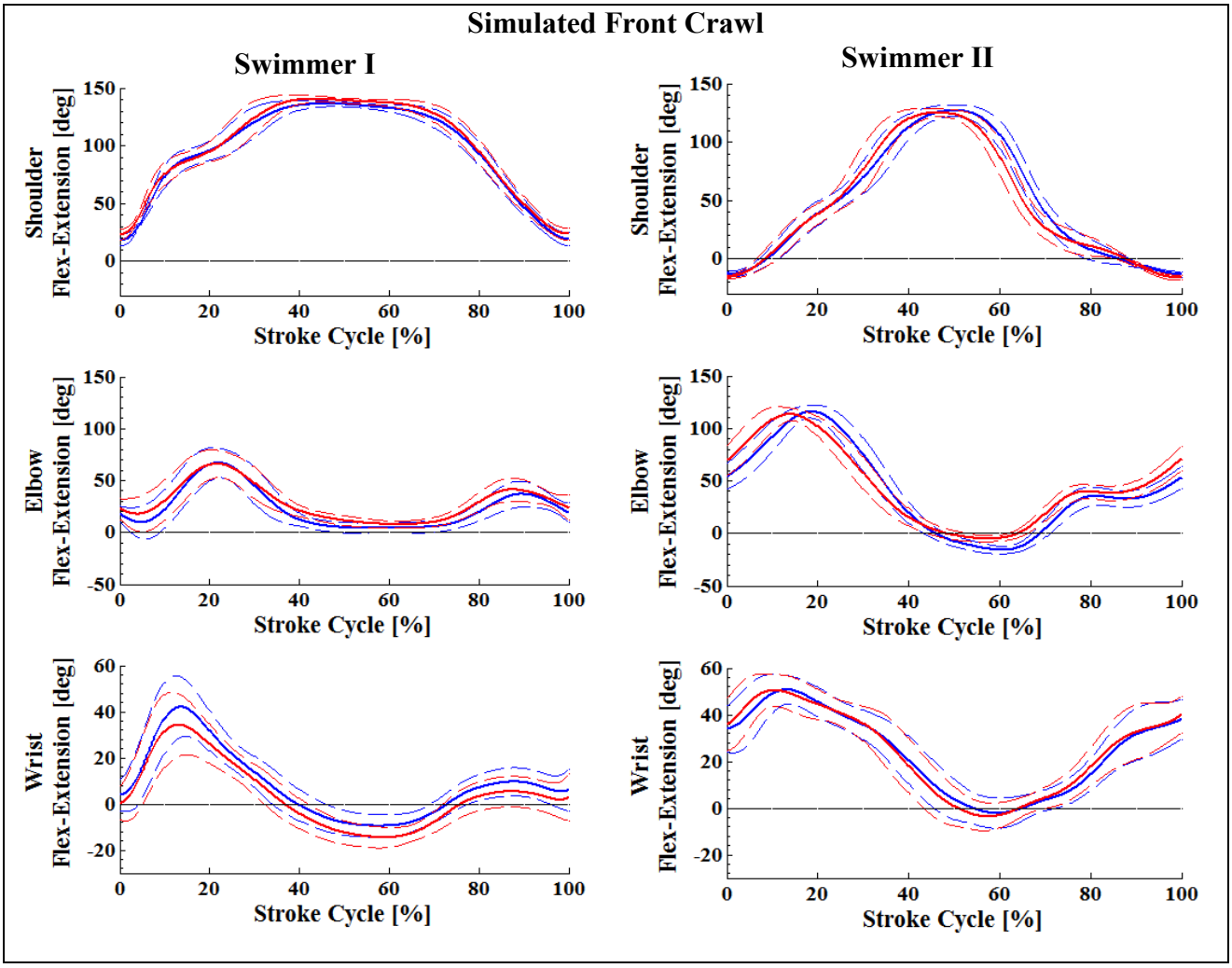

Figure 4.6: Shoulder, elbow and wrist patterns of motion during simulated front crawl. Angles measured by the IMMU (blue lines) and by the SPS (red lines). Columns show the joint kinematics of two swimmers in the sagittal plane, where different motor patterns can be seen. Solid and dashed lines: mean ± standard deviation of all trials, respectively.

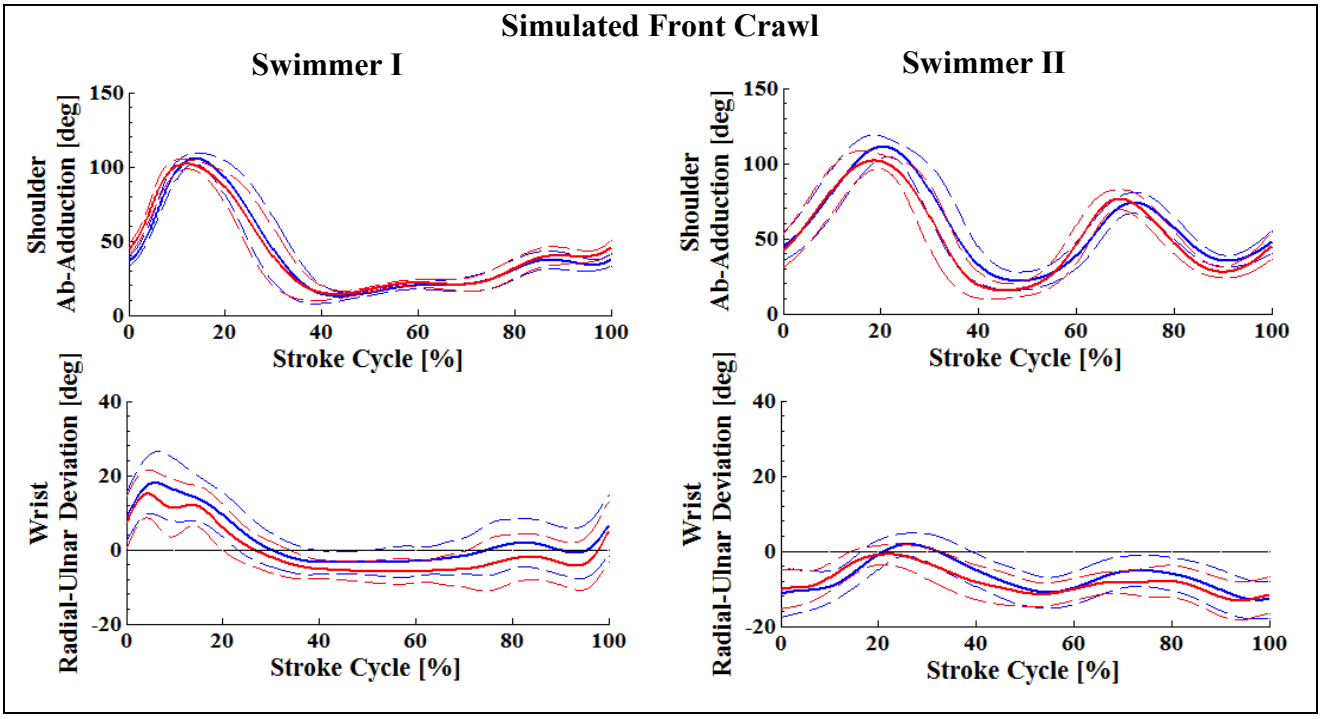

Figure 4.7: Shoulder and wrist patterns of motion during simulated front crawl. Angles measured by the IMMU (blue lines) and by the SPS (red lines). Columns show the joint kinematics of two swimmers in the frontal plane, where different motor patterns can be seen. Solid and dashed lines: mean ± standard deviation of all trials, respectively.

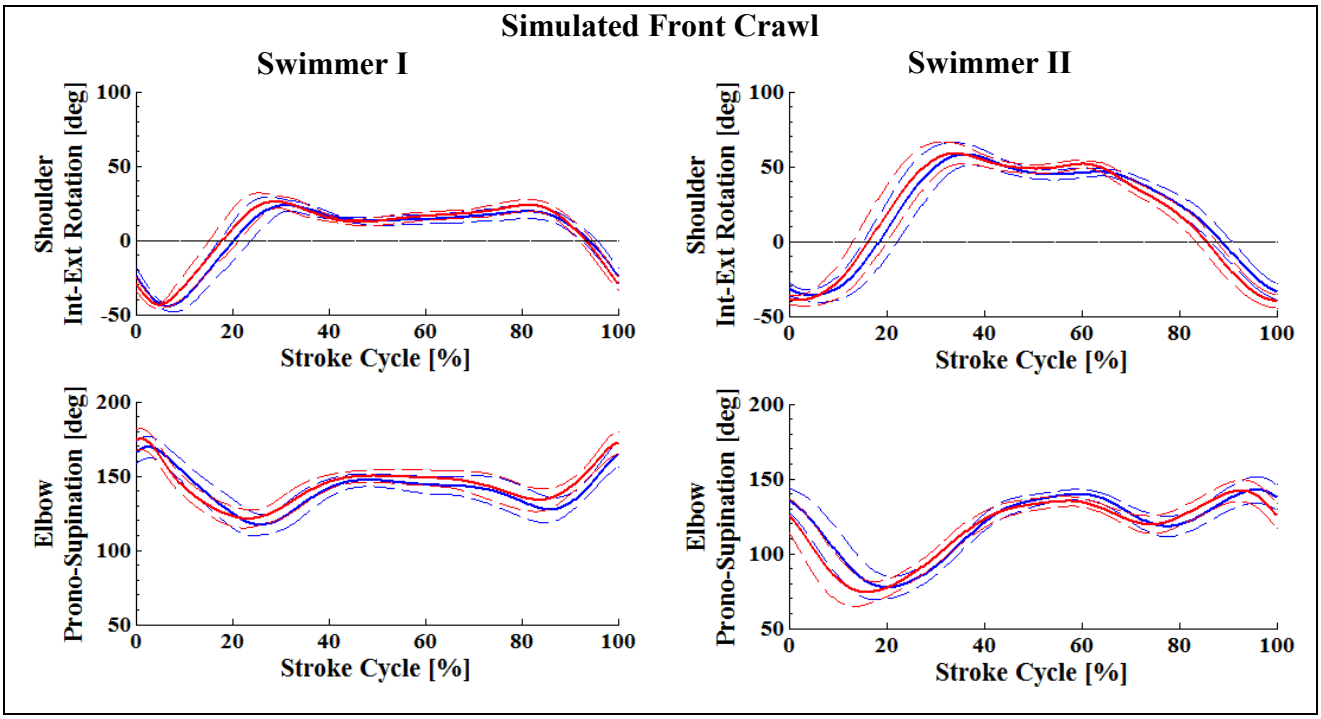

Figure 4.8: Shoulder and elbow patterns of motion during simulated front crawl. Angles measured by the IMMU (blue lines) and by the SPS (red lines). Columns show the joint kinematics of two swimmers in the transverse plane, where different motor patterns can be seen. Solid and dashed lines: mean ± standard deviation of all trials, respectively.

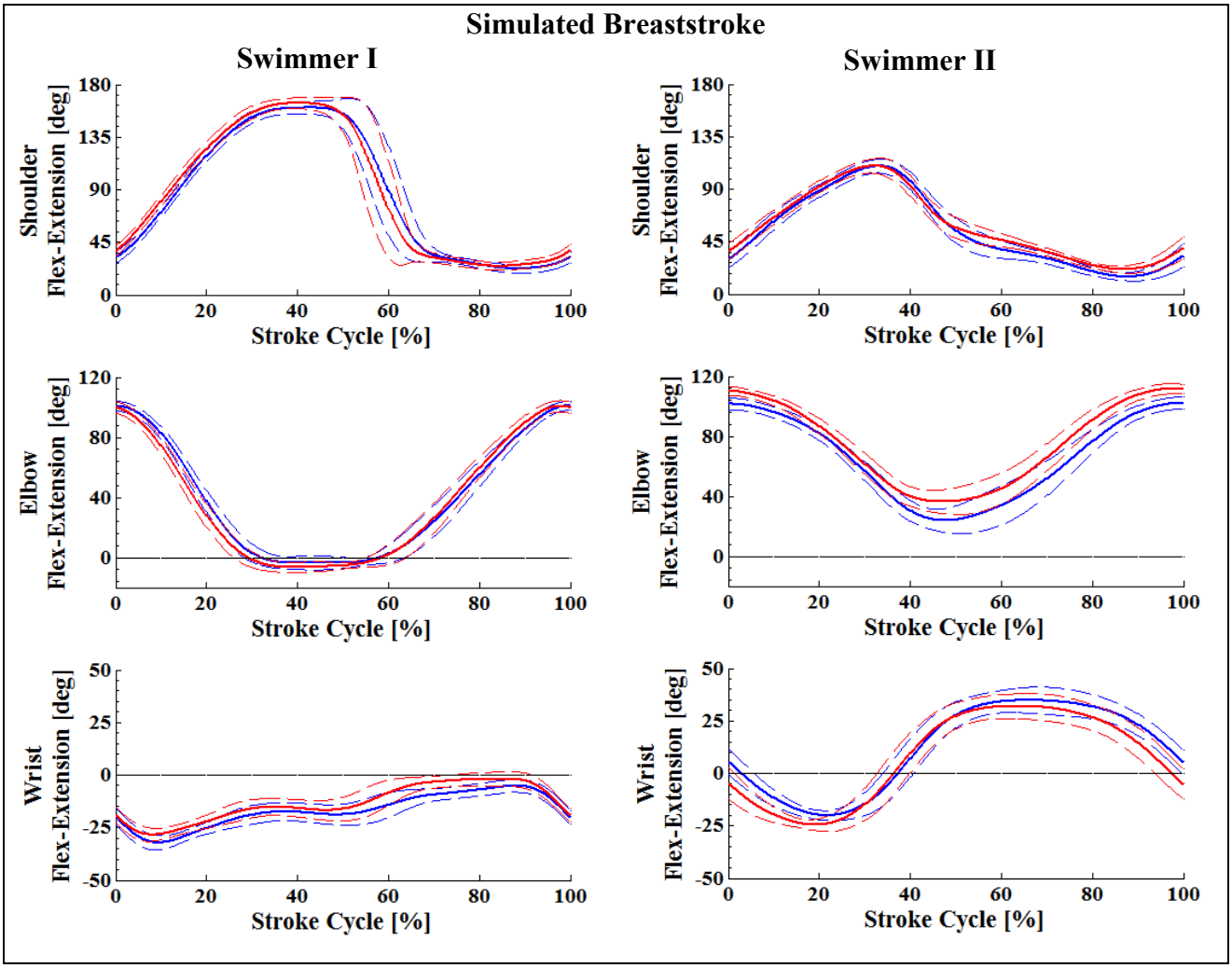

Figure 4.9: Shoulder, elbow and wrist patterns of motion during simulated breaststroke. Angles measured by the IMMU (blue lines) and by the SPS (red lines). Columns show the joint kinematics of two swimmers in the sagittal plane, where different motor patterns can be seen. Solid and dashed lines: mean ± standard deviation of all trials, respectively.

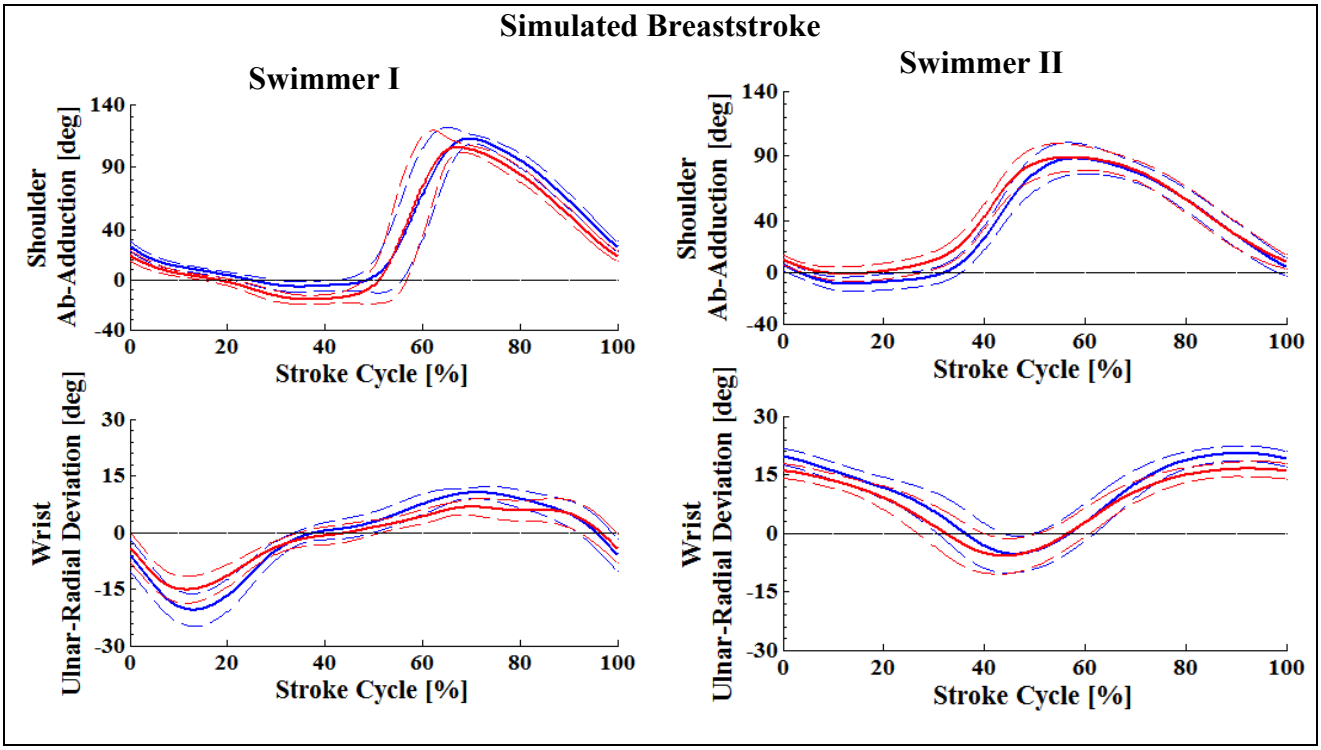

Figure 4.10: Shoulder and patterns of motion during simulated breaststroke. Angles measured by the IMMU (blue lines) and by the SPS (red lines). Columns show the joint kinematics of two swimmers in the sagittal plane, where different motor patterns can be seen. Solid and dashed lines: mean ± standard deviation of all trials, respectively.

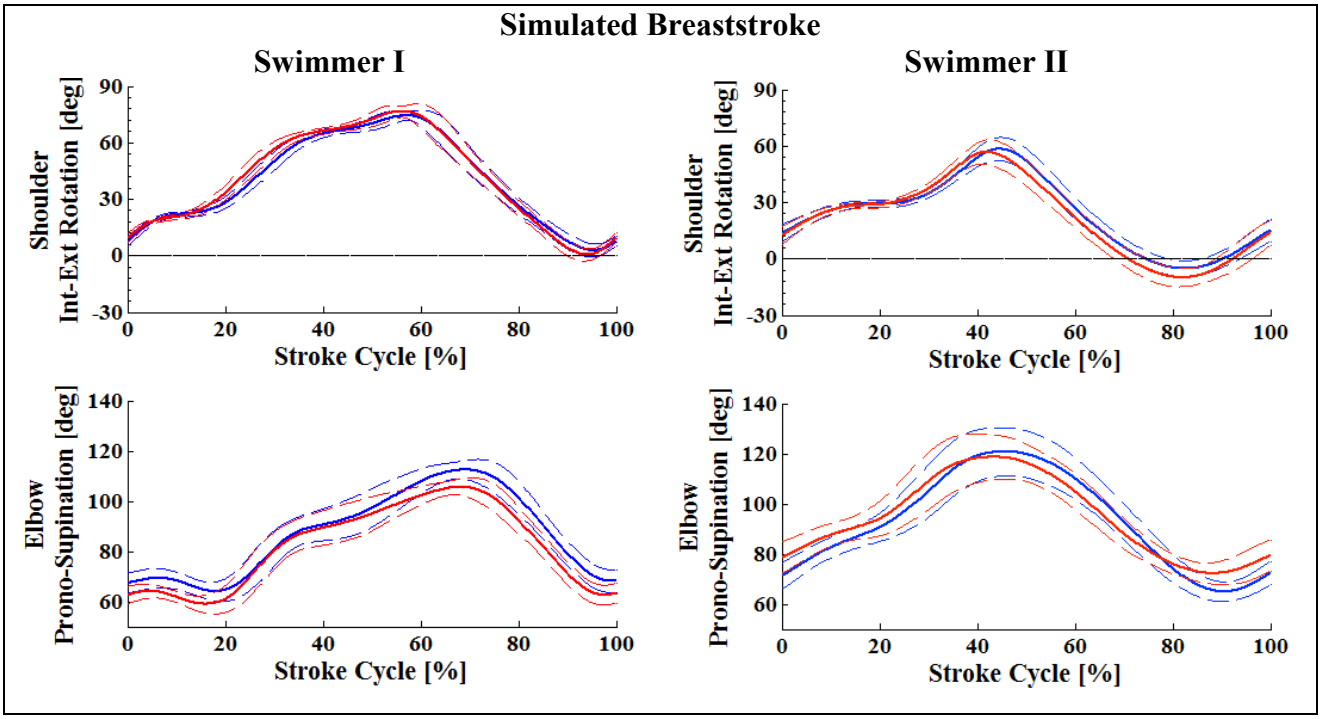

Figure 4.11: Shoulder and elbow patterns of motion during simulated breaststroke. Angles measured by the IMMU (blue lines) and by the SPS (red lines). Columns show the joint kinematics of two swimmers in the sagittal plane, where different motor patterns can be seen. Solid and dashed lines: mean ± standard deviation of all trials, respectively.

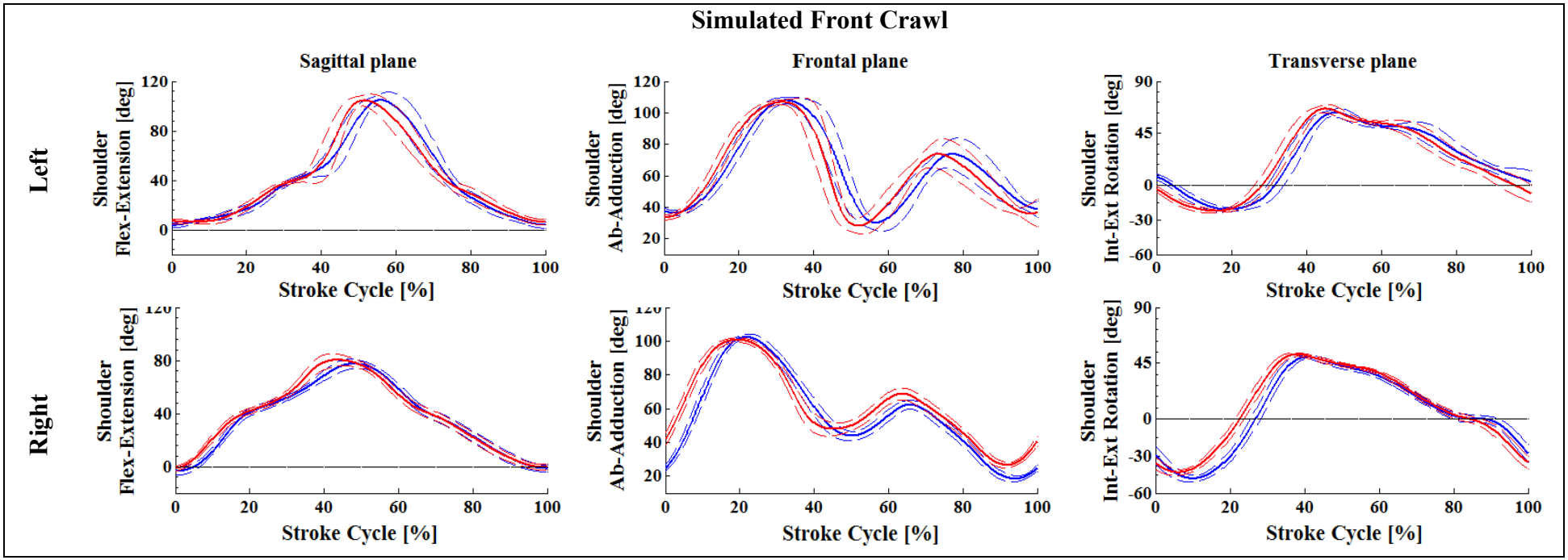

Figure 4.12: Shoulder patterns of motion during simulated front crawl in the three planes.
Angles measured by the IMMU (blue lines) and by the SPS (red lines). Rows show the joint kinematics of both body sides of one swimmer, where different motor patterns can be seen revealing a bilateral asymmetry. Solid and dashed lines: mean ± standard deviation of all trials, respectively.

As would be expected, each athlete had his own style of swimming. Although there is a tendency to follow given shapes, it can be seen in the figures above that individual curves are different not only among the swimmers, but also when for the left versus the right side of the same swimmer. The kinematic analysis is an important tool to compare the swimming technique of different swimmers, eventually taking as a reference the style of top-level swimmers. The sample of this study was composed of high-level swimmers, some of which were finalists in national competitions; however, remarkable differences between them were observed in their swimming styles.

Another issue concerns bilateral asymmetries. By comparing the two sides of the same swimmer, it was possible to observe different patterns of movements between the left and right limbs. Evaluating inter-limb coordination or asymmetries was not within the aim of the present study; however, the figures generated through the protocol may prove to be a useful tool to identify poor coordination between the upper limbs and to recognize functional bilateral asymmetries.

Evaluating swimming in the laboratory using simulated arm strokes is a common practice in the scientific literature (Armstrong and Davies, 1981; Kimura et al., 1990; Lee et al., 2011) because procedures can be more controlled and measurements more easily made. In the case of the present study, the novel method proposed was compared with a SPS. The SPS was used as reference because it is more accurate than the conventional underwater video-camera systems. Each retro-reflective passive marker could be automatically tracked with high accuracy (see section 3.1.2) by the dedicated software (SMART-Tracker, BTS Bioengineering, Italy), enabling precisely the reconstruction of the body segment motions. Whilst this marker-based approach has been widely utilized to analyze the 3D joint kinematics, it cannot be adapted to perform the underwater motion analysis. There is already a SPS available on the market that is able to capture the underwater human motion as reported in the section 2.3.1.1. Nevertheless, besides being even more expensive than the traditional systems, the retro-reflective passive markers used by this system increase the passive drag during underwater motion (Kjendlie and Olstad, 2012). This drawback can negatively affect the swimming performance.

Another advantage of analyzing the simulated arm strokes in laboratory is that the complete arm stroke cycle can be recorded, including the aerial (or recovery) phase. Typically, swimming biomechanics does not consider the aerial phase because it is assumed that the underwater phases are the most important swim phases because they generate propulsion. Moreover, only the underwater phases are acquirable by underwater cameras. Nevertheless, it is important to consider also the aerial phase in order to analyze the entire arm stroke cycles as the aerial phase provides information about the entry and recovery of the stroke. An effective motion capture of the trunk and

upper limbs during the aerial phase is essential to positioning correctly the hand, which acts as a rudder during the propulsive phases. Therefore, when using the marker-based video analysis, only in laboratory is it possible to collect the aerial phase of swimming. To overcome this drawback, IMMU have showed as a solution to this issue even when pool swimming is intended because they are swimmer-centric and have a wide field of view.

4.2 Swimming Test in the Pool

In the swimming test performed in the laboratory, the protocol was highly accurate in estimating the 3D joint kinematics, with a high level of agreement between the measurements of the IMMU and the SPS and low error values (Tables 4.3 and 4.4). The water stage of the test consisted of performing the same analyses during real swimming. Four types of swimming styles were considered: free front crawl, tethered front crawl, free breaststroke and tethered breaststroke. The joint ranges of motion of the free swim, of the tethered swim and of the simulated swim are present in the Figures 4.14 to 4.19. Both free and tethered swim were executed in the pool and the simulated swim was executed in the laboratory, as described in the sections 4.1.4 and 4.1.5. Tethered swimming was overlapped with the simulated swim in those figures because the displayed motor patterns were similar, so it was possible verify the similarities and differences between a simulated and a real swim. The joint ranges of motion values of six swimmers during these three experimental conditions are present in the Table 4.5. Just to clarify, as explained in the section 3.3.1.8, six of the eight swimmers tested in laboratory were tested in the swimming pool. Even if small differences can be found in one or other angle, as found in the shoulder internal-external rotation for the free and tethered breaststroke or in the wrist flexion-extension for the free and simulated front crawl, no remarkable difference in the aggregate values of joint angles was noted when comparing these 3 kinds of swimming.

The differences in the pattern of movement between dry simulated and water swimming increased from the proximal to the distal joints. This might be due to the shortcomings of simulated swimming. During dry land simulations, the swimmers were required to imitate the proper technique of swimming without the usual resistance of the water during the arm strokes. In addition, during the simulations, the swimmers had to support actively their trunk in suspension, a condition that may have limited the body roll and, consequently, reduced the joint ranges of motion. Finally, in water swimming, the upper limbs generate propulsion forces to overcome the water resistance (drag forces) and then push the body forward, which is not true in dry simulations.

Similarly to the dry simulated swim, different patterns of movement in the kinematics of the athletes were noticed during the real swim. Figures 4.20 to 4.22 show a side-by-side comparison

between two swimmers during the free front crawl in the pool, and Figures 4.23 to 4.25 complete this comparison during the free breaststroke in the pool. Those different patterns of movement suggest once again that each swimmer has his own style of swimming, and the same discussion conducted in the section 4.1.5 may be considered here. On the other hand, the majority of the six athletes performed both free front crawl and breaststroke in the pool with very similar motor patterns, indicating that establishing values of references for each swim style based on top swimmers might be a reasonable strategy for coaches to better train swimmers.

The method proposed in this thesis modified a pre-existent protocol in order to analyze the 3D joint kinematics of both upper limbs through an inertial and magnetic measurement units system during swimming. This novel method revealed to be a potent tool to assist coaches, clinicians and researches to evaluate and monitor precisely the underwater motion.

Table 4.5: Joint ranges of motion

	Front Crawl			**Breaststroke**		
	Free	**Tethered**	**Lab**	**Free**	**Tethered**	**Lab**
Sh_Fl-Ex	124 (16)	116 (11)	105 (7)	124 (11)	123 (9)	113 (8)
Sh_In-Ex	47 (7)	56 (8)	90 (5)	40 (8)	74 (6)	70 (6)
Sh_Ab-Ad	94 (14)	96 (9)	82 (6)	109 (10)	108 (8)	83 (8)
El_Fl-Ex	94 (11)	93 (11)	105 (10)	91 (7)	96 (6)	105 (7)
El_Pr-Su	106 (10)	95 (10)	71 (10)	88 (7)	91 (11)	89 (10)
Wr_Fl-Ex	94 (8)	90 (7)	30 (9)	63 (6)	46 (11)	50 (8)
Wr_Dev	25 (6)	30 (5)	20 (7)	20 (4)	24 (6)	26 (5)
Total	94 (10)	93 (9)	82 (7)	88 (7)	91 (8)	83 (8)

Table reports the joint ranges of motion (in degrees) in the three experimental conditions were measured by the IMMU system. Values expressed in median (IQR). Free: free swim in the pool, Tethered: tethered swim in the pool, and Lab: simulated swim in the laboratory. Sh_Fl-Ex: shoulder flexion-extension, Sh_Ab-Ad: shoulder abduction-adduction, Sh_In-Ex: shoulder internal-external rotation, El_Fl-Ex: elbow flexion-extension, El_Pr-Su: elbow pronation-supination, Wr_Fl-Ex: wrist flexion-extension, and Wr_Dev: wrist radial-ulnar deviation.

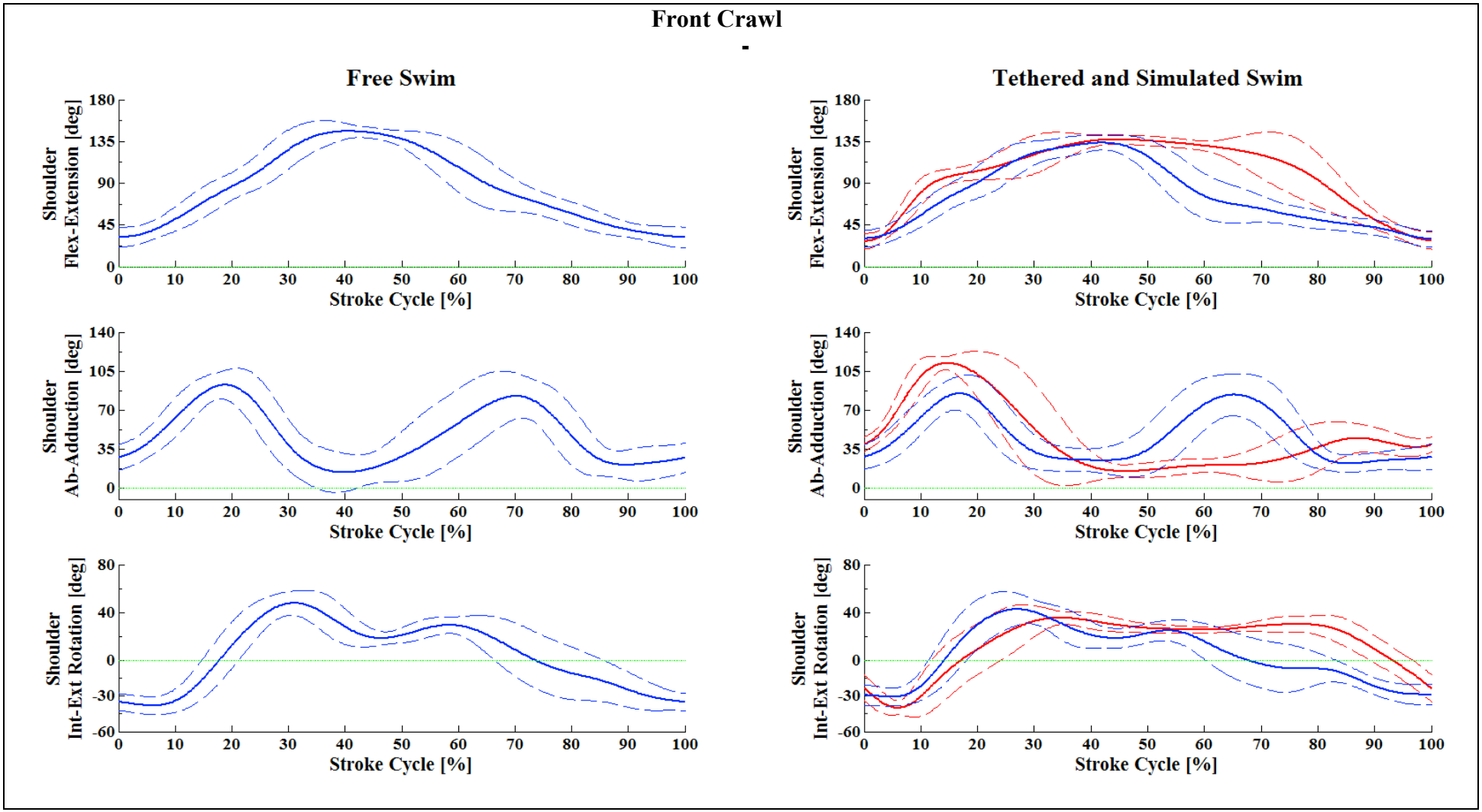

Figure 4.13: Shoulder angles during free, tethered and simulated front crawl.
Free and tethered swim were performed in the pool (IMMU, blue lines) and simulated swim was performed in laboratory (SPS, red lines). Solid and dashed lines: mean ± standard deviation of all trials, respectively.

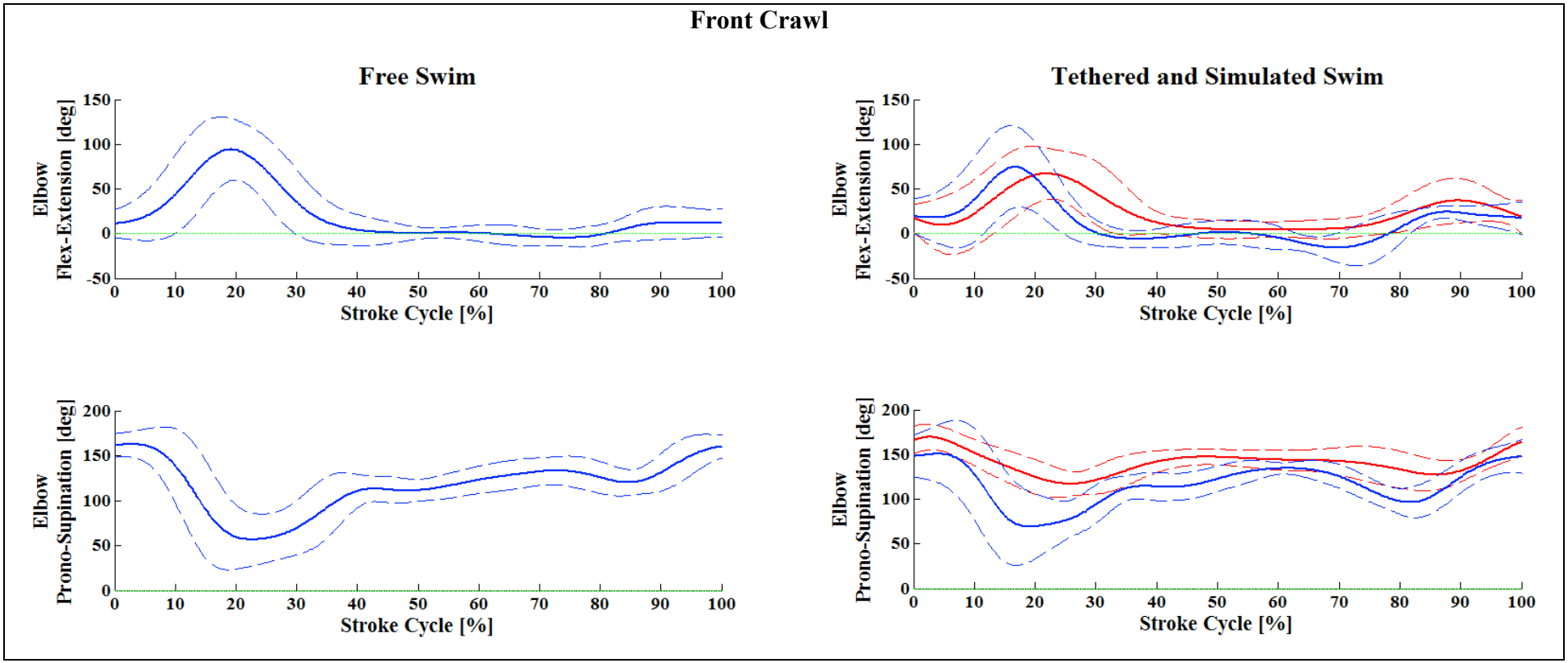

Figure 4.14: Elbow angles during free, tethered and simulated front crawl.
Free and tethered swim were performed in the pool (IMMU, blue lines) and simulated swim was performed in laboratory (SPS, red lines). Solid and dashed lines: mean ± standard deviation of all trials, respectively.

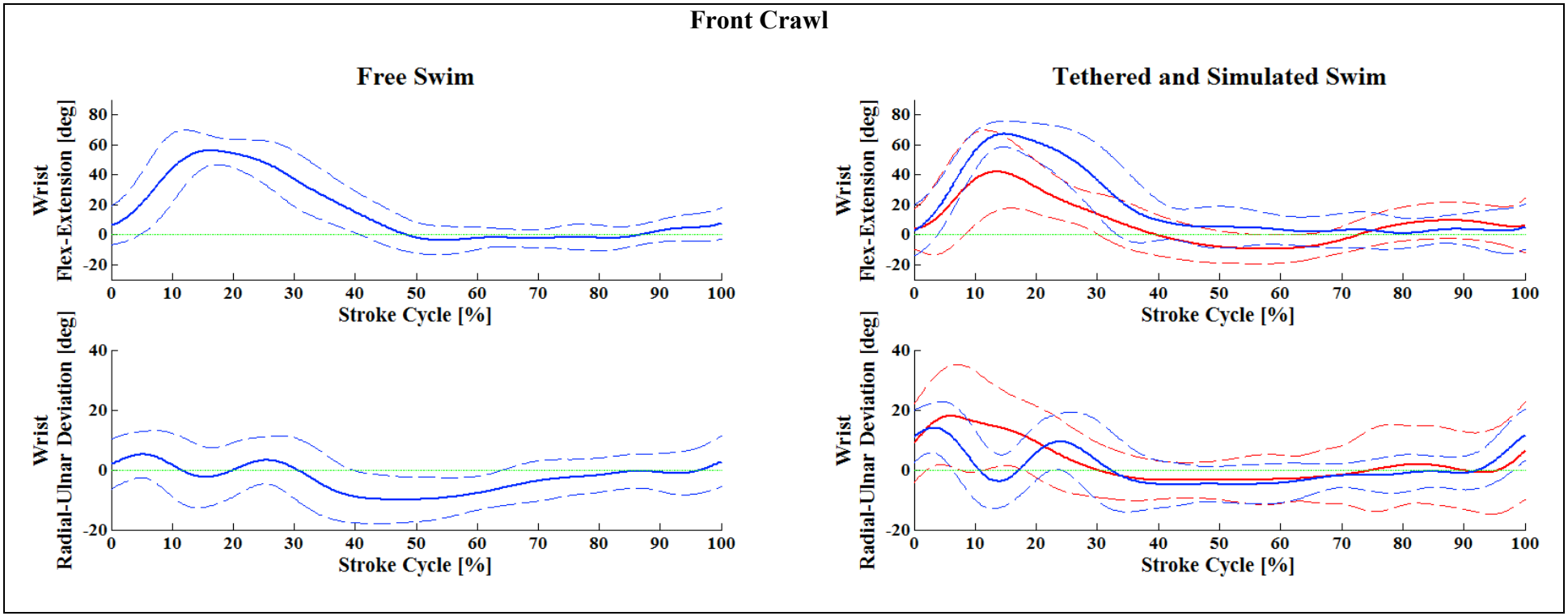

Figure 4.15: Wrist angles during free, tethered and simulated front crawl.
Free and tethered swim were performed in the pool (IMMU, blue lines) and simulated swim was performed in laboratory (SPS, red lines). Solid and dashed lines: mean ± standard deviation of all trials, respectively.

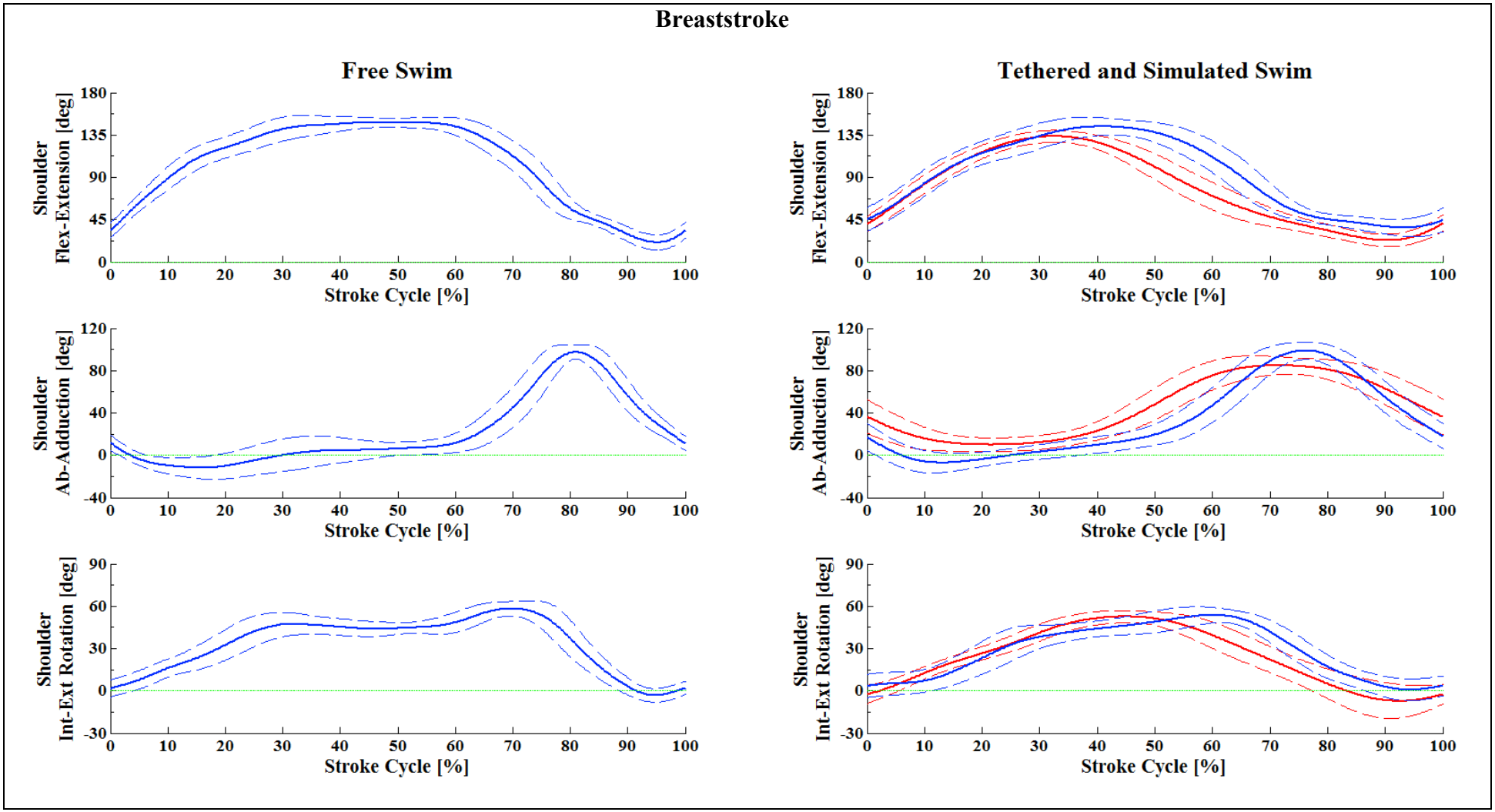

Figure 4.16: Shoulder angles during free, tethered and simulated breaststroke.
Free and tethered swim were performed in the pool (IMMU, blue lines) and simulated swim was performed in laboratory (SPS, red lines). Solid and dashed lines: mean ± standard deviation of all trials, respectively.

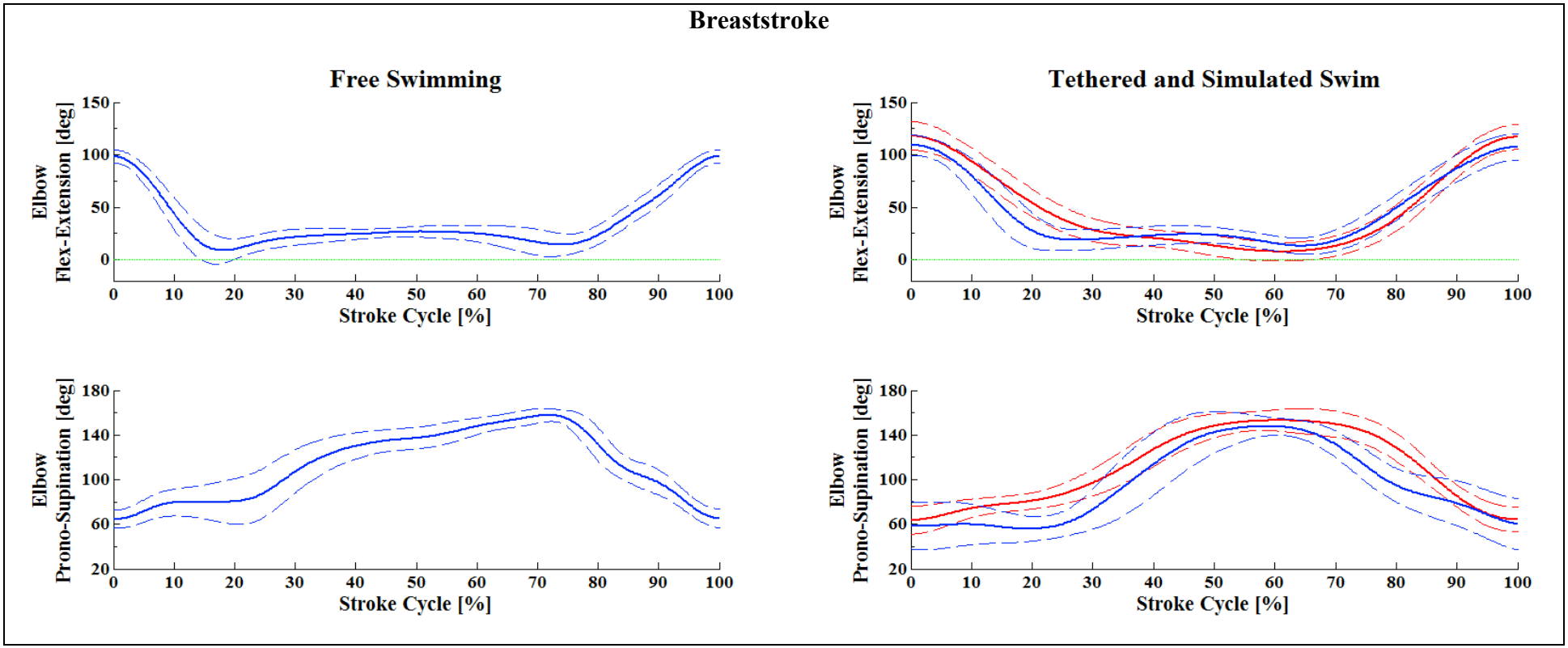

Figure 4.17: Elbow angles during free, tethered and simulated breaststroke.
Free and tethered swim were performed in the pool (IMMU, blue lines) and simulated swim was performed in laboratory (SPS, red lines). Solid and dashed lines: mean ± standard deviation of all trials, respectively.

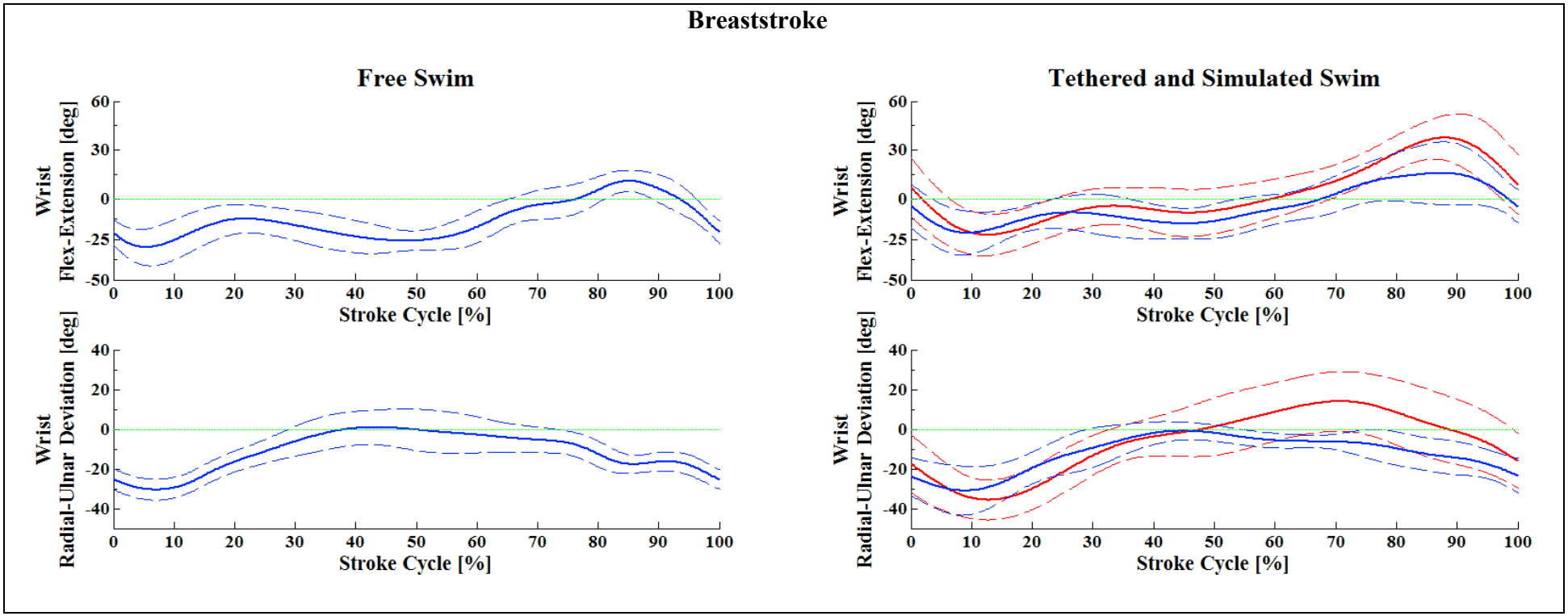

Figure 4.18: Wrist angles during free, tethered and simulated breaststroke.
Free and tethered swim were performed in the pool (IMMU, blue lines) and simulated swim was performed in laboratory (SPS, red lines). Solid and dashed lines: mean ± standard deviation of all trials, respectively.

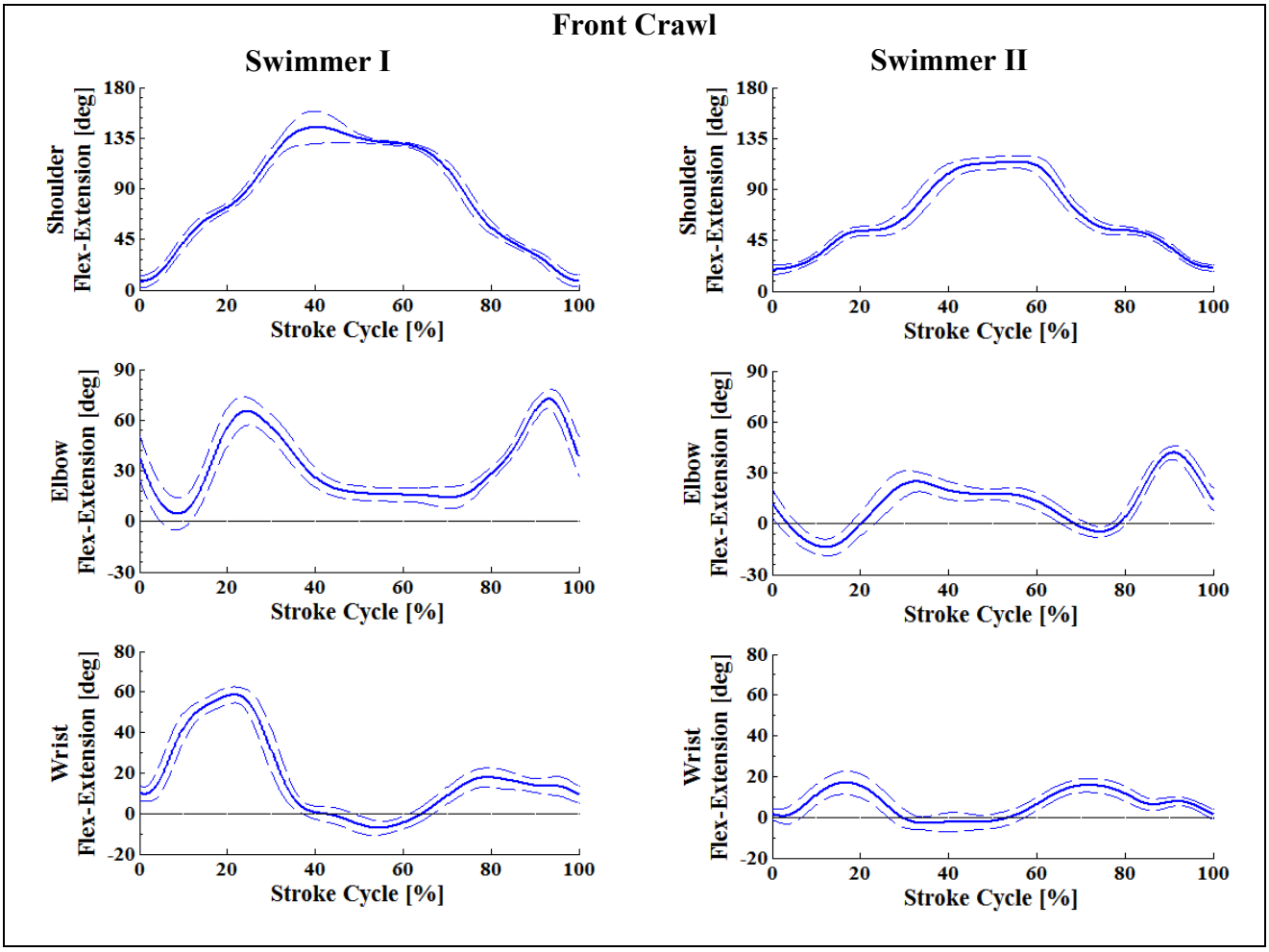

Figure 4.19: Joint angles during free front crawl in the sagittal plane. Angles measured by the IMMU. Columns show the joint kinematics of two swimmers, where different motor patterns can be seen. Solid and dashed lines: mean ± standard deviation of all trials, respectively.

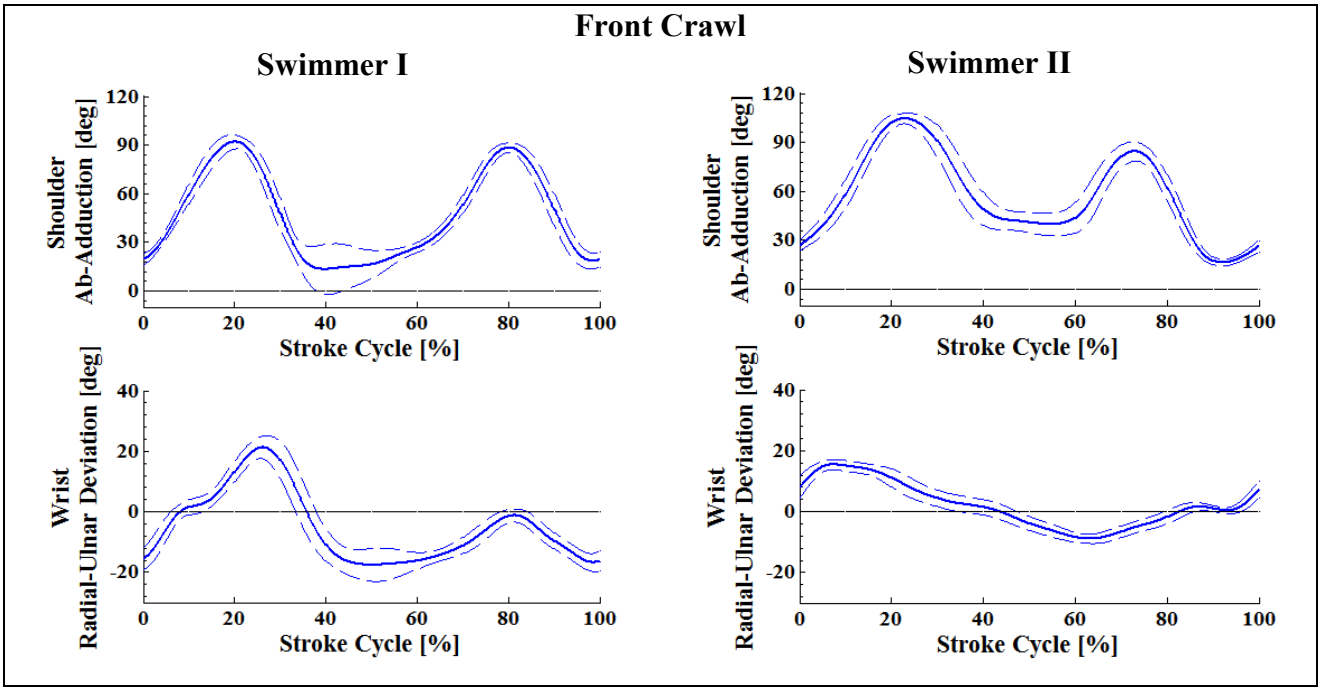

Figure 4.20: Joint angles during free front crawl in the frontal plane.
Angles measured by the IMMU. Columns show the joint kinematics of two swimmers, where different motor patterns can be seen. Solid and dashed lines: mean ± standard deviation of all trials, respectively.

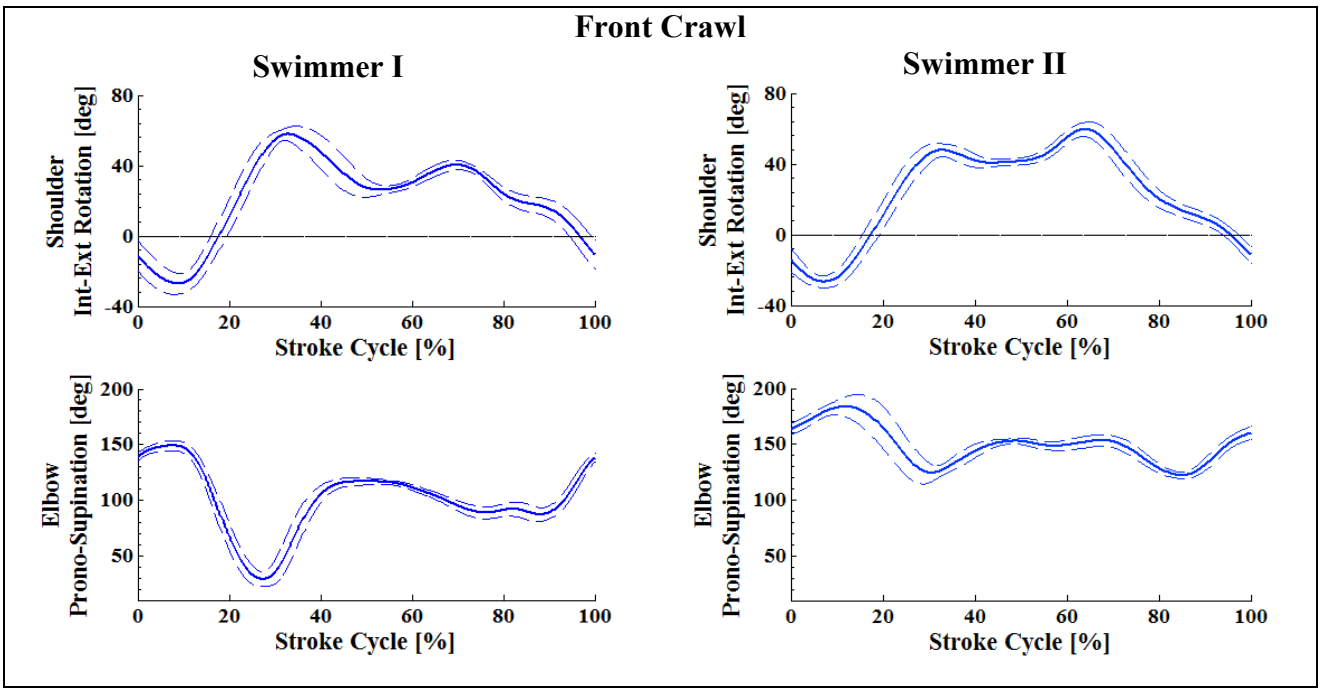

Figure 4.21: Joint angles during free front crawl in the transverse plane.
Angles measured by the IMMU. Columns show the joint kinematics of two swimmers, where different motor patterns can be seen. Solid and dashed lines: mean ± standard deviation of all trials, respectively.

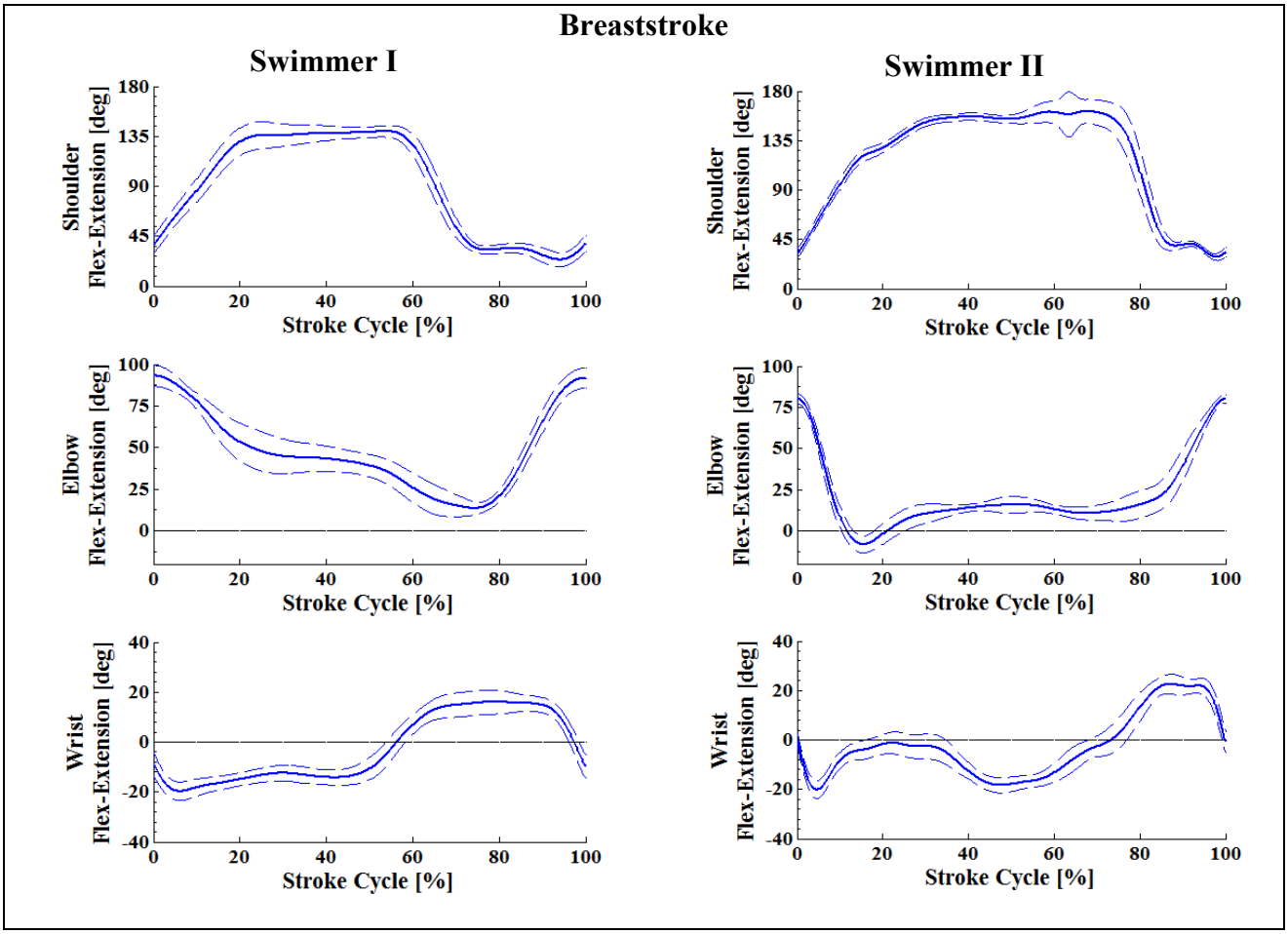

Figure 4.22: Joint angles during free breaststroke in the sagittal plane. Angles measured by the IMMU. Columns show the joint kinematics of two swimmers, where different motor patterns can be seen. Solid and dashed lines: mean ± standard deviation of all trials, respectively.

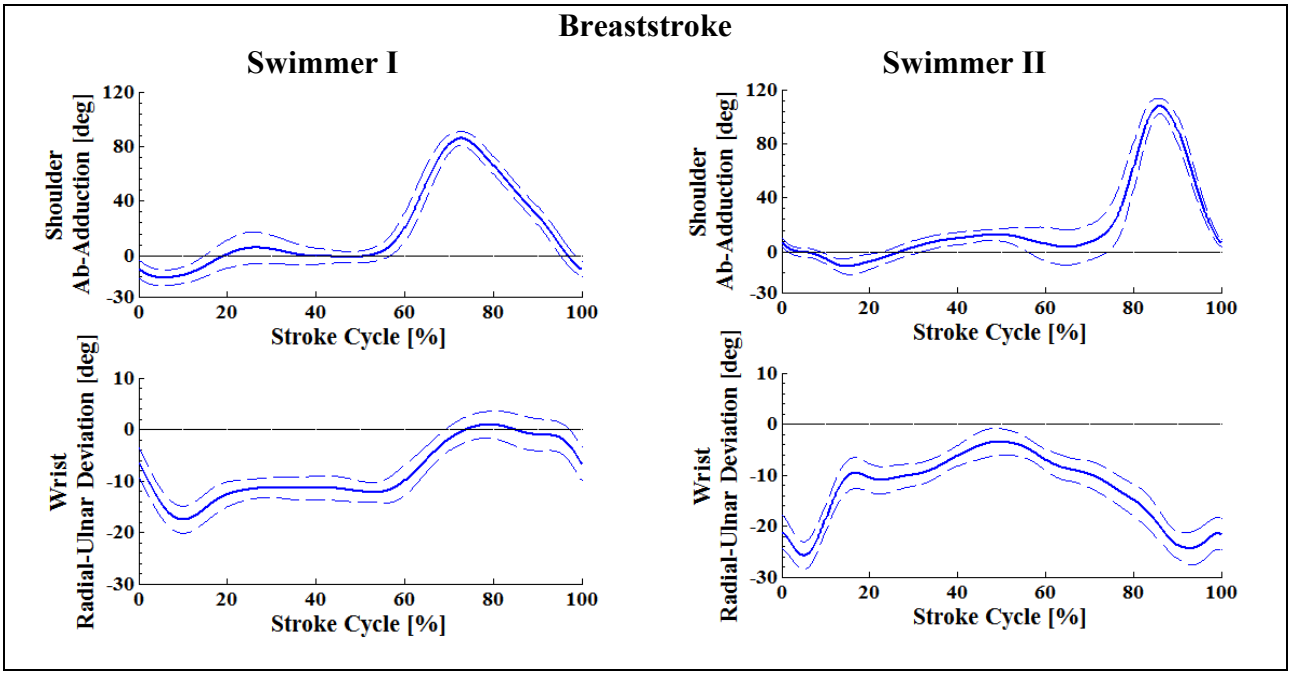

Figure 4.23: Joint angles during free breaststroke in the frontal plane.
Angles measured by the IMMU. Columns show the joint kinematics of two swimmers, where different motor patterns can be seen. Solid and dashed lines: mean ± standard deviation of all trials, respectively.

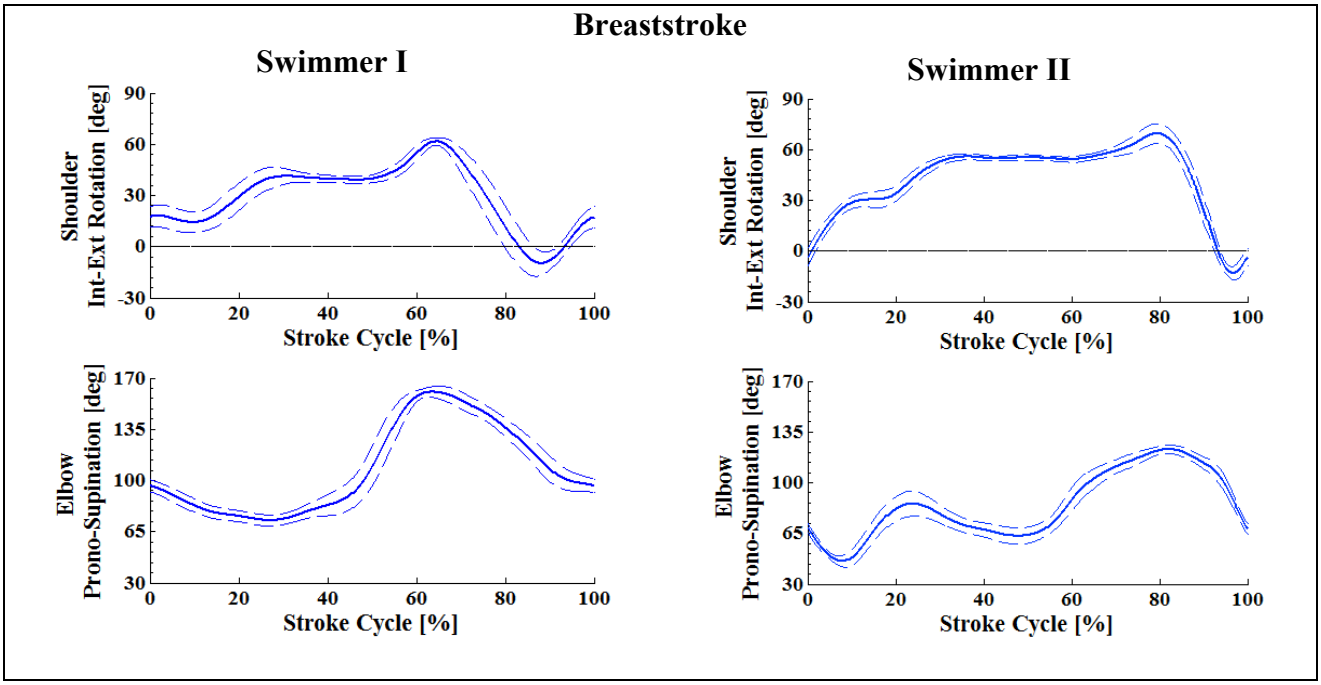

Figure 4.24: Joint angles during free breaststroke in the transverse plane.
Angles measured by the IMMU. Columns show the joint kinematics of two swimmers, where different motor patterns can be seen. Solid and dashed lines: mean ± standard deviation of all trials, respectively.

CHAPTER 5

CONCLUSIONS

5 Conclusions

In this thesis, a protocol initially designed to perform 3D kinematic analysis of upper limbs during simple motor tasks was modified to be used in swimming, and was evaluated both in the laboratory and in the field (swimming pool). In laboratory, simulated swimming trials were carried out in dry-land conditions and recorded by means of inertial and magnetic measurement units (IMMU) and simultaneously by means of a stereo-photogrammetry system (SPS) considered as the reference. For both the front crawl and breaststroke swimming styles and all joint degrees of freedom modeled, the comparison between the SPS and the IMMU showed median values of RMSE lower than 8°, representing 10% of overall joint range of motion, high median values of CMC (0.97) and R (0.96).

Swimming evaluation through accelerometers is an old practice that has been improved over the last two decades due mainly to the micro-electronic evolution. Also other sensors have been aggregated, such as gyroscopes and magnetometers, forming the inertial and magnetic system. Contemporaneously, research on swimming kinematics through IMMU have profited of that evolution by proponing different methods to measure each time more variables useful for performance assessment. The present study contributed with this evolution by offering a novel method so far not encountered in the literature. Consequently, it was not possible to compare these findings with others. Moreover, the literature has only one study that evaluated the 3D kinematics of swimming by means of video recording analysis (Ceccon et al.). Unfortunately, due to different angular conventions in these studies, comparisons between the present outcomes against previous research was once again not possible.

The present study was the first research that aimed to measure 3D joint kinematics of swimming through IMMU and that has been validated by means of a gold standard procedure. This novel method is an useful tool that was easy to set up, did not bother the athletes, and required much less time than

the standard video method during the data collection (about 45min against about 10min for the IMMU), and during the post-processing (2h per each person for video compared with about 3min for the IMMU).

Currently, commercial waterproofed IMMU are not available in the market, and it was not possible to get waterproofed prototypes. The solution applied was similar to most of previous studies that protected the nodes by capsuling them within plastic bags with hermetic sealing (Magalhães, In review). Indeed, this procedure worked well without adding substantial extra weight and volume to the system. Nevertheless, in order to reduce the operational time and to make the proposed method even more convenient, three waterproofing will be explored in next future. The first solution is manufacturing specific size cases to the IMMU for their proper housing and waterproofing; this solution is going to be realized in the near future and tests will be performed as soon as possible. The second solution is contacting a company specialized in waterproofing small electronic devices like music players for swimming (Waterfi, U.S.A., further information can be found at http://waterfi.com, retrieved at 03/07/2013) to render the nodes waterproof; this solution is still running since one node has been be sent to the company for waterproofing. The third and last solution is contacting with a multinational company specialized in sport costumes (Arena, Italy) to create a full body swimsuit with waterproofed IMMU-sized pockets, which is under development.

Another issue, particularly critical due to the environment, is the absence of IMMU capable of synchronization in underwater conditions. Wireless signals propagate over the air within the operating range, but not underwater. Indeed, during the test reported in section 3.4, signal loss was experienced when the IMMU were submerged in depths over 20cm or over 10m from the workstation. Therefore uploading data in real-time during underwater motor tasks still challenges researchers.

Not few solutions can be found in the literature with the aim of providing real-time swimmers feedback (Slawson et al., 2011; Chakravorti et al., 2013; Le Sage et al., 2010; Hagem et al., 2012;

Bächlin et al., 2012). The common point of these studies is the presence of one wireless transmitter device placed either on the back or over the head of the swimmer. These attempts are valuable because offer important performance information useful for coaches and athletes, like stroke counts, rates, length, duration for example. Meanwhile, none study that proposed to perform real-time measurement in swimming have measured 3D joint angles. Whilst new technologies to overcome the IMMU's signal loss underwater are not currently available, the method proposed provide a useful tool that enables 3D kinematics measurement just few minutes after swimming.

Regarding to the validation of the protocol, it was conducted in dry condition because the SPS is more accurate than underwater cameras, thus it can be considered the best gold standard for protocol validation. Furthermore, a large number of arm stroke cycles can be acquired and compared, instead of a maximum of two strokes cycles available with six underwater cameras. In addition, complete arm stroke cycles can be registered in dry condition allowing the analysis of all swim phases including the recovery.

On the other hand, evaluating swimming in dry land lack ecological validity. Even if the instructions given to participants were to swim naturally, these motor tasks were not performed underwater. In the pool, the water's physical proprieties such as drag and thrust demand different patterns of movement from the swimmers when compared to air. Conversely, the comparative analysis between the swimming in the pool and the simulated swimming in the laboratory showed no difference in the joint ranges of motion (Table 4.5). Furthermore, the patterns of movement of the swimmers were found to be comparable with each other in both conditions; and the difference in the patterns of movement between real swimming and simulated swimming diminished from distal toward proximal joints, i.e. from wrists to shoulders joints. Hence, this study validated an IMMU a protocol during movements very similar to real swimming.

The speed of the protocol in delivering kinematic information on swimmers soon after the swim allows coaches to provide the athletes with feedback about their swim-specific technical movements. This is possible due to the low computational load required by the protocol, allowing it to run quickly. Additionally, this protocol is not hardware-dependent. So any systems having technical specifications similar to those presented in section 3.1.1.2 could be used, as long as there is an internal data storage feature, which is the most important requirement. A wireless system is recommended since the use of wires could disturb the natural movements of swimmers.

Besides the use of diverse IMMU, the protocol permits the evaluation of several orientation algorithms. In the present study, three different orientation algorithms were tested. The gyroscopes present in IMMU have a major limitation of drifting during a long trial or during cyclical movements, and a well-adjusted orientation algorithm may be able to compensate for the gyroscope drift by using the accelerometer and/or the magnetometer signals. The analyses of the present study were done utilizing the orientation algorithm based on an extended Kalman filter that presented the best performance in compensating for the gyroscope drift and, in this way, output valid 3D kinematic data. If desirable, other orientation algorithms could be used in this protocol, either with old kinematic data or with a new data collection. The algorithm can be an updated from the IMMU's manufacturer, an open-source or one task specific designed by a developer. In this way, the protocol is easily adjustable to be applied to in numerous experimental conditions.

Underwater motion analysis is of extreme interest for the clinicians because the buoyant force partially cancels the gravitational force so reducing the compression in the joints, which is useful for high body weights or joint injuries. In addition, the water resists limb movement proportional to speed. Thus, obese or overweight people, the elderly, pregnant women and patients with mobility problems and those with neurological impairments or joint pathologies, may benefit from a wide range of aquatic exercises.

Last but not less important, coaches and athletes also frequently utilize resources to perform the underwater motion analysis to improve performance and prevent injuries, as detailed previously. In this way, both coaches/clinicians and athletes/patient may profit by using the IMMU for 3D joint kinematic analyses.

The participants of this thesis showed a tendency of having general patterns of movement for the front crawl and for the breaststroke. Notwithstanding, it was possible to identify individual difference in the patterns of movement of a single swimmer. The main differences noticed among the participants were the higher or lower joint range of motion, and the diverse beginning, ending and duration of each of the stroke phases. Understanding individual variations of the sport movement may help coaches and athletes to plain particular strategies of movement correction and therefore improving performance.

Analysis of the joint angles during sports motion provides professionals and practitioners with important information not only about motor patterns, but also several variables can reliably be estimated. IMMU evaluation in sports could identify lateral asymmetries between the limbs. Investigating the arm symmetry of athletes can help identifying symmetry problems and help improving the swimming technique (Stamm et al., 2012). It may be possible to use IMMU to identify excess fatigue in athletes which the literature suggests is related to both incidence of injuries and declines in sports performance .

In a sport context, the knowledge of the 3D kinematics of the upper limbs in swimming will provide new scenarios for the analysis of the technique used by high-level swimmers, which may be used to improve the performance of beginners, as well as lead to new teaching approaches (i.e., using testing, real-time analysis and feedback, correction, etc.). One of the main advantages of the protocol is that the swimming kinematics can be analyzed throughout the entire training session, whereas waterproofed cameras can only capture a small volume of data.

Consequently, the IMMU is a unique system that allows observing the effects of fatigue on the 3D joint kinematics of swimmers, especially throughout long training sessions or competitions. Moreover, coaches could evaluate not only joint angles but also other biomechanical variables related to the performance, as bilateral symmetries and propulsive forces.

Since only a quick uncomplicated setup is required, daily training use can be supported and encouraged. In the clinical context, an excessive shoulder flexion and/or internal rotation during the stretching phase of the front crawl may lead to undesirable injuries, therefore the protocol can support the identification of possible injury risk factors.

The findings of this thesis support that the protocol accurately estimated the 3D orientation of the shoulders, elbows and wrists joint during simulated swimming. The swimmers were tested during simulated arm strokes in dry land and in the pool during real swimming. Furthermore, an overall correspondence was verified among the swim phases in both simulated and real swimming, and no difference in the overall joint ranges of motion between the real and the simulated swims were observed.

In conclusion, the proposed method to evaluate the 3D joint kinematics through IMMU was revealed to be a useful tool for both sport and clinical contexts. Future research should include extending the protocol to hip, knee and ankle joints in order to perform a complete 3D kinematic analysis of athletes by accomplishing a full-body assessment.

APPENDIX

6 Appendix I: Working and Accuracy of the Inertial and Magnetic Measurement Units.

6.1 Introduction

The working principle of an inertial-based sensor can be illustrated through the human vestibular system, located in the inner ear, a biological system of 3D inertial sensors. This system is able to feel the rotations and linear accelerations of the head and this allows maintenance of the position of the eyes in the environment. Artificial sensors can replicate the above system through micro-electro-mechanical systems technology that allows miniaturization of sensors (accelerometers gyroscopes and magnetometers) and their integration into small portable units or inertial platforms to track the body segments movement of interest on which they are positioned.

6.2 Accelerometers

A single axis accelerometer consists of a mass, suspended by a spring in a housing. Hooke's law governs the linear region of the spring, in which the restoring forces are proportional to the amount of expansion or compression. Specifically,

$$F = kx$$

where k is the constant of proportionality between displacement x and force F. The other important physical principle is the Newton's second law of motion that states that a force operating on a mass that is accelerated will exhibit a force with a magnitude:

$$F = ma$$

This force causes the mass to either compress or expand the spring under the constraint that:

$$F = ma = kx$$

Hence an acceleration will cause the mass to be displaced by:

$$x = \frac{ma}{k}$$

or, if we observe a displacement of x, we know the mass has undergone k an acceleration of

$$a = \frac{kx}{m}$$

In this way, the problem of measuring acceleration m has been turned into one of measuring the displacement of a mass connected to a spring. In order to measure multiple axes of acceleration, this system needs to be duplicated along each of the required axes (Roetenberg, 2006). The accelerometers then are able to provide linear acceleration measurements, including the gravitational component. When the angle between the sensor and the vertical direction is known,

the gravitational component can be subtracted and then by numerical integration the linear velocity and position over time theoretically can be obtained (Garofalo, 2010).

6.3 Gyroscopes

Gyroscopes are instruments that are used to measure angular motion of the underlying body. There are two broad categories: (1) mechanical gyroscopes and (2) optical gyroscopes, within both of these categories, there are many different types available (Roetenberg, 2006). Mechanical gyroscopes operate based on conservation of angular momentum by sensing the change in direction of an angular momentum. According to Newton's second law, the angular momentum of a body will remain unchanged unless a torque acts upon it. Gimbaled and laser gyroscopes are not suitable for human motion analysis due to their large size and high costs. Over the last few years, micro-machined inertial sensors have become more available. Vibrating mass gyroscopes are small, inexpensive and have low power requirements, making them ideal for human movement analysis. A vibrating element (vibrating resonator), when rotated, is subjected to the Coriolis Effect that causes secondary vibration orthogonal to the original vibrating direction. By sensing the secondary vibration, the rate of turn can be measured. The Coriolis Force is given by:

$$\boldsymbol{Fc} = -2m\ (\boldsymbol{\omega} \text{ x } \mathbf{v})$$

where *m* is the mass, v is the momentary speed of the mass relative to the moving object to which it is attached and ω is the angular velocity of that object. Various micro-electromechanical machined geometries are available, of which many use the piezo-electric effect for vibration exert and detection.

6.4 Magnetometers

The magnetometers are sensors that measure the magnetic field, thus functioning as compasses. The magnetic signals are described as the sum of the earth magnetic field vector, a disturbance vector and a white noise term, forming the local magnetic field (Roetenberg, 2006). Near ferromagnetic materials or external magnetic fields, the magnetic flux is most likely to be higher or lower. In real 3D space, the field distribution is more complicated, and therefore, the magnetic inclination should also be taken into account in order to identify a disturbance. The magnetic inclination is the angle the earth magnetic field makes with the surface of the earth. This angle varies depends the position on the earth's surface, being 0◦ at the magnetic equator and 90◦ at each of the magnetic poles (Roetenberg, 2006).

6.5 Sensor Fusion

By combining accelerometers, gyroscopes and magnetometers in a single small unit, the sensor fusion (also known as inertial and magnetic measurement units, IMMU) has been widely used in diverse situations. The traditional application area of IMMU is navigation as well as guidance and stabilization of military systems. Position, velocity and attitude are obtained using accurate, but large gyroscopes and accelerometers, in combination with other measurement devices such as GPS, radar or a baro-altimeter. Generally, signals from these devices are fused using a Kalman filter to obtain quantities of interest. The Kalman filter is useful for combining data from several different indirect and noisy measurements (Kalman, 1960). It weights the sources of information appropriately with knowledge about the signal characteristics based on their models to make the best use of all the data from each of the sensors.

There is no such thing as a perfect measurement device; each type of sensor has its strong and weak points. The idea behind IMMU is that characteristics of one type of sensor are used to overcome the limitations of another sensor. For example, magnetic sensors are used as a reference to prevent the gyroscope integration drift about the vertical axis in the orientation estimates of the attitude and heading reference system. However, iron and other magnetic materials will disturb the local magnetic field and consequently, the orientation estimate. Errors related to magnetic disturbances will have different spatial and temporal properties than gyroscope drift errors (Roetenberg et al., 2005). Using this a priori knowledge, the effects of drift and disturbances can both be minimized.

The IMMU can be mounted on vehicles in such a way they stay leveled and pointed in a fixed direction. This system relies on a set of gimbals and sensors attached on three axes to monitor the angles at all times. Another type of IMMU is the strapdown system that eliminates the use of gimbals, and which is suitable for human motion analysis (Garofalo et al., 2009). In this case, the gyros and accelerometers are mounted directly to the structure of the vehicle or strapped on the body segment. The measurements are made in reference to the local axes of roll, pitch, and heading (or yaw). The clinical reference system provides anatomically meaningful definitions of main segmental movements (e.g. flexion-extension, abduction-adduction or supination-pronation). From this combination or fusion of sensor signals, information is obtained regarding the offsets of the gyroscopes, accelerometers and magnetometers, which can be used to recalibrate the sensors in use.

6.6 Static and Dynamic Accuracy

The large number of scientific papers has demonstrated the applications of the IMMU in the human motion tracking. IMMU use has intensified in the last decade with the technological achievement of miniaturizing the sensors aggregated with new resources such as long battery life, high internal

storage, and wireless transmission. These new features in addition to development of effective algorithms enable the use of the IMMU to perform the 3D joint kinematic analysis in both clinical and sports contexts.

The efficacy of the protocol implemented in this thesis is highly dependent on the static orientation estimation to define the anatomical systems of reference as described in section 3.3. In complement, the orientation algorithm performance based on Kalman filters relies on the accuracy of each sensor in static and dynamic conditions. In this way, the wearable motion capture systems based on IMMU are valid alternatives to optical motion capture for sport applications. Subsequently, several authors have investigated both static and dynamic accuracy of the IMMU.

Usually, manufacturers report in their user guidelines the static and dynamic accuracies. However, due to the different laboratory settings of each research team, and the number and type of instruments presented, substation noise can be aggregated to the raw signals increasing measurement errors. Moreover, the global location of the laboratory where the tests take place also is an important issue to take into consideration. Since the magnetometers performance depends on the earth's magnetic inclination, as stated before, trials performed near to the magnetic equator may present different outcomes than those performed near to the magnetic poles.

In order to check the veracity of the values claimed by the manufacturers, Brodie et al. (2008b) proposed to investigate the static accuracy of 5 different commercial IMMU in measuring 3D orientation in static situations as well as to investigate the calibration of the accelerometers and magnetometers within the IMMU. By using the original factory calibration, these authors found maximum absolute static orientation error of 5.2°, much higher than the value stated by the vendors. Nonetheless, when the IMMU were re-calibrated at the time of measurement, the error was of less than 1°, in agreement with the vendor's specifications. Therefore, they concluded that, for biomechanical research, small relative movements of a body segment from a calibrated position are likely to be more accurate than large-scale global motion that may have an error of up to 9.8°.

Aware of the importance of verifying IMMU accuracy for movement reconstruction, Picerno et al. (2011) proposed a spot check for assessing the IMMU performance in 2 static situations: 9 commercial IMMU aligned to each other on a rigid plank or each one assessed separately by verifying differences between measured and imposed known rotations. They found that, in the first situation, the IMMU defined their orientation differently. This difference was not constant but varied according to the plank's orientation, reaching up to 5.7° for the least consistent IMMU. In the second situation, the same IMMU presenting the highest inaccuracy in the previous test presented once again the worse performance (8.4°). Therefore, these tests demonstrated that IMMU showed different levels of accuracy. The important contribution of this study was that the IMMU

offered a suitable solution for body segments orientation tracking and joint angular kinematics estimation, although the users should be aware of the errors associated with the measurements. At the end, the authors advised others always to check on the accuracy of IMMU, which information may suggest either to recalibrate or to exclude the less reliable IMMU from the data collection.

In another study, Brodie et al. (2008a) investigated the IMMU dynamic accuracy in estimating 3D orientation during simple pendulum motion. The motion of a pendulum swing was measured using both IMMU and video motion capture as a reference. The IMMU raw data were processed by two different orientation algorithms, i.e. by the one supplied by the vendor (Xsens Technology, The Netherlands) and by the one developed by the authors. When comparing the IMMU measurement of pendulum motion using the vendor's orientation against the video motion capture, the results showed RMS errors of between 8.5° and 11.7° depending on the length and type of pendulum swing; sometimes the error exceeded 30° along the trials. On the other hand, comparing the performance of the custom orientation algorithm against the video motion capture, the RMS error was between 0.8° and 1.3°.

In attempt to negate the problems of ferromagnetic materials or other magnetic fields near the IMMU that can disturb the local earth magnetic field and, therefore, the orientation estimation, Roetenberg et al. (2005) proposed a complementary Kalman filter designed to estimate orientation of human body segments through IMMU signals. In this filter, the gyroscope bias error, orientation error, and magnetic disturbance error are estimated. The filter was tested under quasi-static and dynamic conditions with ferromagnetic materials close to the IMMU. The orientation estimated by the filter was compared with the orientation obtained with a video motion capture. Results show accurate and drift-free orientation estimates. The compensation resulted in a significant difference ($p < 0.01$) between the orientation estimates with compensation of magnetic disturbances in comparison to no compensation or only gyroscopes. The average static error was 1.4° in the magnetically disturbed experiments. The dynamic error presented was 2.6°.

Hence, it has be demonstrated that the highest IMMU performance in estimating the 3D human kinematics is strictly dependent of these 2 following issues: 1) proper calibration of each sensor in the epoch and place of measurement, according to the manufacturer’s instructions; and 2) robust orientation algorithm, either specifically developed to that motor task or flexible enough to be adjusted to vary with the experimental situation.

ACKNOWLEDGMENTS

Foremost, I would like to express my sincere gratitude to my supervisor Prof. Silvia Fantozzi for the continuous support of my Ph.D study and research, for her patience, motivation, enthusiasm, and immense knowledge. His guidance helped me in all the time of research and writing of this thesis. In the same way, I would like to thank my co-supervisor Prof. Giorgio Gatta for his high professionalism and good sense of humor. Besides my supervisor and co-supervisor, I would like to thank the rest of my thesis committee: Prof. Ugo Della Croce and Prof. Kamiar Aminian, for their encouragement, insightful comments, and hard questions. My sincere thanks also goes to Prof. Angelo Capello and Prof. Lorenzo Chiari, for offering support during my stay in Bologna. I thank my fellow labmates in the Record Center of the UNIBO: Andrea Giovanardi, Sandro Bartolomei, Rocco di Michelli, Matteo Cortesi, Stefano Maracino, Claudio Fabbri, Ivan Malagoli, Martina Camorani, Franco Merni, Andrea Ceciliani, Gabrielle Semprini, Simone Ciacci e Antonio Cicchella for the stimulating discussions, for the hard works, and for all the fun we have had in the last three years. Special thanks to Mr. Andrea Giovanardi for his dedication, teachings and readiness in help. Also I thank the people from the department of international relations of the UNIBO, particularly to Ms. Livia Mercatelli, and the Projects Monesia for the providing the provision during the last 34 months. I cannot forget to thank Dr. Philip Bishop for his assistance in correcting the english text. Last but not the least, I would like to thank my wife Leandra, daughter Anne, mother Dorinha, father Laerte, sister Pollyana and my in-laws for the care, support, comfort, prayers and fellowship. To all of you, I wish God may bless you by rewarding you according to your deeds.

REFERENCES

Allegrucci, M., Whitney, S.L., Irrgang, J.J., 1994. Clinical implications of secondary impingement of the shoulder in freestyle swimmers. The Journal of orthopaedic and sports physical therapy 20, 307-318.

Armstrong, N., Davies, B., 1981. An ergometric analysis of age group swimmers. British journal of sports medicine 15, 20-26.

Bächlin, M., Förster, K., Tröster, G., 2009. SwimMaster: a wearable assistant for swimmer. In 11th international conference on Ubiquitous computing. Orlando, Florida, USA.

Bächlin, M., Tröster, G., 2009. Pervasive computing in swimming: A model describing acceleration data of body worn sensors in crawl swimming. In Pervasive Computing (JCPC), 2009 Joint Conference on. Tamsui, Taipei.

Bächlin, M., Tröster, G., 2012. Swimming performance and technique evaluation with wearable acceleration sensors. Pervasive and Mobile Computing, 1574-1192.

Bachmann, E.R., Yun, X., Peterson, C.W., 2004. An investigation of the effects of magnetic variations on inertial/magnetic orientation sensors. In Robotics and Automation, 2004. Proceedings. ICRA'04. 2004 IEEE International Conference on.

Barbosa, T., Silva, A.J., Reis, A.M., Costa, M., Garrido, N., Policarpo, F., Reis, V.M., 2010a. Kinematical changes in swimming front Crawl and Breaststroke with the AquaTrainer® snorkel. European journal of applied physiology 109, 1155-1162.

Barbosa, T.M., Bragada, J.A., Reis, V.M., Marinho, D.A., Carvalho, C., Silva, A.J., 2010b. Energetics and biomechanics as determining factors of swimming performance: updating the state of the art. Journal of Science and Medicine in Sport 13, 262-269.

Barbosa, T.M., Marinho, D.A., Costa, M.J., Silva, A.J., 2011. Biomechanics of Competitive Swimming Strokes.

Berger, M.A., de Groot, G., Hollander, A.P., 1995. Hydrodynamic drag and lift forces on human hand/arm models. J Biomech 28, 125-133.

Berthouze, L., Mayston, M., 2011. Design and validation of surface-marker clusters for the quantification of joint rotations in general movements in early infancy. Journal of Biomechanics 44, 1212-1215.

Bixler, B., Pease, D., Fairhurst, F., 2007. The accuracy of computational fluid dynamics analysis of the passive drag of a male swimmer. Sports Biomechanics 6, 81-98.

Brodie, M.A., Walmsley, A., Page, W., 2008a. Dynamic accuracy of inertial measurement units during simple pendulum motion. Computer Methods in Biomechanics and Biomedical Engineering 11, 235-242.

Brodie, M.A., Walmsley, A., Page, W., 2008b. The static accuracy and calibration of inertial measurement units for 3D orientation. Computer Methods in Biomechanics and Biomedical Engineering 11, 641-648.

Capitão, F., Lima, A.B., Gonçalves, P., Morouço, P., Silva, M., Fernandes, R.M., Vilas-Boas, J.P., 2006. Videogrametrically and acelorimetrically assessment intra-cyclic variations of the velocity in breaststroke. In Biomechanics and Medicine in Swimming X. Porto.

Cappozzo, A., Catani, F., Della Croce, U., Leardini, A., 1995. Position and orientation in space of bones during movement: anatomical frame definition and determination. Clinical biomechanics (Bristol, Avon) 10, 171-178.

Ceccon, S., Ceseracciu, E., Sawacha, Z., Gatta, G., Cortesi, M., Cobelli, C., Fantozzi, S., 2013. Motion analysis of front crawl swimming applying CAST technique by means of automatic tracking. Journal of sports sciences 31, 276-287.

Ceseracciu, E., 2011. New frontiers of markerless motion capture: application to swim biomechanics and gait analysis. PhD Thesis, University of Padua.

Ceseracciu, E., Sawacha, Z., Fantozzi, S., Cortesi, M., Gatta, G., Corazza, S., Cobelli, C., 2011. Markerless analysis of front crawl swimming. Journal of Biomechanics 44, 2236-2242.

Chakravorti, N., Le Sage, T., Slawson, S.E., Conway, P.P., West, A.A., 2013. Design and Implementation of an Integrated Performance Monitoring Tool for Swimming to Extract Stroke Information at Real Time. IEEE Transactions on Human-Machine Systems 43, 199-213.

Chollet, D., Tourny-Chollet, C., Gleizes, F., 1999. Evolution of co-ordination in flat breaststroke in relation to velocity. Biomechanics and Medicine in Swimming VIII, 29-32.

Cooper, G., Sheret, I., McMillian, L., Siliverdis, K., Sha, N., Hodgins, D., Kenney, L., Howard, D., 2009. Inertial sensor-based knee flexion/extension angle estimation. Journal of biomechanics 42, 2678-2685.

Corazza, S., Gambaretto, E., Mundermann, L., Andriacchi, T.P., 2010. Automatic generation of a subject-specific model for accurate markerless motion capture and biomechanical applications. Biomedical Engineering, IEEE Transactions on 57, 806-812.

Corazza, S., Mündermann, L., Chaudhari, A., Demattio, T., Cobelli, C., Andriacchi, T., 2006. A markerless motion capture system to study musculoskeletal biomechanics: Visual hull and simulated annealing approach. Annals of biomedical engineering 34, 1019-1029.

Costill, D., Kovaleski, J., Porter, D., Kirwan, J., Fielding, R., King, D., 1985. Energy expenditure during front crawl swimming: predicting success in middle-distance events. International Journal of Sports Medicine 6, 266-270.

Craig, A.B., Skehan, P.L., Pawelczyk, J.A., Boomer, W.L., 1985. Velocity, stroke rate, and distance per stroke during elite swimming competition. Med Sci Sports Exerc 17, 625-634.

Dadashi, F., Crettenand, F., Millet, G., Seifert, L., Komar, J., Aminian, K., 2011. Frontcrawl propulsive phave detection using inertial sensors. In 29 International Conference on Biomechanics in Sports. Porto (Portugal).

Dadashi, F., Crettenand, F., Millet, G.P., Aminian, K., 2012. Front-crawl instantaneous velocity estimation using a wearable inertial measurement unit. Sensors (Basel) 12, 12927-12939.

Dadashi, F., Millet, G., Aminian, K., 2013. Inertial measurement unit and biomechanical analysis of swimming: an update. Schweizerische Zeitschrift für Sportmedizin & Sporttraumatologie 61.

Daukantas, S., Marozas, V., Lukosevicius, A., 2008. Inertial sensor for objective evaluation of swimmer performance. In 11th International Biennial Baltic.

Davey, N.P., Anderson, M., James, D.A., 2008. Validation trial of an accelerometer-based sensor platform for swimming. Sports Tech 1, 202-207.

De Vries, W., Veeger, H., Baten, C., Van Der Helm, F., 2009. Magnetic distortion in motion labs, implications for validating inertial magnetic sensors. Gait & posture 29, 535-541.

Deschodt, V., Rouard, A., Monteil, K., 1996. Relationship between the three coordinates of the upper limb joints with swimming velocity. Biomechanics and Medicine in Swimming VII. London: E & FN Spon, 52-58.

Di Prampero, P., Pendergast, D., Wilson, D., Rennie, D., 1974. Energetics of swimming in man. Journal of applied physiology 37, 1-5.

El-Gohary, M., McNames, J., 2011. Human Joint Angle Tracking with Wearable Inertial Sensors, 33rd Annual International Conference of the IEEE Engineering in Medicine and Biology Society (EMBC '11), Boston, USA.

Favre, J., Chardonnens, J., Aminian, K., 2007. An orientation measuring system suitable for routine uses made by the fusion of a 3D gyroscope and a magnetic tracker. Conf.Proc.IEEE Eng Med Biol.Soc. 2007, 3938-3941.

Ferrari, A., Cutti, A.G., Cappello, A., 2010a. A new formulation of the coefficient of multiple correlation to assess the similarity of waveforms measured synchronously by different motion analysis protocols. Gait & posture 31, 540-542.

Ferrari, A., Cutti, A.G., Garofalo, P., Raggi, M., Heijboer, M., Cappello, A., Davalli, A., 2010b. First in vivo assessment of "Outwalk": a novel protocol for clinical gait analysis based on inertial and magnetic sensors. Med Biol Eng Comput 48, 1-15.

Fulton, S.K., Pyne, D., Burkett, B., 2011. Optimizing kick rate and amplitude for Paralympic swimmers via net force measures. Journal of Sports Sciences 29, 381-387.

Fulton, S.K., Pyne, D.B., Burkett, B., 2009a. Quantifying freestyle kick-count and kick-rate patterns in Paralympic swimming. Journal of Sports Science 27, 1455-1461.

Fulton, S.K., Pyne, D.B., Burkett, B., 2009b. Validity and reliability of kick count and rate in freestyle using inertial sensor technology. J Sports Sci 27, 1051-1058.

Garofalo, P., 2010. Development of motion analysis protocol based on inertial sensors. University of Bologna.

Garofalo, P., Raggi, M., Ferrari, A., Cutti, A.G., Davalli, A., 2009. Development of a clinical software to measure the 3D gait kinematics in every-day-life environments through the outwalk protocol. Gait & posture 30, S30.

Hagem, R.M., Thiel, D.V., O'Keefe, S., Fickenscher, T., 2013. Real-time swimmers' feedback based on smart infrared (SSIR) optical wireless sensor. Electronics Letters 49, 340-341.

Hagem, R.M., Thiel, D.V., O'Keefe, S.G., Dahm, N., Stamm, A., Fickenscher, T., 2012. Smart optical wireless sensor for real time swimmers feedback. In Sensors, 2012 IEEE.

Hollander, A., De Groot, G., van Ingen Schenau, G., Toussaint, H., De Best, H., Peeters, W., Meulemans, A., Schreurs, A., 1986. Measurement of active drag during crawl arm stroke swimming. Journal of Sports Sciences 4, 21-30.

Hollander, A.P., de Groot, G., van Ingen Schenau, G.J., Kahman, R., Toussaint, H.M., 1988. Contribution of the legs to propulsion in front crawl swimming. Swimming science V, 39-43.

Hou, P., 2012. The study on swimming exercises based on 3D accelerometer data analysis. International Journal of Advancements in Computing Technology 4, 239-245.

Hyndman, R.J., Koehler, A.B., 2006. Another look at measures of forecast accuracy. International Journal of Forecasting 22, 679-688.

Ichikawa, H., Ohgi, Y., Miyaji, C., Nomura, T., 2003. Estimation of arm motion in front crawl swimming using accelerometer, in: Chatard, J.C. (Ed.), Biomechanics and Medicine in Swimming IX, Université de St. Etienne, pp. 133 - 138.

Jackman, J., 2007. Bluescreen Compositing. Burlington, USA: Focal Press.

James, D.A., Leadbetter, R.I., Neeli, M.R., Burkett, B.J., Thiel, D.V., Lee, J.B., 2011. An integrated swimming monitoring system for the biomechanical analysis of swimming strokes. Sports Technology 4, 141-150.

Ji-Hwan, K., Nguyen Duc, T., Hyun Sang, S., Rasheed, T., Tae-Seong, K., 2009. Forearm Motion Tracking with Estimating Joint Angles from Inertial Sensor Signals. In Biomedical Engineering and Informatics, 2009. BMEI '09. 2nd International Conference on.

Kalman, R.E., 1960. A new approach to linear filtering and prediction problems. Journal of basic Engineering 82, 35-45.

Khoo, B.H., Lee, B.K.J., Senanayake, S.M.N.A., Wilson, B.D., 2009. System for determining within-stroke variations of speed in swimming (SWiSS). In Advanced Intelligent Mechatronics, 2009. AIM 2009. IEEE/ASME International Conference on.

Kimura, Y., Yeater, R., Martin, R., 1990. Simulated swimming: a useful tool for evaluation the VO2 max of swimmers in the laboratory. British journal of sports medicine 24, 201-206.

Kjendlie, P., Stallman, R.K., 2008. Drag characteristics of competitive swimming children and adults. Journal of Applied Biomechanics 24, 35.

Kjendlie, P.-L., Haljand, R., Fjortoft, O., Stallman, R.K., 2006. Stroke frequency strategies of international and national swimmers in 100-m races. Biomechanics and medicine in swimming X. Port J Sport Sci, Porto, 52-54.

Kjendlie, P.L., Olstad, B.H., 2012. Automatic 3D motion capture of swimming: marker resistance. Medicine & Science in Sports & Exercise 44, S320.

Kolmogorov, S., Duplishcheva, O., 1992. Active drag, useful mechanical power output and hydrodynamic force coefficient in different swimming strokes at maximal velocity. Journal of biomechanics 25, 311-318.

Kontaxis, A., Cutti, A.G., Johnson, G.R., Veeger, H.E.J., 2009. A framework for the definition of standardized protocols for measuring upper-extremity kinematics. Clinical Biomechanics 24, 246-253.

Kudo, S., Vennell, R., Wilson, B., 2013. The effect of unsteady flow due to acceleration on hydrodynamic forces acting on the hand in swimming. Journal of Biomechanics 46, 1697-1704.

Kudo, S., Vennell, R., Wilson, B., Waddell, N., Sato, Y., 2008. Influence of surface penetration on measured fluid force on a hand model. J Biomech 41, 3502-3505.

Le Sage, T., Bindel, A., Conway, P., Justham, L., Slawson, S., Webster, J., West, A., 2012. A Multi-sensor System for Monitoring the Performance of Elite Swimmers, in: Obaidat, M., Tsihrintzis, G., Filipe, J. (Eds.), e-Business and Telecommunications. Springer Berlin Heidelberg, pp. 350-362.

Le Sage, T., Bindel, A., Conway, P., Justham, L., Slawson, S., West, A., 2010a. Development of a real time system for monitoring of swimming performance. Procedia Engineering 2, 2707-2712.

Le Sage, T., Bindel, A., Conway, P., Justham, L., Slawson, S., West, A., 2010b. Kalman filter design for application to an ins analysing swimmer prefornance. In 18th European Signal Processing Conference.

Le Sage, T., Bindel, A., Conway, P., Justham, L., Slawson, S., West, A., 2011. Embedded programming and real-time signal processing of swimming strokes. Sports Engineering 14, 1-14.

Lee, J.B., Burkett, B.J., Thiel, D.V., James, D.A., 2011. Inertial sensor, 3D and 2D assessment of stroke phases in freestyle swimming. Procedia Engineering 13, 148-153.

Lee, J.B., Ohgi, Y., James, D.A., 2012. Sensor fusion: let's enhance the performance of performance enhancement. Procedia Engineering 34, 795-800.

Madgwick, S.O.H., Harrison, A.J.L., Vaidyanathan, R., 2011. Estimation of IMU and MARG orientation using a gradient descent algorithm, IEEE International Conference on Rehabilitation Robotics. IEEE, Zurich, Switzerland, pp. 1-7.

Magalhães, F.A., Sawacha, Z., Di Michele, R., Cortesi, M., Gatta, G., Fantozzi, S., 2013. Effectiveness of an Automatic Tracking Software in Underwater Motion Analysis. Journal of Sports Science and Medicine 12, 660-667.

Magalhães, F.A., Sawacha, Z., Di Michele, R., Cortesi, M., Gatta, G., Fantozzi, S., 2012. Performance analysis of an automatic tracking software in underwater exercises. In XII International Symposium on 3D Analysis of Human Movement. Bologna, Italy.

Magalhães, F.A., Vannozzi, G., Gatta, G., Fantozzi, S., In review. Wearable inertial and magnetic sensors in swimming motion analysis: a systematic review. Submitted to the Journal of Sports Sciences.

Marinho, D.A., Barbosa, T.M., Costa, M.J., Figueiredo, C., Reis, V.M., Silva, A.J., Marques, M.C., 2010. Can 8-weeks of training affect active drag in young swimmers? Journal of Sport Science and Medicine 9, 71-78.

Marinho, D.A., Rouboa, A.I., Alves, F.B., Vilas-Boas, J.P., Machado, L., Reis, V.M., Silva, A.J., 2009. Hydrodynamic analysis of different thumb positions in swimming. Journal of Sports Science and Medicine 8, 58-66.

McCabe, C.B., Psycharakis, S., Sanders, R., 2011. Kinematic differences between front crawl sprint and distance swimmers at sprint pace. Journal of Sports Science. 29, 115-123.

McCabe, C.B., Sanders, R.H., 2012. Kinematic differences between front crawl sprint and distance swimmers at a distance pace. Journal of Sports Science. 30, 601-608.

McMaster, W.C., Troup, J., 1993. A survey of interfering shoulder pain in United States competitive swimmers. Am J Sports Med 21, 67-70.

Moeslund, T.B., Granum, E., 2001. A survey of computer vision-based human motion capture. Computer Vision and Image Understanding 81, 231-268.

Moeslund, T.B., Hilton, A., Kruger, V., 2006. A survey of advances in vision-based human motion capture and analysis. Computer Vision and Image Understanding 104, 90-126.

Mullane, S.L., Chakravorti, N., Conway, P.P., West, A.A., 2011. Design and implementation of a user-centric swimming performance monitoring tool. Proceedings of the Institution of Mechanical Engineers, Part P: Journal of Sports Engineering and Technology 225, 213-229.

Ohgi, Y., 2002. Microcomputer-based acceleration sensor device for sports biomechanics - stroke evaluation by using swimmer's wrist acceleration. In Proceedings of IEEE on Sensors.

Ohgi, Y., Ichikawa, H., 2002. Microcomputer-based data logging device for accelerometry in swimming.

Ohgi, Y., Ichikawa, H., Homma, M., Miyaji, C., 2003. Stroke phase discrimination in breaststroke swimming using a tri-axial acceleration sensor device. Sports Engineering 6, 113-123.

Ohgi, Y., Ichikawa, H., Miyaji, C., 2002. Microcomputer-based Acceleration Sensor Device for Swimming Stroke Monitoring. JSME Int J., Ser. C 45, 960-966.

Ohgi, Y., Yasumura, M., Ichikawa, H., Miyaji, C., 2000. Analysis of stroke technique using acceleration sensor IC in freestyle swimming. In The Engineering of Sport.

Pansiot, J., Lo, B., Guang-Zhong, Y., 2010. Swimming Stroke Kinematic Analysis with BSN. In Body Sensor Networks (BSN), 2010 International Conference on.

Payton, C.J., Bartlett, R.M., 1995. Estimating propulsive forces in swimming from three ‐ dimensional kinematic data. Journal of Sports Sciences 13, 447-454.

Pendergast, D., Capelli, C., Craig, A., Di Prampero, P., Minetti, A., Mollendorf, J., Termin, I., Zamparo, P., 2006. Biophysics in swimming. Rev Port Cien Desp 6, 185-189.

Picerno, P., Cereatti, A., Cappozzo, A., 2008. Joint kinematics estimate using wearable inertial and magnetic sensing modules. Gait Posture 28, 588-595.

Picerno, P., Cereatti, A., Cappozzo, A., 2011. A spot check for assessing static orientation consistency of inertial and magnetic sensing units. Gait Posture 33, 373-378.

Pink, M.M., Tibone, J.E., 2000. The painful shoulder in the swimming athlete. Orthop Clin North Am 31, 247-261.

Pollard, H., Croker, D., 1999. Shoulder pain in elite swimmers. Australasian chiropractic & osteopathy : journal of the Chiropractic & Osteopathic College of Australasia 8, 91-95.

Poppe, R., 2007. Vision-based human motion analysis: An overview. Computer vision and image understanding 108, 4-18.

Psycharakis, S.G., McCabe, C., 2011. Shoulder and hip roll differences between breathing and non-breathing conditions in front crawl swimming. J Biomech 44, 1752-1756.

Psycharakis, S.G., Naemi, R., Connaboy, C., McCabe, C., Sanders, R.H., 2010. Three-dimensional analysis of intracycle velocity fluctuations in frontcrawl swimming. Scand J Med Sci Sports 20, 128-135.

Psycharakis, S.G., Sanders, R.H., 2008. Shoulder and hip roll changes during 200-m front crawl swimming. Medicine & Science in Sports & Exercise 40, 2129-2136.

Psycharakis, S.G., Sanders, R.H., 2009. Validity of the use of a fixed point for intracycle velocity calculations in swimming. Journal of Science and Medicine in Sport 12, 262-265.

Roetenberg, D., 2006. Inertial and magnetic sensing of human motion. University of Twente.

Roetenberg, D., Luinge, H.J., Baten, C.T., Veltink, P.H., 2005. Compensation of magnetic disturbances improves inertial and magnetic sensing of human body segment orientation. IEEE Trans Neural Syst Rehabil Eng 13, 395-405.

Sabatini, A.M., 2011. Estimating three-dimensional orientation of human body parts by inertial/magnetic sensing. Sensors 11, 1489-1525.

Saber-Sheikh, K., Bryant, E.C., Glazzard, C., Hamel, A., Lee, R.Y., 2010. Feasibility of using inertial sensors to assess human movement. Man.Ther. 15, 122-125.

Sanders, R.H., 1999. Hydrodynamic characteristics of a swimmer's hand. Journal of Applied Biomechanics 15, 3-26.

Sanders, R.H., 2007. Kinematics, coordination, variability, and biological noise in the prone flutter kick at different levels of a “learn-to-swim” programme. Journal of sports sciences 25, 213-227.

Schepers, H.M., Roetenberg, D., Veltink, P.H., 2010. Ambulatory human motion tracking by fusion of inertial and magnetic sensing with adaptive actuation. Med Biol Eng Comput 48, 27-37.

Schleihauf, R., 1979. A hydrodynamic analysis of swimming propulsion. Swimming III, 70-109.

Seifert, L., Chehensse, A., Tourny-Chollet, C., Lemaitre, F., Chollet, D., 2008. Effect of breathing pattern on arm coordination symmetry in front crawl. J Strength Cond Res 22, 1670-1676.

Seifert, L., Chollet, D., Allard, P., 2005. Arm coordination symmetry and breathing effect in front crawl. Hum Mov Sci 24, 234-256.

Sein, M.L., Walton, J., Linklater, J., Appleyard, R., Kirkbride, B., Kuah, D., Murrell, G.A., 2010. Shoulder pain in elite swimmers: primarily due to swim-volume-induced supraspinatus tendinopathy. British journal of sports medicine 44, 105-113.

Slawson, S.E., Justham, L.M., Conway, P.P., Le-Sage, T., West, A.A., 2011. Characterizing the swimming tumble turn using acceleration data. Proceedings of the Institution of Mechanical Engineers, Part P: Journal of Sports Engineering and Technology 226, 3-15.

Slawson, S.E., Justham, L.M., West, A.A., Conway, P.P., Caine, M.P., Harrison, R., 2008. Accelerometer Profile Recognition of Swimming Strokes (P17) The Engineering of Sport 7. Springer Paris, pp. 81-87.

Spigelman, T.H., 2009. Coordination of Swimbench Freestyle in Elite and Non-elite Swimmers: A Dynamical System Approach. Doctoral disssertation, University of Kentucky.

Stamm, A., James, D., Thiel, D., 2013. Velocity profiling using inertial sensors for freestyle swimming. Sports Engineering 16, 1-11.

Stamm, A., James, D.A., Hagem, R.M., Thiel, D.V., 2012. Investigating arm symmetry in swimming using inertial sensors. In Sensors, 2012 IEEE.

Stamm, A., Thiel, D.V., Burkett, B., James, D.A., 2011. Towards determining absolute velocity of freestyle swimming using 3-axis accelerometers. Procedia Engineering 13, 120-125.

Takagi, H., Sugimoto, S., Nishijima, N., Wilson, B., 2004. Swimming: Differences in stroke phases, arm‐leg coordination and velocity fluctuation due to event, gender and performance level in breaststroke. Sports Biomechanics 3, 15-27.

Tourny, C., Chollet, D., Micallef, J., Macabies, J., 1992. Comparative analysis of studies of speed variations within a breaststroke cycle. Biomechanics and medicine in swimming, 161-166.

Toussaint, H., Truijens, M., 2005. Biomechanical aspects of peak performance in human swimming. Animal Biology 55, 17-40.

Toussaint, H.M., Carol, A., Kranenborg, H., Truijens, M.J., 2006. Effect of fatigue on stroking characteristics in an arms-only 100-m front-crawl race. Medicine and science in sports and exercise 38, 1635.

Vannozzi, G., Donati, M., Gatta, G., 2010. Analysis of swim turning, underwater gliding and stroke resumption phases in top division swimmers using a wearable inertial sensor device., Biomechanics and Medicine in Swimming XI, Oslo (NW) pp. 178-180.

Veltink, P.H., Bussmann, H., de Vries, W., Martens, W., Van Lummel, R.C., 1996. Detection of static and dynamic activities using uniaxial accelerometers. Rehabilitation Engineering, IEEE Transactions on 4, 375-385.

Vezos, N., Gourgoulis, V., Aggeloussis, N., Kasimatis, P., Christoforidis, C., Mavromatis, G., 2007. Underwater stroke kinematics during breathing and breath-holding front crawl swimming. J Sports Sci & Med 6, 58-62.

Vilas-Boas, J.P., Fernandes, R.J., Barbosa, T.M., 2010. Intra-cycle velocity variations, swimming economy, performance and training in swimming. World book of swimming: from science to performance, 120-140.

Woltring, H.J., Long, K., Osterbauer, P.J., Fuhr, A.W., 1994. Instantaneous helical axis estimation from 3-D video data in neck kinematics for whiplash diagnostics. Journal of Biomechanics 27, 1415-1432.

Wu, G., Van der Helm, F.C., Veeger, H., Makhsous, M., Van Roy, P., Anglin, C., Nagels, J., Karduna, A.R., McQuade, K., Wang, X., 2005. ISB recommendation on definitions of joint coordinate systems of various joints for the reporting of human joint motion—Part II: shoulder, elbow, wrist and hand. Journal of biomechanics 38, 981-992.

Zaidi, H., Taiar, R., Fohanno, S., Polidori, G., 2008. Analysis of the effect of swimmer's head position on swimming performance using computational fluid dynamics. Journal of biomechanics 41, 1350-1358.

Zamparo, P., 2006. Effects of age and gender on the propelling efficiency of the arm stroke. Eur J Appl Physiol 97, 52-58.

Zhou, H., Hu, H., 2005. Kinematic model aided inertial motion tracking of human upper limb. In Information Acquisition, 2005 IEEE International Conference on.